


Spring 5-8-2021

Neural Oscillatory Activity Serving Sensorimotor Control is Regulated by the Mitochondrial Redox Environment in Health and Disease

Rachel Spooner
University of Nebraska Medical Center

Tell us how you used this information in this [short survey](#).

Follow this and additional works at: <https://digitalcommons.unmc.edu/etd>

 Part of the [Multivariate Analysis Commons](#), [Neurosciences Commons](#), [Physiological Processes Commons](#), and the [Virus Diseases Commons](#)

Recommended Citation

Spooner, Rachel, "Neural Oscillatory Activity Serving Sensorimotor Control is Regulated by the Mitochondrial Redox Environment in Health and Disease" (2021). *Theses & Dissertations*. 521.
<https://digitalcommons.unmc.edu/etd/521>

This Dissertation is brought to you for free and open access by the Graduate Studies at DigitalCommons@UNMC. It has been accepted for inclusion in Theses & Dissertations by an authorized administrator of DigitalCommons@UNMC. For more information, please contact digitalcommons@unmc.edu.

**Neural Oscillatory Activity Serving Sensorimotor Control is Regulated by
the Mitochondrial Redox Environment in Health and Disease**

by

Rachel K. Spooner

A DISSERTATION

Presented to the Faculty of
The Graduate College at the University of Nebraska
In Partial Fulfillment of Requirements
For the Degree of Doctor of Philosophy

Interdisciplinary Graduate Program in Biomedical Sciences
(Neuroscience)

Under the Supervision of Dr. Tony W. Wilson

University of Nebraska Medical Center
Omaha, Nebraska

March, 2021

Supervisory Committee:

Janelle Beadle, Ph.D.
Elizabeth Heinrichs-Graham, Ph.D.
Max J. Kurz, Ph.D.
David E. Warren, Ph.D.
Matthew C. Zimmerman, Ph.D.

ACKNOWLEDGMENTS

First, I would like to thank my mentor, Dr. Tony W. Wilson, who has supported my development as a scientist and my research progress over the last five years. My successes as a student and my completion of a project of this caliber that integrates data across multiple scientific disciplines would not be without his endless support of new ideas and innovative techniques, his encouragement of collaboration to develop and broaden our expertise, and his unmatched involvement in all aspects of his student's scientific and academic career development. From the beginning, he has created a welcoming environment where students can feel comfortable expressing their ideas and pursuing their research interests with the guidance and support of the laboratory and for that I am truly grateful. I would also like to thank my fellow graduate students and the research staff who have not only advanced science within the lab, but who have also provided friendship during a pivotal time in my life. This includes Christine Embury, Brandon Lew, Yasra Arif, Abraham Killanin, Chloe Meehan, Mikki Schantell, Seth Springer, Dr. Brittany Taylor, Marie McCusker, Maddie Fung, Chloe Casagrande, Nick Christopher-Hayes, Samantha Penhale, Lauren Ott, Emily Fitzgerald, Cosette Rhoads, Rebecca Losh, Katie Losh, Jacob Eastman, Michaela Frenzel, Hallie Johnson, Maddie Willet, Lisa Houseman, Nichole Knott, Melissa Welch-Lazoritz, as well as previous members including Dr. Amy Proskovec, Dr. Alex Wiesman, Boman Groff, Sam Koshy, Abril Rangel-Pacheco, Josylnn Hoburg, Michael Rezich, Mackenzie Mills, Tim McDermott and Nathan Coolidge.

I want to give special thanks to Drs. Elizabeth Heinrichs-Graham, Amy Proskovec and Alex Wiesman for their guidance and support over the last five years, as they were prior students in the lab who were integral to my training and development. I would like to give special thanks to Christine Embury and Brandon Lew, as their graduate training directly paralleled my own, which allowed us each to learn and grow together. In addition, this project would not have been possible

without the expertise of Dr. Brittany Taylor, who taught me the advanced statistical modeling approaches that helped illuminate the findings in this document and will motivate future studies. Further, I am greatly appreciative of the support of my collaborators including Drs. Matthew Zimmerman, Iman Ahmad, Adam Case, Howard Fox, Kelly Stauch, Susan Swindells, Sara Bares, Jennifer O'Neill, Mauren Kubat, Pamela May, Max Kurz, David Warren and Janelle Beadle, all of whom have guided my development as a student and future scientist. I also want to express gratitude towards my early experiences in undergraduate under the mentorship of Drs. Ashley Scolaro, Paulina Mena and Nicole Palenske.

Most importantly, I would like to thank my loved ones including my parents Greg and Steph Spooner, as well as Dan and Carol Davis, Ron and Sherrie Spooner, Tiffany Nguyen, Melanie Breza and Nathan Coolidge, for their endless support and belief in me throughout all stages of my life. Finally, I would like to dedicate this dissertation to my grandfather, Dan Davis. He has and will continue to be the inspiration for the work that I do and the passion I have for continuing scientific discovery and progress in clinical disease.

This research was supported by grants to my advisor, Tony W. Wilson from the National Institutes of Mental Health (R01-MH116782, R01-MH118013, RF1-MH117032), the National Institutes on Drug Abuse (R01-DA047828), and the National Science Foundation (#1539067). In addition, my training was supported by a T32 National Institutes of Neurological Disorders and Stroke Institutional Research Training Grant (T32-NS105594) and supplemented by research awards from the NASA Nebraska Space Grant Fellowship, the Cognitive Neuroscience of Development and Aging (CoNDA) Center Mini-grant, and the Office of Graduate Studies at the University of Nebraska Medical Center. This work was also supported by a travel award from the National Institutes of Health BRAIN Initiative Investigator's Meeting. In addition, this research was supported by program grants to my collaborators from the National Institutes of Health (P30-

MH062261 to Howard S. Fox; P30-GM103335 to Matthew C. Zimmerman and the EPR Spectroscopy Core). Finally, I would like to thank all the volunteers who completed this study.

ABSTRACT

Despite effective regimens of combination antiretroviral therapy, individuals with HIV are still at higher risk for developing forms of cognitive impairment, with one of the most common behavioral abnormalities to manifest being motor dysfunction. This is an important consideration, as deficits in motor control likely contribute to higher-order cognitive impairments, which together, lead to functional dependencies in the ever-growing aging population of HIV-infected adults. While the neuroanatomical bases of motor dysfunction have recently been illuminated in people living with HIV (PLWH), there remains an open question regarding the molecular processes supporting the circuit-level neuronal dynamics that potentially serve these behavioral aberrations. One theorized contributor to neurocognitive variability is a mitochondrial-induced redox imbalance of the system, although their direct impact on *human* neurophysiological function is unknown. Herein, we used state-of-the-art systems biology and neuroscience approaches including peripheral measures of mitochondrial respiration and superoxide concentration using Seahorse Analyzer and Electron Paramagnetic Resonance Spectroscopy, respectively, as well as antioxidant activity assays and magnetoencephalography to directly quantify spatially- and spectrally-distinct neural oscillatory dynamics serving motor function in a large sample of virally-suppressed PLWH and demographically-matched controls. First, we characterize aberrations in mitochondrial function and the redox environment in PLWH compared to their seronegative counterparts (Chapter 1) and determine their role in modulating movement-related beta oscillations and behavioral performance, sequentially, in the healthy system (Chapter 2). Next, we examine the divergent predictive capacities of the mitochondrial redox environment on sensorimotor brain-behavior dynamics in PLWH (Chapter 3). Finally, we interrogate the contribution of important HIV clinical risk factors and demographics for modulating bioenergetic-neural-behavioral pathways in the sensorimotor system of PLWH (Chapter 4). These findings

provide novel mechanistic insight regarding redox-regulated neuronal dynamics in health and disease and importantly, highlight the precursors that may serve as effective targets to ameliorate age- and disease-related declines in cognitive-motor function in the future.

TABLE OF CONTENTS

ACKNOWLEDGEMENTS	ii
ABSTRACT	v
LIST OF FIGURES	viii
LIST OF TABLES	ix
LIST OF ABBREVIATIONS	x
INTRODUCTION	1
Neurocognitive Impairment in People Living with HIV	1
Neural Substrates of Motor Dysfunction in PLWH	2
An Oscillatory Perspective to Motor Control	3
Redox Biology, Mitochondrial Energetics and neuroHIV	6
Goals of the Current Studies	8
CHAPTER 1: MITOCHONDRIAL FUNCTION AND REDOX STATUS IN PEOPLE LIVING WITH HIV	10
Introduction:	10
Methods:	12
Results:	15
Discussion:	18
CHAPTER 2: NEURAL OSCILLATORY DYNAMICS SERVING HEALTHY SENSORIMOTOR CONTROL ARE REGULATED BY THE MITOCHONDRIAL REDOX ENVIRONMENT	24
Introduction:	24
Methods:	26
Results:	32
Discussion:	38
CHAPTER 3: SUPEROXIDE-SENSITIVE REDOX ENVIRONMENTS DIFFERENTIALLY PREDICT SENSORIMOTOR BRAIN-BEHAVIOR DYNAMICS IN PEOPLE LIVING WITH HIV	44
Introduction:	44
Methods:	47
Results:	52
Discussion:	60
CHAPTER 4: CLINICAL MARKERS OF HIV PREDICT REDOX-REGULATED NEURAL AND BEHAVIORAL FUNCTION IN THE SENSORIMOTOR SYSTEM	65
Introduction:	65
Methods:	67
Results:	73
Discussion:	80
CONCLUSIONS	85
BIBLIOGRAPHY	91

LIST OF FIGURES

Figure 1. Mitochondrial Energetics Disrupted in PLWH	15
Figure 2. Evaluation of Superoxide-Sensitive Features of the Redox Environment in PLWH	16
Figure 3. H ₂ O ₂ -sensitive Features of the Redox Environment in PLWH	17
Figure 4. Mitochondrial Respiration Predicts the Redox Environment in PLWH	18
Figure 5. Motor Sequence Paradigm	27
Figure 6. Movement-related Oscillations at the Sensor and Source Level	33
Figure 7. Superoxide-sensitive Mitochondrial Redox Environments Modulate Neural Oscillations Serving Motor Function	35
Figure 8. H ₂ O ₂ -sensitive Redox Features Do Not Predict Movement-related Brain-Behavior Relationships	37
Figure 9. Sensor- and Anatomical-Space Movement-related Oscillations in PLWH and Uninfected Controls	54
Figure 10. Superoxide-sensitive Parameters Differentially Modulate Sensorimotor Performance in PLWH	55
Figure 11. H ₂ O ₂ -pertinent Antioxidants Differentially Predict Sensorimotor Brain-Behavior in PLWH	59
Figure 12. Sensor- and Source-Level Oscillatory Responses to Movement in PLWH	74
Figure 13. HIV-relevant Clinical Markers Predict Superoxide-sensitive Redox Environments in PLWH	76
Figure 14. Levels of SOD Activity and Reaction Time Fully Mediated the HIV-related Alterations in Movement Duration	78
Figure 15. HIV-relevant Clinical Markers Do Not Predict H ₂ O ₂ -Sensitive Redox Environments in PLWH	79

LIST OF TABLES

Table 1. Participant Demographics and Clinical Metrics	12
Table 2. Results of the Mediation Analyses of Mitochondrial Function on Brain-Behavior through Superoxide-Pertinent Redox Parameters	36
Table 3. Results of the Group-based Superoxide-Sensitive Mediation Analyses using Structural Equation Modeling	57
Table 4. HIV-infected Participant Demographics and Clinical Metrics	68

LIST OF ABBREVIATIONS

AD	Alzheimer's disease
ALS	Amyotrophic lateral sclerosis
cART	Combination antiretroviral therapy
CMH	1-hydroxy-3-methoxycarbonyl1-2,2,5,5-tetramethylpyrrolidine
CNS	Central nervous system
EEG	Electroencephalography
EPR	Electron paramagnetic resonance
ETC	Electron transport chain
FCCP	1 μ M fluoro-carbonyl cyanide phenylhydrazone
fMRI	Functional magnetic resonance imaging
GABA	Gamma-aminobutyric acid
GSH	Reduced glutathione
GSSG	Oxidized glutathione
GSSG/tGSH	Glutathione reducing capacity
H ₂ O ₂	Hydrogen peroxide
HAD	HIV-associated dementia
HAND	HIV-associated neurocognitive disorder
HDMS	HIV Dementia Motor Scale
HIV	Human immunodeficiency virus
M1	Primary motor cortices
MCMD	HIV-associated mild cognitive-motor disorder
MEG	Magnetoencephalography
MFRTA	Mitochondrial free radical theory of aging
MPP+	1-methyl-4-phenylpyridinium
MPTP	1-Methy-4-phenyl-1,2,3,6-tetrahydropyridine
Non-Mt	Non-mitochondrial linked respiration
NOX	NADPH oxidase enzymes
OCR	Oxygen consumption rate
PBMC	Peripheral blood mononuclear cells
PD	Parkinson's disease
PLWH	People living with HIV
ROI	Region of interest
ROS	Reactive oxygen species
rot/AA	14 μ M rotenone + 14 μ M antimycin A
S1	Primary somatosensory cortices
SMA	Supplementary motor areas
sMRI	Structural magnetic resonance imaging
SOD	Superoxide dismutase
SRC	Spare respiratory capacity
tGSH	Total glutathione
UPDRS	Unified Parkinson's Disease Rating Scale

INTRODUCTION

Neurocognitive Impairment in People Living with HIV:

The widespread use of combination antiretroviral therapy (cART) has made HIV-infection a chronic, but manageable condition, with life expectancies now approaching those seen in the seronegative population. However, increased longevity often coincides with a host of age-related comorbidities including neurocognitive impairment. While effective regimens of cART have dramatically decreased the prevalence of HIV-associated dementia (HAD), the risk for developing mild to moderate forms of cognitive impairment (i.e., HIV-associated neurocognitive disorder: HAND) remains a major concern in approximately 35-70% of all people living with HIV (PLWH) (1–8). In addition to aging, this functional decline may be attributable, at least in part, to the imperfect delivery of anti-HIV drugs to the central nervous system (CNS), which likely enables ongoing viral replication and the downstream release of inflammatory cytokines that disrupt neuronal processing and behavior, sequentially (9). Nevertheless, patients with HAND are more likely to be unemployed, have poorer medication adherence, and have lower quality of life than their unimpaired or seronegative counterparts (10–15), making the study of neurocognitive dysfunction in PLWH particularly important.

The cognitive symptoms present in HIV-infected adults span across numerous functional domains including attention, memory and executive functioning to name a few (1, 16, 17). However, one of the first and most common behavioral abnormalities that manifests is that of motor dysfunction (18–23). This is further supported when considering the original nomenclature for mild to moderate forms of HAND, which included a condition termed HIV-associated mild cognitive-motor disorder (MCMD) (1, 18). To date, several assessments are used to characterize the degree of motor dysfunction in PLWH including the Unified Parkinson's Disease Rating Scale (UPDRS), HIV Dementia Motor Scale (HDMS/HMS), and traditional neuropsychological batteries

(e.g., Grooved Pegboard Test). Broadly, these assessments demonstrate that both cART-treated and treatment-naïve PLWH exhibit discrete disruptions in motor processing including deficits in gait, coordination and motor dexterity, as well as the slowing of gross hand movements and action tremors (19–22). Unlike some of the cognitive symptoms that have remained stable following the initiation of cART, motor deficits have been shown to steadily decline over time (20), are exaggerated by the aging process (19), and are accentuated in those with comorbidities (e.g., cerebrovascular disease) or who have poorer baseline cognitive abilities (20, 21). Thus, thorough evaluation of the mechanisms underlying motor dysfunction in the modern cART era is critical for understanding neurocognitive impairment in HIV, as deficits in motor control contribute to non-motor symptoms and will profoundly impact a person's functional dependence in later life.

Neural Substrates of Motor Dysfunction in PLWH:

HIV-infection is associated with numerous structural and functional neural changes in regions pertinent to sensorimotor processing and behavioral control. For example, studies using structural magnetic resonance imaging (sMRI) have demonstrated atrophy in an extended cortical and subcortical network including the basal ganglia, frontoparietal regions, primary motor and somatosensory cortices (M1 and S1, respectively) and the cerebellum (24–27). Importantly, these distributed patterns of atrophy have often been associated with neurocognitive and motor deficits (e.g., reduced psychomotor speed, gross motor dysfunction, increased global deficit scores (27–30)) and further, are tightly linked to HIV clinical risk factors such as CD4 nadir (i.e., lowest lifetime CD4+ T-cell count), time since diagnosis, delay in cART initiation, and plasma HIV RNA levels (24, 25, 27, 28, 31). For instance, CD4+ T-cells are important qualifiers for immune system stability, with levels dramatically depleting immediately upon infection with HIV and gradually increasing with viral suppression (32, 33). Not only have lower levels of CD4+ T-cells (i.e., worse immune system integrity) been associated with cortical thinning and subcortical volume

loss, but they are also predictive of accelerated aging phenotypes (e.g., DNA methylation) and behavioral deficits in PLWH (28, 34–39). However, despite this relationship to HIV disease status, some studies suggest that brain atrophy metrics may not be enough to effectively distinguish those with and without functional impairment in PLWH (26, 29, 40), emphasizing the need for other neural markers that may better index neurocognitive and motor decline in PLWH.

In contrast, studies of brain *function* have primarily used functional MRI (fMRI) to study neural networks in PLWH. Broadly, these studies suggest that PLWH exhibit reduced degrees of activation in primary sensory cortices (e.g., visual cortex), with greater degrees of activation present in association cortices (e.g., prefrontal and parietal) to support more difficult task performance (41–46), albeit the evaluation of motor cortical networks during behavior is less well characterized. Interestingly, a few prior ROI-based studies of motor function suggest that fMRI signal characteristics (e.g., amplitude, temporal evolution) were not different between PLWH compared to uninfected controls during movement tasks (47, 48). However, when considering cognitive ability and cART regimens, differences in these metrics emerged, with greater change in those who were impaired and those on cART regimens with low-CNS penetrance (47, 48). While these structural and functional studies have made progress in characterizing the neuroanatomical origins supporting sensorimotor processing in PLWH, there remains a substantial gap in our knowledge regarding the circuit-level neuronal dynamics that serve sensorimotor processing and behavioral performance as it evolves on the millisecond timescale.

An Oscillatory Perspective to Motor Control:

Volitional motor control requires desired movement kinematics to be transformed into discrete plans to successfully execute and terminate motor actions. After repeated exposure to a particular action or movement sequence, an internal model is generated within the sensorimotor system, and this is continuously and adaptively updated to fulfill task demands (49–52). Such

motor control requires a coordinated ensemble of population-level neural oscillatory activity during distinct phases of the movement (i.e., planning, execution and termination). Briefly, recent neurophysiological studies of movement-related neural oscillations have used magnetoencephalography (MEG), which is a noninvasive imaging method that measures the minute magnetic fields (10^{-15} T) that naturally emanate from the brain using a whole-head sensor array. Importantly, because magnetic fields are not susceptible to attenuation by intervening tissues (e.g., skull, scalp, cerebrospinal fluid) like the electrical activity recorded using electroencephalography (EEG), MEG is afforded good spatial precision (~ 3 -5 mm) that is accompanied by unmatched temporal resolution (millisecond level), making it a superior neuroimaging method to measure the dynamic interactions among spatially- and spectrally-defined neuronal populations directly (53).

During movement, sustained decreases in oscillatory alpha (e.g., 8-12 Hz) and beta (e.g., 15-30 Hz) activity are evident prior to and during motor execution (e.g., -1000 to 500 ms surrounding movement), and are thought to reflect the active engagement of the motor network including hubs in bilateral M1, SMA, parietal cortices and S1 (54–57). Interestingly, peri-movement oscillations in the beta range have been shown to be especially pertinent to higher-order planning and movement selection factors, as characteristics of beta responses (e.g., amplitude, connectivity) within this network have been shown to scale linearly with the certainty of the action to be performed (54, 55, 57–59), the complexity of the movement (60), and the degree of response interference (61–63), and critically, are intimately tied to task performance. Thus, the study of movement-related oscillatory dynamics within the beta range may be critical for uncovering divergent mechanisms of behavioral modification in health and disease.

In addition to peri-movement alpha and beta neural responses, there is a robust increase in M1 beta activity that follows motor execution termed the post-movement beta rebound

(PMBR). While the PMBR may simply reflect the motor cortex returning to idling beta levels, this response has also been linked to the active inhibition of motor cortical neurons and/or somatosensory reafference to the motor cortex (64–68). Lastly, motor control is also known to involve transient increases in lower and higher frequency oscillations in the theta (e.g., 4-8 Hz) and gamma (e.g., 60-90 Hz) bands during movement onset, respectively. While the precise role of M1 theta and gamma power is unclear, these responses may serve as temporal coordinators (69, 70) and robust execution signals for motor action (56, 71–73), albeit recent evidence suggests that these responses may also be modulated by increased cognitive demand including multiple sources of interference and the reorienting of attention (61–63, 74, 75).

In regard to HIV-infection, only two prior studies have examined motor cortical oscillations during movement and at rest. For instance, a study by Wilson and colleagues used a pseudo-paced finger tapping paradigm during MEG and observed robust peri-movement decreases in beta oscillations in the bilateral M1 and SMA in PLWH and healthy controls (76). However, PLWH exhibited significantly weaker beta responses in these regions compared to uninfected controls, while increases in beta power were observed in the frontal cortices of HIV-infected adults (76). This pattern of findings aligns well with prior fMRI studies that suggest that PLWH exhibit hypoactivation in primary sensory regions during basic sensory tasks (e.g., visual stimulation task), and hyperactivation in association cortices to fulfill more cognitively demanding task goals (41–44). Interestingly, the study by Wilson et al., demonstrated these patterns of hypo- and hyperactivation in concert during finger tapping, which may reflect a compensatory recruitment of prefrontal cortices to overcome neural inefficiencies in the primary motor network of PLWH. In a second study, Becker et al., evaluated network-level oscillatory dynamics during rest and importantly, observed robust reductions in beta power in bilateral superior parietal regions, left SMA, and the paracentral lobule of older PLWH compared to age-matched uninfected

controls (77). Additionally, reductions in sensorimotor beta responses were related to the degree of neuropsychological impairment in HIV-infected adults. Taken together, these studies, and the aforementioned studies of normative motor control, provide substantial support for the role of neural oscillations in sensorimotor processing and motor function and further, illuminate the potential utility of MEG as a future test for characterizing neurocognitive and motor impairments in PLWH. However, the origin of these disease-related changes in neural dynamics serving motor function are not known, nor are the factors influencing the magnitude of impairment in PLWH.

Redox Biology, Mitochondrial Energetics and neuroHIV:

Mitochondrial integrity and associated redox interactions in concert are one of the well-theorized contributors to the neural and behavioral viability observed in health and disease (78–83). Under normal physiological conditions, the mitochondria serve as primary producers of cellular energy and oxygen consumption in the system, which is concomitant with circulating redox parameters (e.g., reactive oxygen species (ROS), enzymatic and non-enzymatic antioxidants) that are essential for downstream signaling mechanisms, giving rise to a host of normative cellular processes (e.g., inflammation) (83–86). In regard to the brain, neuronal function (e.g., synaptic vesicle pool development, neurotransmitter release) is known to be regulated by mitochondria through various mechanisms including changes in mitochondrial morphology, motility, oxygen consumption, ATP generation and more (82, 87, 88), however its role in *human* neurophysiology is unknown. Further, the generation of ROS (e.g., superoxide and hydrogen peroxide (H_2O_2)), concomitant with attenuations in their antioxidant defenses (e.g., superoxide dismutase (SOD), catalase, glutathione) may also contribute to functional aberrations in brain and behavior (89, 90), and further, this phenomenon is known as a mitochondrial-induced redox imbalance in the system (79).

Interestingly, one of the first demonstrations of the role of the mitochondrial redox environment in brain and behavioral function involved the motor system. For example, early models of oxidative damage and neurodegeneration targeted depletions to important antioxidant scavengers (i.e., SOD) to mimic amyotrophic lateral sclerosis (ALS). Essentially, gene mutations in the cytosolic form of SOD leads to dramatic reductions in SOD activity levels, which in turn, results in increased levels of ROS that give rise to the progressive atrophy and functional dependencies seen in motor neuron diseases (91, 92). In addition, the aging process has been associated with depleted levels of SOD, greater ROS production and functional decline in the sensorimotor domain (e.g., increased tail flick latency, reduced exploration time) (93–95). Finally, the 1-Methyl-4-phenyl-1,2,3,6-tetrahydropyridine (MPTP) model of Parkinson's disease (PD) serves as one of the best examples of the role of mitochondrial dysfunction in sensorimotor aberrations (82, 96–98). Briefly, upon crossing the blood brain barrier, MPTP is rapidly converted to 1-methyl-4-phenylpyridinium (MPP⁺), which is the neurotoxin that accumulates in the mitochondrial matrix of dopaminergic neurons. This accumulation effectively shuts down mitochondrial respiration via inhibition of Complex I in the electron transport chain (ETC), which in turn, results in the generation of superoxide and the impaired production of ATP, leading to the death of dopaminergic cells and subsequent symptom profiles observed in animal models of PD (96). *En masse*, these studies provide substantial support for the role of mitochondrial energetics and redox profiles in animal sensorimotor processing and behavior, making the evaluation of these constructs in human neurophysiology an attractive avenue of investigation.

Regarding neuroHIV, there is currently a lack of literature linking mitochondrial and redox parameters to brain and behavioral function in HIV-infected adults, albeit there is some work characterizing these profiles in the context of their chronic immunocompromised states. For example, during acute responses to infections or pathogens, the mitochondria experience a shift

in functionality as primary producers of cellular energy to purposeful generators of ROS through elevations in oxygen consumption to elicit the appropriate immune response and promote inflammation (84–86, 99). This is particularly important when considering those who are chronically immunocompromised, as persistent inflammation despite effective virologic suppression in the modern cART era is thought to be a key contributor to neurocognitive impairment in PLWH (100). In contrast to acute infection, PLWH tend to exhibit decrements in oxygen consumption and spare respiratory capacity (SRC) of the mitochondria, reflecting a decreased energetic reserve available to meet changing energy demands and subsequent increased ROS production in the periphery (101). Importantly, these data, combined with the well-established literature implicating mitochondrial functionality and redox profiles to a host of age- and disease-related comorbidities (79–81, 102, 103), suggest that the analysis of mitochondrial redox environments may provide novel mechanistic insight into the neural and motor dysfunction observed PLWH.

Goals of the Current Studies:

The goals of the current studies are to fill the knowledge gaps regarding the molecular and neural mechanisms underlying motor dysfunction in virally-suppressed PLWH using advanced systems biology and neurophysiology techniques. Specifically, we aim to comprehensively quantify features of mitochondrial respiration and redox profiles sensitive to superoxide and H_2O_2 in a large sample of seropositive adults with virologic suppression (Chapter 1). In addition, we aim to assess the predictive capacity of these parameters on the spatiotemporally-precise neural oscillations that underly motor planning and execution and subsequent behavioral performance in health and disease (Chapters 2 and 3) and finally, to interrogate the influence of key clinical and demographic risk factors on the extant bioenergetic-neural-behavioral pathways serving sensorimotor function in PLWH (Chapter 4). As a result of these studies, we can expect to gain a

better understanding of the functional role of the mitochondrial redox environment in the context of *human* neurophysiology and behavior for the first time. Furthermore, the molecular precursors (i.e., blood-based measures of mitochondrial respiration and redox status) as evaluated in the current studies will profoundly influence future work in clinical populations who also present with symptoms of motor dysfunction and neurocognitive decline (e.g., Parkinson's disease, Alzheimer's disease), as the development of peripheral, less-invasive markers of disease progression (i.e., neurophysiological aberrations and behavioral decline) will be of utmost importance to potentially drive diagnostic accuracy and clinical distinction in the future.

CHAPTER 1. MITOCHONDRIAL FUNCTION AND REDOX STATUS IN PEOPLE LIVING WITH HIV

Introduction:

While combination antiretroviral therapy (cART) has dramatically decreased the prevalence of HIV-associated dementia, 35-70% of all people living with HIV (PLWH) still develop some form of cognitive impairment. Importantly, the prevalence of cognitive dysfunction has remained the same or increased during the era of cART (1–8), and with PLWH living longer than ever before and often exhibiting premature or accelerated aging phenotypes (34, 104, 105), the study of the mechanisms contributing to HIV-related cognitive and behavioral dysfunction is of particular importance.

One well-theorized contributor to disease- and age-related cognitive decline is a mitochondrial-induced redox imbalance in the system (e.g., mitochondrial free radical theory of aging: MFRTA) (79–81). Broadly, theories like MFRTA suggest that aging and disease phenotypes are the result of free radical-induced damage to the cell, namely due to changes in mitochondrial structure and function. Specifically, this damage typically involves both the accumulation of reactive oxygen species (ROS) and the attenuation of antioxidant defense mechanisms leading to systemic redox imbalance (80, 81, 106). Additionally, these alterations in the mitochondrial redox environment are not only tied to nervous system functionality (78, 82, 87, 88, 107, 108) but may also be concomitant with declines in behavioral performance (90–95), however this link has only been previously established in animal models. Furthermore, discrete alterations to mitochondrial function and associated redox profiles are essential to effectively carry out the immune system's response to invading pathogens and infections (84–86, 99), making mitochondrial redox biology an attractive avenue for probing functional dependencies induced by chronic immune dysregulation as seen in HIV.

In regard to HIV-infection, only a few studies have evaluated changes in the mitochondrial redox environment in response to these chronic immunocompromised states, especially in the context of human physiology. In contrast to acute immune system activation where increases in mitochondrial-produced energy, oxygen consumption and ROS are initiated to propagate the appropriate immune response, mitochondrial respiration (i.e., oxygen consumption rate: OCR) seems to decrease, such that seropositive adults exhibit discrete decreases in basal and maximal OCR, leading to reduced spare respiratory capacity (SRC; i.e., the cell's adaptability to changing energy demands), concomitant with increased ROS production in the periphery (101). However, these results should be considered with caution, as these studies included adults with and without cART-induced viral suppression, and cART has been shown to directly impact cellular respiratory and redox profiles, regardless of HIV exposure (109, 110). Importantly, these data, combined with the well-established literature linking mitochondrial functionality and redox interactions (e.g., ROS and antioxidant defense mechanisms) to a host of age- and disease-related comorbidities (81, 102, 103), suggest that analysis of mitochondrial function and redox environment may provide novel mechanistic insight into the neural and behavioral dysfunction that persists despite effective viral suppression in PLWH.

Thus, the goal of the current study was to comprehensively quantify features of mitochondrial function and the redox environment, and to assess the interaction amongst these parameters in PLWH versus uninfected controls using structural equation modeling. To this end, we recruited 40 PLWH with virologic suppression who were on a stable regimen of cART and 40 demographically-matched uninfected controls. Unlike previous studies using qualitative or indirect measures of the redox environment (e.g., fluorescence), we used state-of-the-art systems biology approaches to directly quantify mitochondrial respiration in real time using Seahorse Analyzer, total intracellular superoxide levels using Electron Paramagnetic Resonance (EPR)

Spectroscopy, and commercially-available enzymatic and non-enzymatic antioxidant activity assays. We hypothesized that oxygen consumption rates of mitochondria would be reduced in PLWH, resulting in a less efficient bioenergetic capacity which would be concomitant with elevated levels of superoxide and attenuated antioxidant defenses (e.g., superoxide dismutase, catalase, glutathione), indicative of a redox imbalance in the system. In addition, we hypothesized that mitochondrial respiratory parameters disrupted in PLWH would differentially predict superoxide- and hydrogen peroxide (H₂O₂)-pertinent redox profiles in PLWH versus uninfected controls.

Methods:

Participant Demographics

Eighty adults (range: 20-66 years old; 40 PLWH and 40 controls) were enrolled. All PLWH were receiving effective cART and had viral suppression defined as <50 copies/mL. Exclusion criteria included any medical illness affecting CNS function (other than HIV), any psychiatric or neurological disorder, history of head trauma, current pregnancy and current substance use. Uninfected controls were enrolled to demographically match PLWH based on their age ($p = .857$), sex ($p = .095$), handedness ($p = .999$) and body mass index (BMI: $p = .267$) (for a comprehensive list, see Table 1). The University of Nebraska Medical Center Institutional Review Board approved the study and all participants provided written informed consent.

Demographics (Mean \pm SD)	Controls	PLWH
N	40	40
Age (yrs)	45.1 \pm 13.9	44.5 \pm 13.8
Sex (% males)	57.5	77.5
Handedness (% right handed)	92.5	90.0
Education (yrs)	15.9 \pm 2.2	13.6 \pm 2.7
BMI	27.9 \pm 5.6	29.3 \pm 6.0
CD4 Nadir (cells/ μ L)	--	282 \pm 232
Current CD4 (cells/ μ L)	--	768 \pm 322
Time since diagnosis (yrs)	--	12.8 \pm 9.1
Time on ART (yrs)	--	10.1 \pm 7.1
Exposure Time (yrs)	--	2.9 \pm 5.3

Table 1. Participant Demographics and Clinical Metrics.

Isolation of Peripheral Blood Mononuclear Cells and Respiration Analysis

Whole blood (~45 mL) was collected into EDTA tubes by venous puncture for all participants. Buffy coats were submitted to a Ficoll-Paque Plus (GE Healthcare) gradient centrifugation for isolation of the mononuclear fraction. Peripheral blood mononuclear cells (PBMC) were cryopreserved in Fetal Bovine Serum with 10% DMSO. Cells were thawed within 6 weeks of isolation and underwent assessment using the Seahorse XF96 Analyzer (Seahorse Bioscience) to quantify oxygen consumption rate (OCR) using the mitochondrial stress test assay. Specifically, PBMCs were plated at 500,000 cells/well and 3 OCR measurements were taken sequentially on 5-6 technical replicate wells prior to and upon serial injection of 3.5 μ M oligomycin (Sigma; complex V inhibitor), 1 μ M fluoro-carbonyl cyanide phenylhydrazone (FCCP; Sigma; mitochondrial oxidative phosphorylation uncoupler) and 14 μ M rotenone + 14 μ M antimycin A (Sigma; complex I and III inhibitors, respectively) to evaluate measures of mitochondrial respiration including basal respiration, ATP-linked respiration, proton leak, maximal respiration, spare respiratory capacity (SRC) and non-mitochondrial respiration. All bioenergetic data were normalized to protein in the well for subsequent analyses. For data calculation, the Seahorse Wave software (v2.2.0) was used.

Quantification of the Redox Environment

Cellular levels of superoxide were assessed using Electron Paramagnetic Resonance (EPR) Spectroscopy of whole blood incubated with a superoxide-sensitive spin probe (1-hydroxy-3-methoxycarbonyl-1,2,2,5,5-tetramethylpyrrolidine: CMH) for 1 hour under physiologic conditions (37°C), as previously described (111). Specifically, immediately after sample collection, 200 μ M of CMH was reconstituted into EPR buffer (Krebs Hepes Buffer) supplemented with metal chelators (5 μ M sodium diethyldithiocarbamate trihydrate and 25 μ M deferoxamine) and incubated with 200 μ L of whole blood. EPR measurements were performed with a Bruker eScan EPR

spectrometer (Bruker BioSpin GmbH, Rheinstetten/Karlsruhe, Germany), with the following parameters: field sweep width, 100.0 G; center field, 3482 G; microwave frequency, 9.75 kHz; microwave power, 1.10 mW; modulation amplitude, 5.94 G; conversion time, 10.24 ms; time constant, 40.96 ms. The resulting EPR spectra amplitude is expressed as arbitrary units (a.u.) that are directly proportional to the amount of total cellular superoxide in the sample.

Antioxidant activity levels were quantified in erythrocytes for key enzymatic and non-enzymatic contributors to the mitochondrial redox environment including superoxide dismutase (SOD), catalase, and glutathione. Specifically, we used the SOD Assay Kit-WST (DOJINDO, Inc.) to measure total SOD activity, the OxiSelect Catalase Activity Assay Kit (Cell Biolabs, Inc.) for catalase, and the GSSG/GSH Quantification kit (DOJINDO, Inc.) for total (tGSH), oxidized (GSSG) and reduced glutathione (GSH) according to the manufacturers' guidelines.

Statistical Analysis

To evaluate HIV-related changes in mitochondrial redox environments, relevant parameters of mitochondrial function (e.g., basal respiration) and the redox environment (e.g., superoxide levels) underwent independent samples t-tests following standard data evaluation procedures. Briefly, measures that exceeded 2.5 standard deviations above or below the group's mean were excluded from subsequent analyses. Next, we evaluated assumptions of equal variance using the Levene's test ($p < .05$) and conducted independent samples t-tests (one-tailed) on these mitochondrial redox parameters as function of HIV-infection assuming non-equal variance where appropriate. All group-wise comparisons were conducted using IBM SPSS (v.25).

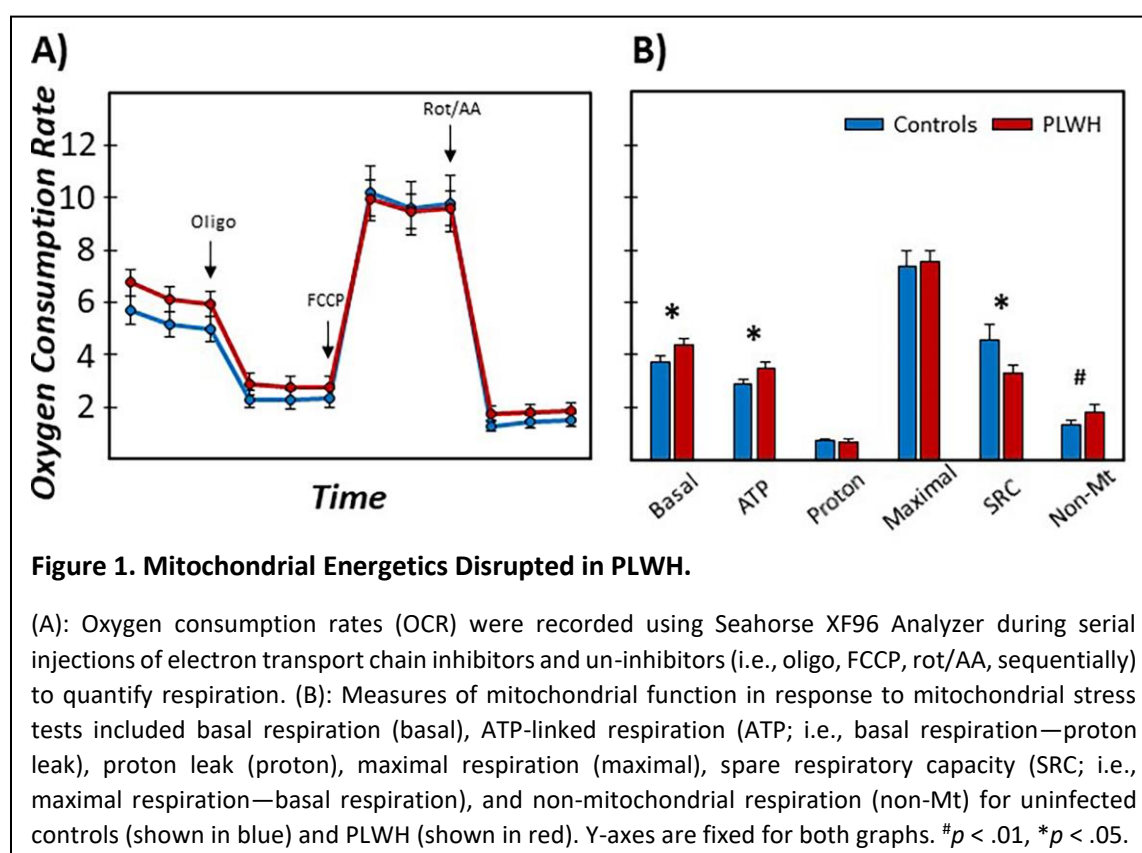
Finally, we aimed to interrogate the predictive capacity of mitochondrial respiration on the redox environment using variables that demonstrated discrete alterations as a function of HIV-infection using structural equation modeling. Specifically, we conducted a group-based path analysis with measures of mitochondrial function (i.e., spare respiratory capacity: SRC, ATP-linked

respiration and non-mitochondrial respiration) as predictors of the redox environment (i.e., superoxide, SOD, catalase, and GSSG/tGSH ratio), which yields parameter estimates for PLWH versus uninfected controls (all two-tailed *p*-values reported). Of note, we did not include measures of basal OCR in this analysis as other parameters of mitochondrial function (i.e., SRC, ATP-linked OCR) are directly dependent on levels of basal respiration and thus could lead to inaccurate model estimations. All path analyses were conducted with full information maximum likelihood estimation for missing data using MPlus (v.8.1).

Results:

Mitochondrial Respiration in PLWH

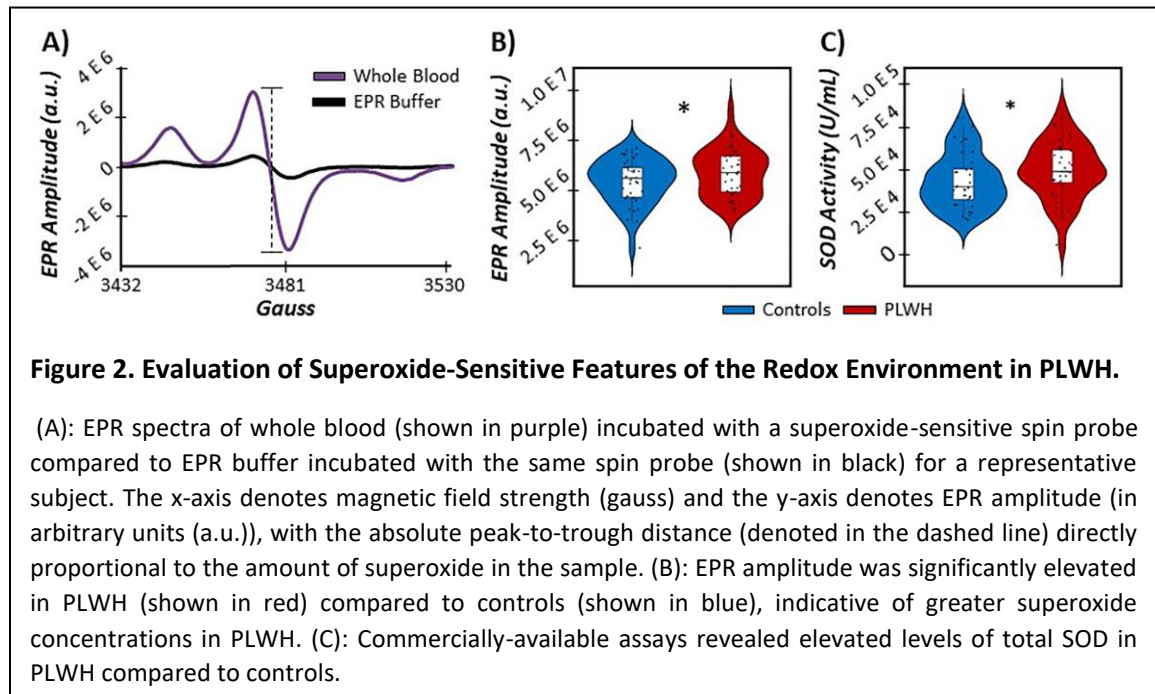
Bioenergetic data of PBMCs revealed distinct alterations in mitochondrial respiration as a function of HIV-infection (Figure 1). Interestingly, we observed significant increases in basal oxygen consumption rates (OCR; $t(74) = 2.03$, $p = .023$), ATP-linked OCR (i.e., basal respiration—



proton leak; $t(76) = 2.09$, $p = .020$) and marginally increased levels of non-mitochondrial respiration in PLWH compared to uninfected controls ($t(74) = 1.35$, $p = .090$; Figure 1). In contrast, PLWH exhibited significant reductions in the spare respiratory capacity (SRC; maximal respiration – basal respiration; $t(76) = -1.85$, $p = .034$) of the mitochondria compared to controls, suggesting that mitochondria in PLWH have an impaired adaptability when faced with increased energy demands.

Superoxide and H_2O_2 Redox Profiles in PLWH

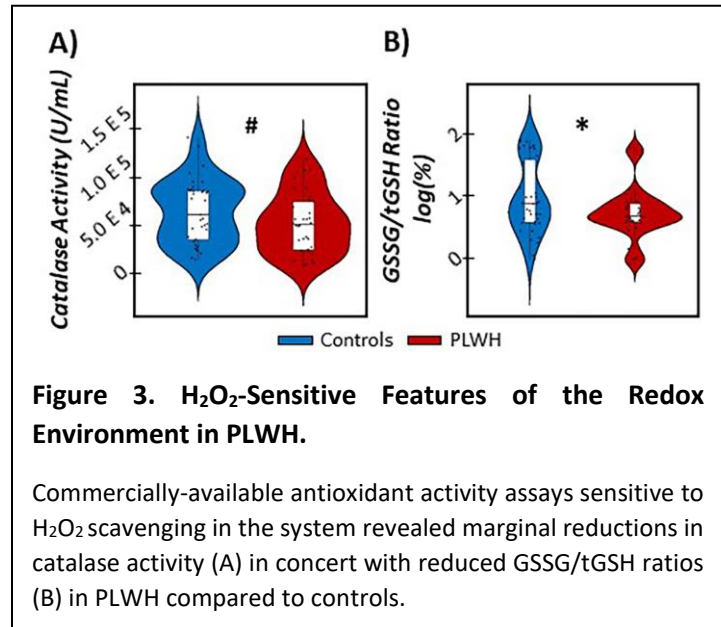
In order to comprehensively quantify the redox environment in our participants, we conducted EPR spectroscopy on whole blood incubated with a superoxide-sensitive spin probe (i.e., CMH) to evaluate total levels of cellular superoxide in the periphery. In addition,



commercially-available assays were collected on erythrocytes for key antioxidants known to scavenge ROS. In regard to superoxide-sensitive redox environments, we observed significant elevations in superoxide concentrations (i.e., EPR amplitude; $t(75) = 1.70$, $p = .047$), concomitant

with elevations in total SOD activity (i.e., the antioxidant important for scavenging superoxide; $t(74) = 1.76, p = .041$) in PLWH compared to controls (Figure 2).

In contrast, antioxidants important for scavenging H_2O_2 were differentially modulated as a function of HIV-infection (Figure 3). Specifically, we observed marginal reductions in catalase activity in PLWH ($t(71) = -1.59, p = .059$). Additionally, we assessed levels of total (tGSH), oxidized

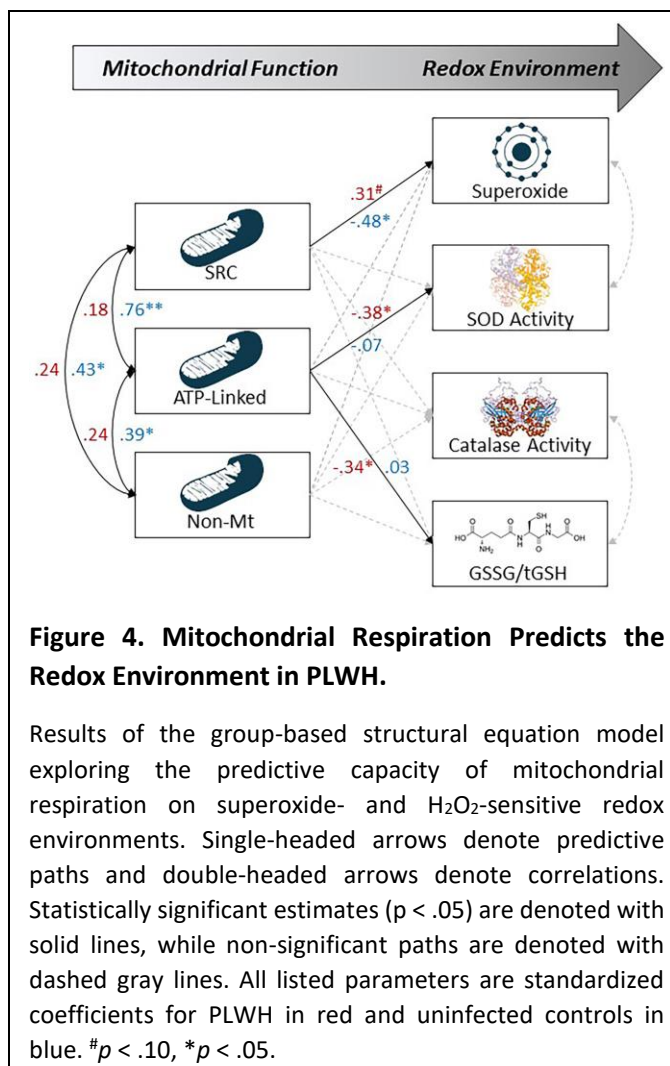


(GSSG), and reduced (GSH) forms of glutathione, and observed significant reductions in GSSG in PLWH ($t(75) = -3.03, p = .002$), while tGSH and GSH were unaffected by HIV-infection ($ps > .183$). Ultimately, this reduction in GSSG likely resulted in the significantly reduced log transformed GSSG/tGSH ratios also observed in PLWH compared to controls ($t(72) = -2.123, p = .019$), with lower values indicative of larger glutathione reducing capacities (i.e., greater ability to scavenge peroxides) in PLWH. Taken together, these results suggest that both superoxide- and H_2O_2 -sensitive redox profiles are disrupted in PLWH.

Mitochondrial Function Differentially Modulates the Redox Environment in PLWH

Finally, we evaluated the predictive capacity of mitochondrial function on superoxide-sensitive (i.e., superoxide, SOD) and H_2O_2 -sensitive (i.e., catalase, GSSG/tGSH ratio) redox parameters using variables exhibiting discrete alterations as a function of HIV-infection (Figure 4). Interestingly, mitochondrial SRC significantly predicted levels of superoxide, such that increases in SRC were predictive of decreased levels of superoxide in uninfected controls ($\beta = -.48, p = .024$),

while decreases in SRC were marginally predictive of decreased levels of superoxide in PLWH ($\beta = .31$, $p = .053$). In addition, ATP-linked respiration was predictive of superoxide- and H_2O_2 -sensitive antioxidant scavengers in PLWH, such that increases in ATP-linked OCR were associated with decreased levels of total SOD activity ($\beta = -.38$, $p = .036$) and attenuated glutathione reducing capacities ($\beta = -.34$, $p = .043$; i.e., higher GSSG/tGSH ratio). Finally, direct comparisons between the unstandardized coefficients of each



path revealed significantly different predictive capacities between PLWH and uninfected controls in the relationships among mitochondrial SRC and superoxide ($\Delta b = 0.04$, $p = .004$), suggesting a differential modulation of superoxide-sensitive redox parameters that are specific to the energetic capacity of the mitochondria (i.e., SRC), as opposed to other respiratory metrics disrupted in HIV-infection.

Discussion:

Using advanced, quantitative measurements of mitochondrial function and the redox environment, we interrogated the predictive capacity of mitochondrial respiratory profiles on superoxide- and H_2O_2 -sensitive redox parameters in a group of PLWH with viral-suppression and

uninfected controls. Specifically, we observed discrete disruptions in mitochondrial respiration, such that basal, ATP-linked and non-mitochondrial respiration were increased in concert with a marked reduction in mitochondrial energetic reserves (i.e., spare respiratory capacity) in PLWH compared to controls. In regard to the redox environment, we observed significant increases in superoxide-sensitive features, including elevated levels of superoxide and the antioxidant important for scavenging it (i.e., superoxide dismutase). In contrast, PLWH exhibited reductions in catalase and oxidized forms of glutathione, suggesting that H_2O_2 -involved pathways may also be disrupted in PLWH. Finally, our study was the first to effectively link key features of real-time mitochondrial respiration to aberrant redox profiles in our sample. We discuss the implications of these novel findings below.

Previous investigations regarding the role of mitochondria in immune system integrity suggest a preferential shift of functionality in response to foreign pathogens/infections. Amongst these changes in mitochondrial metabolism are increases in the consumption of oxygen concomitant with increases in ROS production for downstream signaling mechanisms upon T-cell activation, although the opposite directionality (i.e., decreased oxygen consumption with increased ROS) has been shown during instances of chronic infection as seen in HIV (101, 112, 113). In line with our hypotheses, we observed robust reductions in the SRC of mitochondria in PLWH, indicative of reduced bioenergetic capacities when faced with changing energy demands. Interestingly, this result was likely attributable to the *increases* in basal OCR observed in PLWH, which contradicts previous reports in humans and animals. For example, only one prior study has evaluated the dynamic changes in the OCR of immune cells in PLWH and found significant *decreases* in basal and maximal OCR, leading to impaired SRC (101), while other reports have corroborated this trajectory in animal models treated with the HIV protein gp-120 (112, 113). One factor that could contribute to this discrepancy is the cellular architecture comprising our PBMC

samples. For instance, previous work suggests that immune cells (e.g., T-lymphocytes, B-lymphocytes) have disparate respiratory profiles relating to subsequent changes in cellular activation (101). Thus, the discrepant trajectories observed in the current study could be attributable, at least in part, to the cellular composition of our PBMC samples that were not further purified into their respective cell types for subsequent respiratory analyses. Future work could use methods such as flow cytometry to directly quantify the contribution of these cellular profiles. Nevertheless, our data and previous reports suggest that immune cell mitochondrial adaptability is impaired in PLWH (i.e., reduced SRC), albeit the mechanism leading to this inefficiency may be dependent on sample characteristics.

In regard to the redox environment, we observed increases in total cellular superoxide concomitant with increased activity of the antioxidant important for scavenging it (i.e., total SOD) in PLWH compared to uninfected controls, suggesting that elevated levels of SOD activity may be a compensatory strategy employed to combat the increased levels of superoxide in PLWH (101, 114, 115). In addition, we observed differential modulations of H_2O_2 -involved scavengers, such that activity levels of catalase and oxidized glutathione were reduced in HIV-infected adults. These results were somewhat surprising, as previous studies have shown either no change or opposing trajectories of catalase and glutathione levels, indicative of an overall decrease in the reducing capacity of H_2O_2 in PLWH (114, 116, 117). Nevertheless, the diverse alterations in antioxidant defense systems observed in the current sample potentially point to a H_2O_2 -pertinent mechanism also contributing to the oxidative environment in PLWH. As the direct product of the superoxide-SOD scavenging reaction is H_2O_2 , increases in both superoxide and SOD may result in elevated levels of H_2O_2 , which aligns well with the reductions observed for the main scavenger of it (i.e., catalase) (118). However, the stronger reducing capacity of peroxides by glutathione (i.e., reduced GSSG/tGSH ratio) observed in the current study may be working to assist the catalase-deficient

scavenging of H_2O_2 . Although we did not directly quantify levels of H_2O_2 in our sample, our study is the first to provide comprehensive evidence for discrete alterations in *both* superoxide- and H_2O_2 -sensitive mitochondrial redox environments as a function of HIV-infection, and future work directly evaluating levels of H_2O_2 will be invaluable to fully unravel this relationship.

Our most important finding was likely the differential contribution of mitochondrial respiratory parameters on the redox environment in PLWH compared to uninfected controls. Briefly, we observed strong links between increased ATP-linked mitochondrial OCR and decreased SOD activity levels, as well as attenuated glutathione reducing capacities in PLWH, but not in uninfected controls. In contrast, we observed a differential modulation of intracellular superoxide levels by mitochondrial SRC in PLWH and their seronegative counterparts as evidenced by direct comparisons of unstandardized coefficients for each predictive path. Essentially, decreased levels of SRC were associated with decreased intracellular superoxide levels in HIV-infected adults, while a negative association was observed for controls. This result was somewhat surprising, as reductions in mitochondrial bioenergetic capacity are often associated with increased ROS production in HIV-infection (101, 119), perhaps induced by the incredible stress placed on the mitochondria by electron transport chain (ETC) inhibitors and uncouplers during Seahorse. Again, this discrepancy could be attributable to the cellular composition of our samples, likely reflecting a more variable environment than if select immune cells (e.g., T-cells) were interrogated in isolation. Alternatively, this discrepancy may also suggest that intracellular levels of superoxide as measured in the current study are produced by other cellular sources (e.g., NADPH Oxidase (NOX) enzymes) in addition to mitochondrial-produced ROS alone (120). Future work would benefit from quantifying superoxide directly within the mitochondria to clarify this mechanism.

In conclusion, our study was the first to directly link quantitative measures of mitochondrial function to the redox environment in virally-suppressed PLWH and uninfected

adults. Importantly, our results provide evidence for a mitochondrial-regulated redox profile that differs in PLWH compared to seronegative controls, which is directly related to discrete alterations in the bioenergetic capacity of the mitochondria (i.e., SRC), as opposed to other mitochondrial-dependent mechanisms in the system. While the existing literature provided valuable insight regarding aberrant redox environments in PLWH, the connection between mitochondrial functionality and comprehensively quantified redox profiles in PLWH was poorly understood, especially in the context of human physiology and those with virologic suppression. Finally, it is important to consider several methodological differences and limitations that could be attributable to some of the discrepant findings reported in this study. To begin, our study was the first to evaluate a large sample of HIV-infected adults with *virologic suppression*. This is an important consideration, as prior work has evaluated these mitochondrial-redox constructs in smaller samples of HIV-infected adults with and without virologic suppression (101), which is unfortunate, as various regimens of cART have been directly tied to alterations in mitochondrial toxicity and subsequent redox imbalances even in the absence of HIV exposure (109, 110, 121, 122). Second, our sample was considerably larger (~4x larger) than prior studies in humans, which could have also contributed to some of the directionality differences when comparing to the current literature. Finally, future work would greatly benefit from the direct intracellular quantification of H_2O_2 , as our results suggest a differential involvement of H_2O_2 -sensitive scavengers in HIV-infection. Similarly, it will be valuable for future studies to quantify levels of ROS and antioxidants directly within the mitochondria (e.g., MnSOD: mitochondrial origin of SOD) to further corroborate our evidence for aberrant mitochondrial-specific redox environments. Nevertheless, our study provides unique, mechanistic insight into the role of the mitochondria in aberrant redox profiles evident in PLWH and healthy controls. Importantly, precursors to age- and disease-related comorbidities (i.e., parameters of the mitochondrial redox environment) as

evaluated in the current study through the lens of chronic immunocompromised states may provide effective proxies for other instances of chronic inflammation (e.g., aging, neurodegenerative diseases) and further, may serve as effective targets to modulate downstream functional decline in the future.

CHAPTER 2. NEURAL OSCILLATORY DYNAMICS SERVING HEALTHY SENSORIMOTOR CONTROL ARE REGULATED BY THE MITOCHONDRIAL REDOX ENVIRONMENT

Introduction:

Motor control requires desired movement kinematics to be transformed into discrete plans to successfully execute volitional actions. In the brain, the planning and execution of volitional movement is implemented through multispectral population-level neural oscillatory activity, particularly in the beta band (e.g., 15-30 Hz). Specifically, robust decreases in beta power occur prior to and during movement onset, often reflecting the active engagement of the motor network during planning and execution periods in the bilateral primary motor cortices (M1) and secondary motor regions (54, 55, 57, 123). Importantly, while prior work suggests that this pattern of activity is not particularly susceptible to changes in the movement kinematics themselves (e.g., speed, force applied, muscle groups engaged (124)), beta power has been shown to be especially pertinent to higher-order planning and movement selection factors such as response certainty (54, 55, 57–59) and movement complexity (60), making its role in behavioral modulation to achieve desired outcomes profoundly important. Further, these well-established sensorimotor brain-behavior dynamics in humans appear to be extremely sensitive to participant characteristics such as chronological age and neurodegeneration (125–127)), although the precise mechanisms serving individual alterations in sensorimotor brain-behavior trajectories remains unclear.

One proposed contributor to the neural and behavioral variability observed in health and disease is the bioenergetic capacity of the mitochondria and associated redox environment (78, 79, 82). The importance of mitochondria in an organ as energetically expensive as the brain is highlighted by its increased dysregulation in a host of neurodegenerative diseases, including Alzheimer's disease (102), Parkinson's disease (103), and even healthy aging (79), often leading to cognitive and behavioral abnormalities observed most commonly in animal models. Essentially, neuronal function (e.g., synaptic vesicle release, neurotransmitter release) is known to be

regulated by mitochondria through various mechanisms, including changes in mitochondrial motility, morphology, ATP production and oxygen consumption (82, 87, 88), albeit its role in *human* neurophysiology and behavior is less well understood. Furthermore, as a result of these changes to mitochondrial structure and function, the generation of reactive oxygen species (ROS; e.g., superoxide, hydrogen peroxide (H_2O_2)), concomitant with alterations in their antioxidant scavengers (e.g., superoxide dismutase (SOD), catalase, glutathione) may also contribute to functional aberrations in brain and behavior (89, 90). For example, in aging mice, those with damage to important antioxidant defenses (i.e., SOD knock out models) exhibit significant deficits in sensory and motor neural functions (e.g., tail flick latency (93)), implicating a role for superoxide-sensitive mechanisms in the peripheral *and* central nervous system. Importantly, mitochondrial function and discrete alterations to the redox environment have also been shown to differentially modulate inhibitory interneuronal pools in animal models of psychiatric and neurodegenerative disorders (128–131). This is of particular interest to the current study, as substantial evidence implicates inhibitory interneuronal drive on local pyramidal cells as critical to population-level oscillatory responses, including the beta oscillations pertinent to human sensorimotor control (72, 132–138). Taken together, these data suggest that evaluation of the mitochondrial redox environment may provide novel mechanistic insight into changes in the oscillatory brain dynamics pertinent to healthy human behavior and sensorimotor processing.

The key goals of the current study were to comprehensively quantify parameters of mitochondrial function and the redox environment and to assess their predictive capacity on the neuronal functions serving sensorimotor performance. To this end, 40 healthy adults completed a movement sequence paradigm during magnetoencephalography (MEG) to characterize beta oscillatory activity during distinct phases of motor control (i.e., planning and execution). In addition, we used state-of-the-art systems biology approaches to directly quantify real-time

mitochondrial respiration using Seahorse Analyzer of mitochondrial stress tests, total intracellular superoxide levels using Electron Paramagnetic Resonance (EPR) Spectroscopy, and numerous antioxidant assays sensitive to superoxide and hydrogen peroxide (H_2O_2) redox pathways in the periphery. Of note, recent evidence suggests that bioenergetic features of the redox environment (e.g., mitochondrial respiration) measured in the periphery correspond closely to those measured from isolated mitochondria in the CNS (139), making the evaluation of blood-based markers an attractive avenue for investigation in humans. Using structural equation modeling, we tested the hypothesis that changes in the bioenergetic capacity of the mitochondria (i.e., spare respiratory capacity) would be differentially predictive of redox environments (i.e., ROS concentration, antioxidant defenses) sensitive to superoxide and H_2O_2 pathways, separately. In addition, we hypothesized that the generation of ROS in concert with increased antioxidant defenses would differentially modulate neural oscillatory activity during the planning and execution phases of movement, with significant impacts on subsequent behavioral task performance.

Methods:

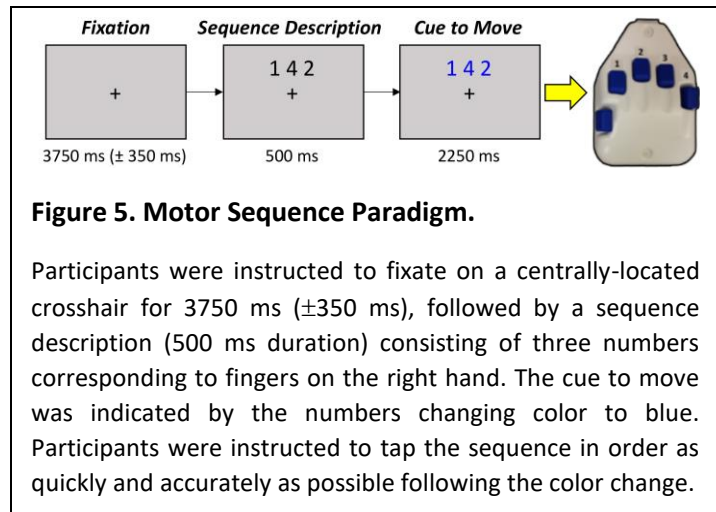
Participant Demographics

Forty adults ($M_{\text{age}} = 45.1$ years old, range: 20-66 years old; 17 females, 37 right handed) were enrolled in the current study. Exclusion criteria included any medical illness affecting CNS function, any psychiatric or neurological disorder, history of head trauma, current pregnancy, and current substance use. The University of Nebraska Medical Center Institutional Review Board approved the study and all participants provided written informed consent.

Experimental Paradigm

Participants were seated in a nonmagnetic chair with their head positioned within the MEG helmet-shaped sensor array. Participants were initially asked to fixate on a crosshair for 3750 ms (± 350 ms), followed by a presentation of three numbers for 500 ms, each corresponding to a

finger on the hand (Figure 5). Upon the presentation of a visual cue (i.e., numbers turning blue), participants were asked to tap the fingers corresponding to the numbers sequentially and given 2250 ms to complete the movement. A total of 160 trials



were completed, making the overall recording time approximately 17 minutes.

For each participant, reaction time (RT: the time to respond to the first number in the sequence) and movement duration (MD: the time to complete the entire motor sequence) data were extracted for each trial and incorrect trials were excluded from all analyses. In addition, individual trial data was initially rejected based on behavioral performance metrics that exceeded a standard threshold that would ultimately impact MEG data analyses (i.e., RT > 1250 ms and MD > 3000 ms). The remaining RT and MD data was then averaged per participant and subjected to subsequent statistical analyses using structural equation modeling.

MEG Data Acquisition and Coregistration with Structural MRI

All recordings were performed in a one-layer magnetically-shielded room with active shielding engaged for environmental noise compensation. With an acquisition bandwidth of 0.1-330 Hz, neuromagnetic responses were sampled continuously at 1 kHz using an MEGIN/Elekta MEG system (MEGIN, Helsinki, Finland) with 306 magnetic sensors, including 204 planar gradiometers and 102 magnetometers. Throughout data acquisition, participants were monitored using a real-time audio-video feed from inside the magnetically-shielded room. MEG data from each participant were individually corrected for head motion and subjected to noise reduction

using the signal space separation method with a temporal extension (140). Each participant's MEG data were coregistered with their structural T1-weighted MRI data prior to imaging analyses using BESA MRI (Version 2.0). Structural MRI data were aligned parallel to the anterior and posterior commissures and transformed into standardized space. After beamformer analysis (see below), each subject's functional images were transformed into standardized space using the transform that was previously applied to the structural MRI volume and spatially resampled.

MEG Preprocessing and Sensor-Level Statistics

Cardiac and ocular artifacts were removed from the data using signal-space projection (SSP) and the projection operator was accounted for during source reconstruction (141). Epochs of 6150 ms duration were defined (i.e., -2050 to 4100 ms) with 0 ms defined as movement onset and the baseline being the -2050 to -1550 ms window. Initially, we rejected trials based on having a reaction time longer than 1250 ms or taking more than 3000 ms to complete the entire motor sequence, which would disrupt the baseline period of the subsequent trial. Next, epochs containing artifacts were rejected based on a fixed threshold method, supplemented with visual inspection. On average, 123 trials per participant were used for further analysis.

Artifact-free epochs were transformed into the time-frequency domain using complex demodulation (142), and the resulting spectral power estimations per sensor were averaged over trials to generate time-frequency plots of mean spectral density. The sensor-level data per time-frequency bin were normalized using the mean power within that frequency bin during the -2050 to -1550 ms baseline period. The specific time-frequency windows used for imaging were determined through a two-stage, data-driven approach involving statistical analysis of the sensor-level spectrograms across all participants and trials. First, paired-sample t-tests against baseline were conducted on each data point, with the output spectrogram of t-values initially thresholded at $p < .05$ to define time-frequency bins containing potentially significant oscillatory deviations.

To reduce the risk of false positive results due to multiple comparisons, the time-frequency bins that survived that initial threshold were temporally and/or spectrally clustered with neighboring bins that were also significant, and a cluster value was derived by summing all of the t-values of all data points in the cluster. Nonparametric permutation testing (10,000 permutations) was then used to derive a distribution of cluster values and the significance level of the observed clusters were tested directly using this distribution. Based on this analysis, the time-frequency periods that contained significant oscillatory events across all participants were subjected to beamforming analyses. Note that we limited our source analyses and modeling to the significant time-frequency extent surrounding the peri-movement beta response in the current study, given our focus on motor planning and execution responses. Further details of our MEG data processing pipeline can be found in recent manuscripts (62, 75, 143, 144).

MEG Source Imaging

Cortical oscillatory responses were imaged through the dynamic imaging of coherent sources (DICS) beamformer (145), which uses the cross-spectral density matrices to calculate source power for the entire brain volume. These images are typically referred to as pseudo-t maps, with units (pseudo-t) that reflect noise-normalized power differences (i.e., active vs. passive) per voxel. Following convention, we computed noise-normalized, source power per voxel in each participant using baseline periods of equal duration and bandwidth (146). MEG preprocessing and imaging used the Brain Electrical Source Analysis (Version 7.0; BESA) software.

Normalized source power was computed over the entire brain volume per participant at $4.0 \times 4.0 \times 4.0$ mm resolution for the peri-movement beta time-frequency periods identified through the sensor level analyses. Prior to statistical analysis, each participant's MEG data, which were coregistered to native space structural MRI prior to beamforming, were transformed into standardized space using the transform previously applied to the structural MRI volume and

spatially resampled. The resulting 3D maps of brain activity were averaged across all participants to assess the neuroanatomical basis of the peri-movement beta oscillatory responses identified through the sensor-level analysis. Source power was then extracted from peak voxels per time bin (i.e., planning and execution phases) and participant and underwent statistical modeling.

Isolation of Peripheral Blood Mononuclear Cells and Respiration Analysis

Whole blood was collected into EDTA tubes by venous puncture for all participants. Buffy coats were submitted to a Ficoll-Paque Plus (GE Healthcare) gradient centrifugation for isolation of the mononuclear fraction. Peripheral blood mononuclear cells (PBMC) were cryopreserved in Fetal Bovine Serum with 10% DMSO. Cells were thawed within 6 weeks of isolation and underwent assessment using the Seahorse XF96 Analyzer (Seahorse Bioscience) to quantify oxygen consumption rate (OCR) using the mitochondrial stress test assay. Specifically, PBMCs were plated at 500,000 cells/well and 3 OCR measurements were taken sequentially on 5-6 technical replicate wells prior to and upon serial injection of 3.5 μ M oligomycin (Sigma; complex V inhibitor), 1 μ M fluoro-carbonyl cyanide phenylhydrazone (FCCP; Sigma; mitochondrial oxidative phosphorylation uncoupler) and 14 μ M rotenone + 14 μ M antimycin A (Sigma; complex I and III inhibitors, respectively) to evaluate measures of mitochondrial respiration including basal respiration, ATP-linked respiration, proton leak, maximal respiration, spare respiratory capacity (SRC) and non-mitochondrial respiration. All bioenergetic data were normalized to protein in the well for subsequent analyses. For data calculation, the Seahorse Wave software (v2.2.0) was used.

Quantification of the Redox Environment

Cellular levels of superoxide were assessed using Electron Paramagnetic Resonance (EPR) Spectroscopy of whole blood incubated with a superoxide-sensitive spin probe (1-hydroxy-3-methoxycarbonyl-1,2,2,5,5-tetramethylpyrrolidine: CMH) for 1 hour under physiologic conditions (37°C), as previously described (111). Specifically, immediately after sample collection, 200 μ M of

CMH was reconstituted into EPR buffer (Krebs Hepes Buffer) supplemented with metal chelators (5 μ M sodium diethyldithiocarbamate trihydrate and 25 μ M deferoxamine) and incubated with 200 μ L of whole blood. EPR measurements were performed with a Bruker eScan EPR spectrometer (Bruker BioSpin GmbH, Rheinstetten/Karlsruhe, Germany), with the following parameters: field sweep width, 100.0 G; center field, 3482 G; microwave frequency, 9.75 kHz; microwave power, 1.10 mW; modulation amplitude, 5.94 G; conversion time, 10.24 ms; time constant, 40.96 ms. The resulting EPR spectra amplitude is expressed as arbitrary units (a.u.) that are directly proportional to the amount of total cellular superoxide in the sample.

Antioxidant activity levels were quantified in erythrocytes for key enzymatic and non-enzymatic contributors to the mitochondrial redox environment including superoxide dismutase (SOD), catalase, and glutathione. Specifically, we used the SOD Assay Kit-WST (DOJINDO, Inc.) to measure total SOD activity, the OxiSelect Catalase Activity Assay Kit (Cell Biolabs, Inc.) for catalase, and the GSSG/GSH Quantification kit (DOJINDO, Inc.) for total (tGSH), oxidized (GSSG) and reduced glutathione (GSH) according to the manufacturers' guidelines.

Statistical Analysis

To evaluate the predictive capacity of the mitochondrial redox environment on movement-related neural oscillations serving motor function, we used structural equation modeling following standard data trimming procedures. Briefly, measures that exceeded 2.5 standard deviations above or below the group's mean were excluded from subsequent analyses. Our primary hypotheses were that movement-related beta oscillatory activity during planning and execution phases of movement would predict task performance, and that these dynamics would be modulated by the mitochondrial redox environment. In regard to the brain and behavior, we predicted that beta activity prior to movement (i.e., planning) would predict reaction time and beta decreases in the contralateral M1 during motor execution. These variables would then

predict the time to complete the entire motor sequence (i.e., movement duration). In addition, we conducted a multiple mediation model whereby measures of mitochondrial function (i.e., spare respiratory capacity) predicted movement-related oscillations and subsequent behavioral performance through changes in the redox environment (i.e., superoxide, SOD, catalase, GSSG/tGSH ratio), for superoxide-sensitive and H₂O₂-sensitive paths, separately. Importantly, we examined the 95% confidence intervals of bias-corrected bootstrapped confidence intervals based on 1000 bootstrapped samples (147). This method provides a robust estimate of mediation effects that are asymmetrical (148), as traditional tests of indirect effects (e.g., Sobel test) often violate the assumption of normality. All analyses were conducted with full information maximum likelihood estimation for missing data using MPlus (v.8.1).

Results:

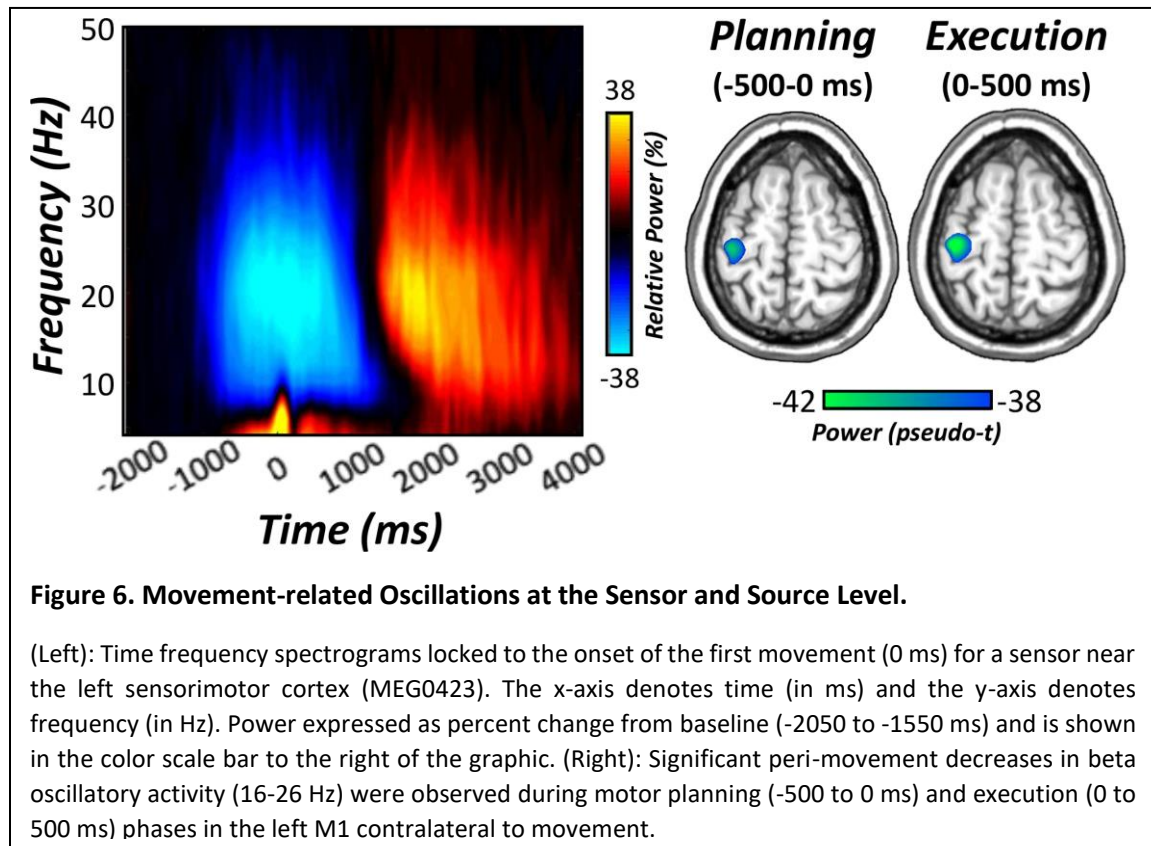
Sequential Movement Performance

Following removal of trials with anomalous performance (e.g., reaction times > 1250 ms; movement durations > 3000 ms), an average of 123 trials per participant remained for subsequent statistical modeling. Participants performed generally well on the task, with an average accuracy of $93.93 \pm 4.69\%$. Average reaction time (i.e., response time to complete the first button press) was 479.17 ± 137.91 ms, while the average movement duration (i.e., time to complete the entire motor sequence) was 831.44 ± 234.47 ms, which aligns well with prior studies of healthy adults (60).

MEG Sensor- and Source-level Analyses

Time-frequency analyses of movement-locked MEG data indicated significant multispectral peri- and post-movement oscillatory responses. These responses were robust in gradiometers near the contralateral sensorimotor strip across all participants ($p < .001$, Figure 6). Specifically, decreases in peri-movement beta activity (16-26 Hz) were observed prior to and

following movement onset (i.e., -500 to 0 ms and 0 to 500 ms, respectively). In addition, we observed transient increases in theta activity near movement onset, as well as weaker sustained decreases in the alpha range (10-14 Hz; Figure 6). Finally, we observed post-movement increases in beta activity following motor termination. However, given the known role of beta oscillations in motor planning and performance, we focused subsequent analyses on these responses and did not further examine the theta, alpha, or post-movement beta activity.



To identify the neural origins of oscillations detected during the discrete phases of motor control, planning and execution windows were imaged separately using a beamformer. The resulting maps indicated that peri-movement decreases in beta power originated from the left M1 contralateral to movement (Figure 6), with identical peak locations observed for motor planning (i.e., -500-0 ms) and execution (i.e., 0-500 ms) phases. Peak voxel values (i.e., pseudo-t)

were then extracted from the left M1 per time bin and these were used for subsequent statistical modeling.

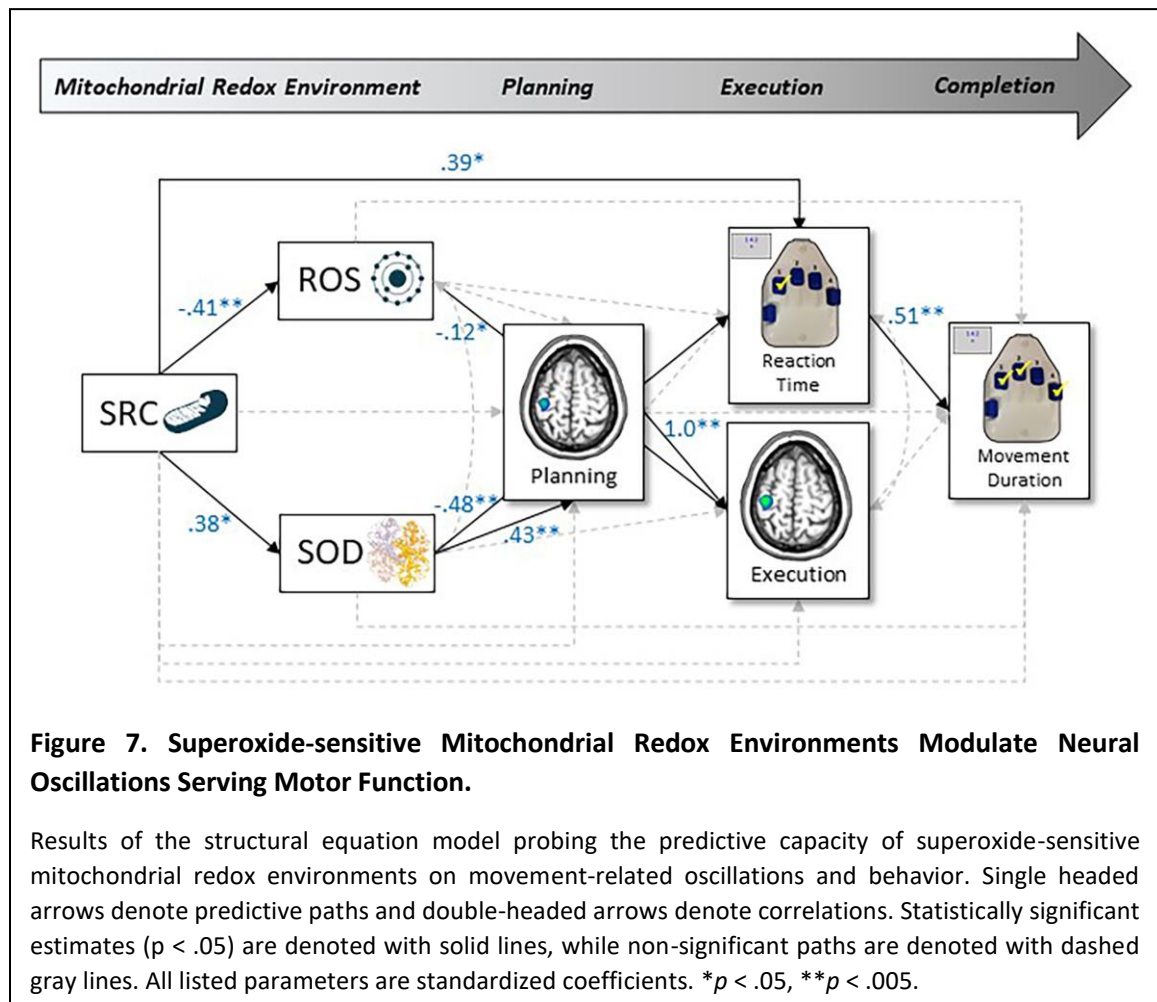
Superoxide-sensitive Redox Environments Predict Movement-related Dynamics

We tested a multiple mediation model (see Methods) whereby measures of the mitochondrial redox environment sensitive to superoxide (i.e., spare respiratory capacity (SRC), superoxide, superoxide dismutase (SOD) activity) predicted brain-behavior relationships serving motor performance. Specifically, our brain-behavior relationships included paths whereby beta oscillatory activity during motor planning (-500 to 0 ms) predicted reaction time, as well as beta activity during motor execution (0 to 500 ms). Variables during planning and execution phases then predicted movement duration (i.e., time to complete the entire sequence). For a full model visualization, see Figure 7.

As expected, reaction time was a robust predictor of movement duration, such that faster responses to the first number in the sequence led to faster sequence completion time ($\beta = .51, p < .001$). In addition, beta activity during the planning period strongly predicted activity during the execution phase in the left M1 contralateral to movement, such that greater decreases in beta oscillatory activity prior to movement were predictive of greater decreases during sequence execution ($\beta = 1.0, p < .001$). Interestingly, while beta activity prior to movement did not significantly predict reaction time nor movement duration ($ps > .109$), weaker beta responses during motor execution were marginally predictive of faster sequence completion times (i.e., movement duration; $\beta = -1.09, p = .061$).

In regard to superoxide-sensitive redox environments, we observed no direct effects of mitochondrial function on peri-movement oscillatory activity in the contralateral M1 nor movement duration ($ps > .105$), although decreases in SRC were predictive of faster reaction times ($\beta = .39, p = .027$; Figure 7). In contrast, we observed robust direct effects of the redox

environment on brain and behavioral function (Figure 7). Specifically, levels of cellular superoxide were robust predictors of beta activity during motor execution, such that increased levels of superoxide were predictive of weaker beta responses ($\beta = -.12, p = .012$), while increased activity levels of superoxide's scavenger (i.e., SOD) were predictive of weaker planning-related decreases in the left M1 ($\beta = .43, p = .004$) and faster reaction times on the motor sequence task ($\beta = -.48, p = .003$).



Next, we examined all potential mediating effects of the redox environment on mitochondrial-related changes in motor cortical dynamics and behavioral performance. As described in the methods, statistical significance of these indirect effects were determined by using bias-corrected bootstrapped confidence intervals (147, 148), thus exact p-values are not

<i>Mitochondrial SRC to Movement Duration</i>			
Path	Total	Direct	Indirect
SRC→SOD→RT→MD	.13	.02	-.09*
<i>Mitochondrial SRC to Reaction Time</i>			
SRC→SOD→RT	.16*	.39*	-.18*
<i>Mitochondrial SRC to Motor Execution</i>			
SRC→EPR→Exec	-.13*	-.08*	.05*
SRC→SOD→Plan→Exec	-.13*	-.08*	.16*
<i>Mitochondrial SRC to Motor Planning</i>			
SRC→SOD→Plan	-.09	-.19*	.16*

Table 2. Results of the Mediation Analyses of Mitochondrial Function on Brain-Behavior through Superoxide-Pertinent Redox Parameters.

Indirect effects were assessed for statistical significance using the bias-corrected bootstrapped confidence intervals. All reported parameters are standardized coefficients. * $p < .05$.

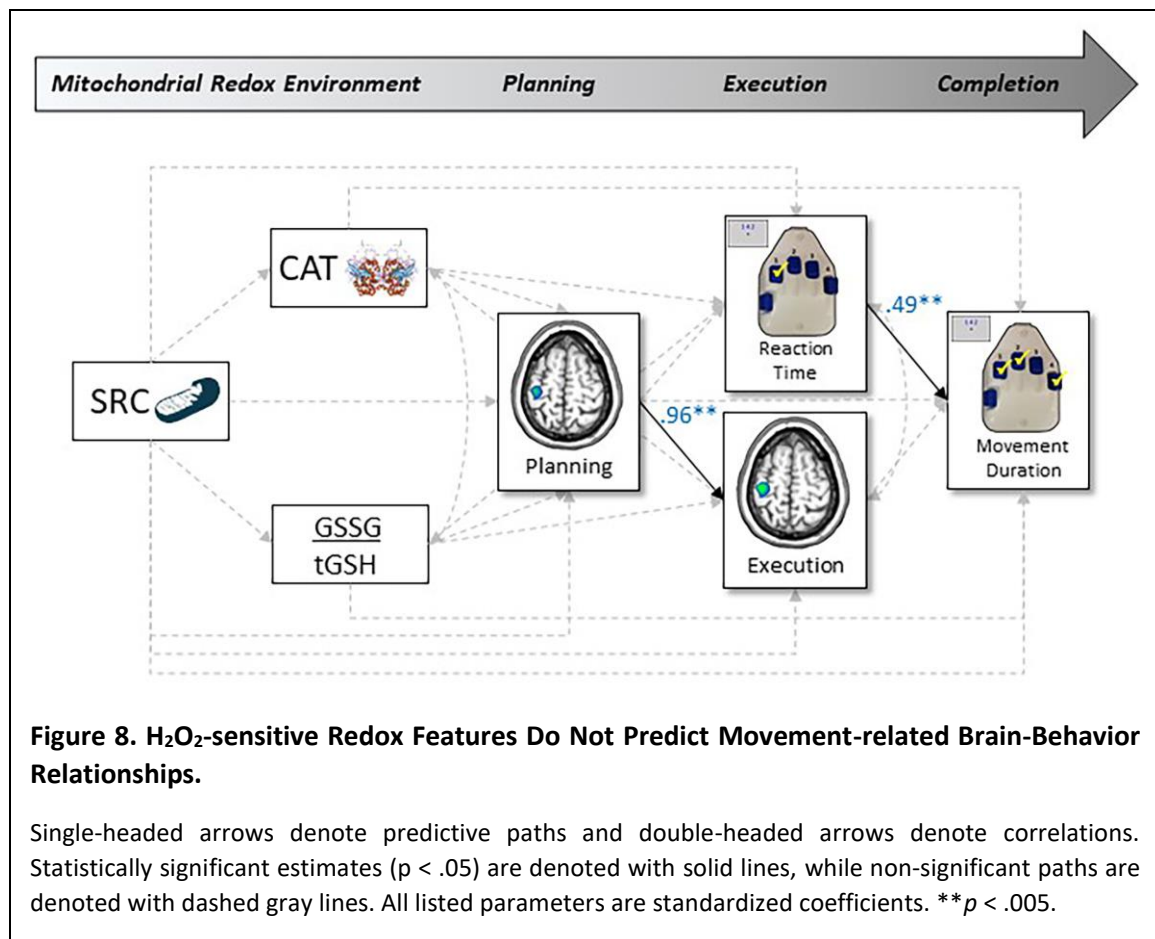
available for indirect effects. In total, we observed five statistically significant indirect effects (see Table 2, $p < .05$). First, there was a full mediation of mitochondrial SRC on movement duration through levels of SOD and reaction time ($\beta_{\text{indirect}} = -.09$, $b_{\text{indirect}} = -7.41$, 95% CI: [-26.55, -0.95]), such that increases in SRC were associated with increases in SOD activity levels ($\beta = .38$, $p = .013$), which were associated with

faster reaction times ($\beta = -.48$, $p = .006$) and subsequently shorter time to complete the entire motor sequence ($\beta = .51$, $p = .001$). Similarly, the relationship between mitochondrial function and reaction time was partially mediated by levels of SOD activity ($\beta_{\text{indirect}} = -.18$, $b_{\text{indirect}} = -8.62$, 95% CI: [-23.51, -2.27]) in the same fashion described above. In regard to the brain, planning and execution-related beta oscillations were mediated by measures of the redox environment through disparate mechanisms, such that superoxide was a partial mediator of the relationship between SRC and neural activity during motor execution ($\beta_{\text{indirect}} = .05$, $b_{\text{indirect}} = .51$, 95% CI: [0.01, 1.56]), while SOD partially mediated changes in planning-related neural oscillations ($\beta_{\text{indirect}} = .16$, $b_{\text{indirect}} = 1.67$, 95% CI: [0.15, 4.71]). Interestingly, decreases in mitochondrial SRC were associated with increased levels of superoxide ($\beta = -.41$, $p = .005$), which were associated with weaker execution-related decreases in beta activity in the contralateral M1 ($\beta = -.12$, $p = .007$). In contrast, when accounting for increasing levels of SOD, we observed a multiple mediation of the relationship between mitochondrial SRC and execution-related beta oscillations through

planning-related decreases in the contralateral M1 ($\beta_{\text{indirect}} = .16$, $b_{\text{indirect}} = 1.67$, 95% CI: [0.16, 4.84]). Essentially, greater mitochondrial energetic reserve was associated with increased activity levels of SOD ($\beta = .38$, $p = .013$), which significantly predicted weaker planning-related beta power ($\beta = .43$, $p = .008$) and subsequent beta decreases during movement execution in the contralateral M1 ($\beta = 1.0$, $p < .001$). Importantly, superoxide-sensitive features of the redox environment and mitochondrial function accounted for 34.9% of the variance in movement duration ($p < .001$).

H₂O₂-sensitive Pathways Do Not Predict Motor Cortical Dynamics and Behavior

Next, we evaluated the predictive capacity of H₂O₂-sensitive redox environments and mitochondrial function on brain-behavior relationships serving sensorimotor control using the same regression equation described above. However, in this model, our measures of the redox environment were now comprised of catalase activity and GSSG/tGSH ratios as continuous



predictors of movement-related beta activity during motor planning and execution phases, as well as behavior on the task. As with the first model, reaction time was a robust predictor of movement durations ($\beta = .49, p = .001$; Figure 8), such that faster responses to the first number in the sequence led to shorter times to complete the full movement. In regard to the brain, movement-related beta oscillations during the planning period were robust modulators of execution-related decreases in beta activity ($\beta = .96, p < .001$; Figure 8). In addition, weaker oscillatory activity during motor execution in the contralateral M1 was marginally predictive of shorter movement completion times ($\beta = -.99, p = .068$). As per H_2O_2 -sensitive mitochondrial redox environments, we observed no direct effects of mitochondrial SRC nor H_2O_2 -sensitive antioxidants on brain or behavioral indices in our sample. In addition, we observed no mediating effects of the redox environment between mitochondrial function, neural, or behavioral metrics.

Discussion:

In the current study, we used advanced neurophysiology and systems biology approaches to evaluate the predictive capacity of mitochondrial function and the redox environment on motor cortical function and behavioral performance in a large sample of healthy adults. Specifically, we observed robust direct effects of superoxide-sensitive redox environments, such that increases in superoxide were robust predictors of execution-related beta oscillations in the contralateral M1, while increases in SOD were predictive of planning-related beta power. In addition, both superoxide and SOD were strong mediators of the relationship between mitochondrial energetic reserve and brain-behavior relationships serving sensorimotor function through disparate mechanisms. Taken together, superoxide-sensitive features of the mitochondrial redox environment accounted for a substantial proportion of the variance (34.9%) in movement duration. Finally, our data suggest that unlike superoxide-related mechanisms, features involved in H_2O_2 -pertinent redox pathways were not predictors of sensorimotor brain-

behavior dynamics in healthy adults. Below, we discuss the implications of these novel findings for understanding the contribution of mitochondrial redox environments in normative human neurophysiology and sensorimotor control.

Our most important finding was likely the contribution of superoxide-sensitive features of the redox environment on the neural dynamics serving sensorimotor control in humans. Specifically, increases in superoxide were robust predictors of weaker beta oscillations in the M1 contralateral to movement during motor execution. In contrast, increases in total SOD activity (i.e., the antioxidant important for scavenging superoxide) were associated with weaker beta oscillations during the planning phase and faster reaction times on the task. Importantly, these results coincided with a well-established pattern of findings in the healthy motor system, such that weaker planning-related beta oscillations in M1 were predictive of weaker beta oscillations during motor execution and shorter movement durations on the task (i.e., time to complete the entire sequence (125, 143)). The idea that superoxide-sensitive redox pathways modulate motor cortical oscillations and subsequent performance in humans is not surprising, albeit prior work has solely interrogated these relationships in animal models. For example, deficiencies in the cytosolic isoform of SOD have long been revered as key contributors to age- and disease-related functional dependencies, with the most common demonstration of this seen in mouse models of amyotrophic lateral sclerosis (ALS) (91). Essentially, gene mutations in SOD lead to sharp reductions in SOD activity levels, which in turn, results in increased levels of ROS that give rise to the progressive atrophy and paralysis seen in motor neuron diseases (i.e., ALS; (91, 92)). In addition, reductions in SOD activity levels have been linked to the healthy aging process in mice, such that increasing age is associated with reduced SOD activity, greater ROS production (e.g., lipid peroxidation, nitrated proteins, superoxide generation) and impaired functionality (e.g., reduced exploration time, increased tail flick latency) (93–95). Importantly, our study is the first

to describe the modulation of sensorimotor brain-behavior relationships by the redox environment in normative human physiology and further, our results suggest that in *healthy* systems, *increases* in SOD and superoxide are associated with more optimal oscillatory response profiles and *better* motor performance.

In agreement with the notion that superoxide-sensitive redox pathways govern more optimal brain-behavior dynamics, we observed robust mediations of the mitochondrial bioenergetic-neural pathway when accounting for increasing levels of superoxide and SOD. Contrary to our hypotheses, we observed no direct effects of mitochondrial SRC on movement-related cortical oscillations nor movement duration. This was somewhat surprising, as there is substantial evidence implicating mitochondrial functionality in modulating brain-behavior dynamics in animals (78, 79, 88, 90). For example, Hara et al., demonstrated a relationship between mitochondrial morphology and content with better working memory performance in aged monkeys, such that increased total number of straight mitochondria were associated with better accuracy on the task, while increased prevalence of donut and blob-shaped mitochondria in presynaptic boutons (i.e., a marker of oxidative stress) were associated with smaller active zones, fewer docked synaptic vesicle pools, and working memory impairment (88). In a different study, Khacho and colleagues observed discrete alterations to motor, learning and memory function (i.e., reduced time on the rotarod, inability to improve over trials, increased latency to platform in Morris water maze, respectively) in aging mice with sustained mitochondrial damage compared to their developing counterparts (90). Importantly, the current findings suggest that when accounting for increasing levels of SOD in the system, mitochondrial SRC predicted weaker planning-related beta oscillations in M1 and faster reaction times on the task. In addition, increased levels of superoxide mediated the relationship between mitochondrial function and movement-related beta power during the execution phase in the contralateral M1. Finally,

decreases in SRC were predictive of faster reaction times and in turn, faster movement durations across our sample when accounting for elevated oxidative states. While the integrity of the mitochondria and its associated functional properties (e.g., oxygen consumption, ATP production, Ca^{2+} sequestering) have been implicated in neurophysiological changes in health and disease (78, 82, 87), our study suggests that features of the redox environment (i.e., superoxide and SOD) are critical modulators of the brain-behavior dynamics serving human motor control. Furthermore, our findings demonstrate that these superoxide-sensitive redox parameters are not merely byproducts of mitochondrial metabolism but exhibit dissociable mechanisms of action on planning and execution-related neural oscillatory activity serving motor function in M1, which had yet to be reported in the context of human neurophysiology.

Mechanistically, our mitochondrial redox-regulated beta oscillatory responses could be attributable, at least in part, to changes in GABAergic inhibitory interneurons. Briefly, there is substantial evidence implicating GABAergic-mediated inhibitory drive in the modulation of pyramidal cells, giving rise to specific oscillatory profiles including the generation of higher frequency beta and gamma oscillations (132, 133, 149–151), especially within the motor and visual networks (72, 137, 138, 152, 153). In regard to the redox environment, the generation of higher frequency oscillators requires the most energy expenditure in the brain (129, 130), and pharmacologically disrupting superoxide and H_2O_2 -sensitive features of this environment has direct consequences on the integrity of inhibitory interneuronal pools including substantial losses in absolute number of interneurons detected, as well as decreased parvalbumin expression in animal models (128). Thus, we propose that the mitochondrial redox-regulated mechanisms observed in the current study could be acting through modulation of GABAergic inhibitory interneuronal pools to modulate the strength of population-level neural oscillations in the beta

range and future work in this area will be invaluable to fully unravel the nature of bioenergetic-oscillatory coupling in the sensorimotor cortices.

In conclusion, our study is the first to directly link quantitative measures of mitochondrial respiration and the redox environment to the neural oscillatory responses underlying motor function in healthy adults. Importantly, our results provide evidence that the beta oscillations serving motor planning and execution are regulated by the redox environment and sensitive to superoxide redox parameters as opposed to H_2O_2 -pertinent mechanisms in the system. In fact, we observed both direct and mediating effects of superoxide-sensitive mitochondrial redox features that accounted for 34.9% of the variance in behavioral performance on the motor sequence task, while we observed no predictive paths on brain or behavioral function in humans when considering H_2O_2 -sensitive redox parameters. Future work will undoubtedly benefit from a direct intracellular quantification of H_2O_2 to clarify the involvement of H_2O_2 in human behavior, albeit our results currently suggest a lack of involvement of H_2O_2 -sensitive scavengers in human sensorimotor control. Further, while our results implicated mitochondrial energetic reserves and associated superoxide and SOD involvement in modulating brain and behavior in the current sample, future work would greatly benefit from the quantification of ROS and antioxidants directly within the mitochondria (e.g., mitochondrial isoform of SOD) to corroborate our findings on mitochondrial-specific redox environments in human neurophysiology. Nevertheless, our study demonstrated a strong link between mitochondrial function, the redox environment, brain and behavioral function in healthy adults, such that alterations in mitochondrial energetic capacities were predictive of weaker peri-movement beta responses in the contralateral primary motor cortices and further, faster reaction times and shorter movement durations through discrete elevations in superoxide and its antioxidant scavenger, SOD. To close, our study suggests that molecular precursors to brain-behavior dynamics (i.e., blood-based markers of mitochondrial

redox pathways) as evaluated in the current study may provide critical insights to behavior and brain function in humans and further, may serve as effective targets in the future to ameliorate age- and disease-related declines in motor function in adults.

CHAPTER 3. SUPEROXIDE-SENSITIVE REDOX ENVIRONMENTS DIFFERENTIALLY PREDICT SENSORIMOTOR BRAIN-BEHAVIOR DYNAMICS IN PEOPLE LIVING WITH HIV

Introduction:

HIV-infection is associated with a host of comorbidities, including cognitive and behavioral dysfunction that persists despite effective and stable regimens of combination antiretroviral therapy (cART) (1–8). Interestingly, one of the first behavioral abnormalities that manifests in those with HIV-associated neurocognitive disorders (HAND) is that of motor dysfunction (2, 19–22), so much so that the original terminology for characterizing mild to moderate forms of HAND included a condition termed HIV-associated mild cognitive-motor disorder (MCMD) (18, 154). While previous investigations have done well to characterize the structural and functional aberrations that occur within the sensorimotor cortical and subcortical networks in people living with HIV (PLWH) (24, 25, 28, 155, 156), little is known about the underlying neuronal dynamics and key molecular pathways that govern this marked decline in motor function. This is unfortunate, as HIV-related deficits in motor control may play an important role in the non-motor symptoms that persist in the modern cART era.

In regard to the brain, motor control requires a coordinated ensemble of spatiotemporally-precise neural oscillations during the planning, execution and termination phases of movement. Recent neurophysiological studies have primarily focused on movement-related oscillations in the beta range (i.e., 15-30 Hz), which exhibit robust decreases in power prior to and following movement onset in an extended motor network including bilateral primary motor cortices (M1), supplementary motor areas (SMA), and parietal cortices (54, 55, 57, 123). Importantly, this distinct pattern of oscillatory activity is thought to reflect the active engagement of neuronal pools and further, is pertinent to higher-order cognitive demands of the action to be performed (e.g., response certainty (54, 55, 57–59), complexity (60), interference (61–63)), making its role in behavioral modification particularly important. To date, only one prior study has

evaluated the impact of HIV-infection on beta oscillations during movement. In 2013, Wilson et al., used a simple finger tapping paradigm during magnetoencephalography (MEG) and observed a strong attenuation of peri-movement beta oscillations (i.e., -350 to 250 ms surrounding movement onset) in the bilateral M1 and the SMA in PLWH compared to uninfected controls (76). In contrast, PLWH exhibited stronger beta responses during movement onset in prefrontal regions (76), which aligns well with prior functional magnetic resonance imaging (fMRI) literature demonstrating hypoactivity in primary sensory regions (157–159) and hyperactivity in association cortices that govern task performance in HIV-infected adults (41–44). Importantly, while the study by Wilson et al., provided novel insight regarding aberrant peri-movement beta oscillatory profiles in PLWH, it is less well understood how these dynamics relate to task behavior, as more complex motor tasks would be better equipped to elicit behavioral differences that could be quantified in real time alongside neuromagnetic recordings.

Beyond the neural oscillatory profiles that govern motor function are the potential molecular mechanisms that are theorized contributors to the age- and disease-related decline in brain-behavior dynamics. One such mechanism involves a mitochondrial-induced redox imbalance of the system, which suggests that mitochondrial dysfunction (e.g., deficient oxygen consumption) leads to an accumulation of reactive oxygen species (ROS), concomitant with an attenuation of their antioxidant defenses, leading to a host of comorbidities observed in aging and clinical populations (78, 79, 82, 87, 88, 94, 102, 103). This is of particular interest in the context of chronic immunocompromised states as seen in HIV-infection, as the mitochondrial redox environment is also essential for regulating normative immune responses to invading pathogens (84–86, 99) and as shown in Chapter 1, is aberrant despite virologic suppression in PLWH. Importantly, prior work by our lab was the first to effectively link parameters of the mitochondrial redox environment to motor cortical oscillations serving motor function in a sample of healthy

adults (see Chapter 2). Essentially, we observed that parameters sensitive to superoxide in the periphery (i.e., intracellular superoxide levels, mitochondrial energetic capacity, superoxide dismutase activity), but not hydrogen peroxide (H_2O_2 ; i.e., catalase activity, glutathione reducing capacity) were robust predictors of planning- and execution-related beta oscillations in the contralateral M1 and further, increasing levels of superoxide and its scavenger, SOD, were robust mediators of the relationship between mitochondrial energetics and sensorimotor brain-behavior relationships. While Chapter 2 provided novel mechanistic insight regarding the modulation of optimal oscillatory profiles that govern *better* motor function in healthy systems, the role of the mitochondrial redox environment in sensorimotor brain-behavior dynamics in those exhibiting motor dysfunction (i.e., PLWH) is less well understood.

Thus, the goal of the current study was to evaluate the predictive capacity of mitochondrial-redox parameters disrupted in HIV-infection on the peri-movement neural oscillations serving motor control in a large virally-suppressed sample of HIV-infected adults and demographically-matched uninfected controls. We employed advanced systems biology and neuroscience approaches including Seahorse Analyzer of mitochondrial respiration, Electron Paramagnetic Resonance (EPR) Spectroscopy of whole blood to quantify intracellular superoxide levels, commercially-available antioxidant activity assays and MEG to directly quantify neural oscillatory activity during a motor sequence task. In addition, we used a group-based path analysis and direct comparisons of unstandardized coefficients for each predictive path to test the following hypotheses: (1) mitochondrial energetic capacities (i.e., adaptability to changing energetic demands) would differentially predict parameters of the redox environment sensitive to superoxide and H_2O_2 -mechanisms, separately. In addition, we expect that (2) features sensitive to superoxide mechanisms in the system, but not H_2O_2 , will differentially predict brain-behavior relationships evaluated using MEG in PLWH versus uninfected controls.

Methods:

Participant Demographics

Eighty adults (range: 20-66 years old; 40 PLWH and 40 controls) were enrolled. All PLWH were receiving effective cART and had viral suppression defined as <50 copies/mL. Exclusion criteria included any medical illness affecting CNS function (other than HIV), any psychiatric or neurological disorder, history of head trauma, current pregnancy and current substance use. Uninfected controls were enrolled to demographically match PLWH based on their age ($p = .857$), sex ($p = .095$), handedness ($p = .999$) and body mass index (BMI: $p = .267$) (for a comprehensive list, see Table 1). The University of Nebraska Medical Center Institutional Review Board approved the study and all participants provided written informed consent.

Experimental Paradigm

Participants were seated in a nonmagnetic chair with their head positioned within the MEG helmet-shaped sensor array. Participants were initially asked to fixate on a crosshair for 3750 ms (± 350 ms), followed by a presentation of three numbers for 500 ms, each corresponding to a finger on the hand (Figure 5). Upon the presentation of a visual cue (i.e., numbers turning blue), participants were asked to tap the fingers corresponding to the numbers sequentially and given 2250 ms to complete the movement. A total of 160 trials were completed, making the overall recording time approximately 17 minutes.

For each participant, reaction time (RT: the time to respond to the first number in the sequence) and movement duration (MD: the time to complete the entire motor sequence) data were extracted for each trial and incorrect trials were excluded from all analyses. In addition, individual trial data was initially rejected based on behavioral performance metrics that exceeded a standard threshold that would ultimately impact MEG data analyses (i.e., RT > 1250 ms and MD

> 3000 ms). The remaining RT and MD data was then averaged per participant and subjected to subsequent statistical analyses using structural equation modeling.

MEG Data Acquisition and Coregistration with Structural MRI

All recordings were performed in a one-layer magnetically-shielded room with active shielding engaged for environmental noise compensation. With an acquisition bandwidth of 0.1-330 Hz, neuromagnetic responses were sampled continuously at 1 kHz using an MEGIN/Elekta MEG system (MEGIN, Helsinki, Finland) with 306 magnetic sensors, including 204 planar gradiometers and 102 magnetometers. Throughout data acquisition, participants were monitored using a real-time audio-video feed from inside the magnetically-shielded room. MEG data from each participant were individually corrected for head motion and subjected to noise reduction using the signal space separation method with a temporal extension (140). Each participant's MEG data were coregistered with their structural T1-weighted MRI data prior to imaging analyses using BESA MRI (Version 2.0). Structural MRI data were aligned parallel to the anterior and posterior commissures and transformed into standardized space. After beamformer analysis (see below), each subject's functional images were transformed into standardized space using the transform that was previously applied to the structural MRI volume and spatially resampled.

MEG Preprocessing and Sensor-Level Statistics

Cardiac and ocular artifacts were removed from the data using signal-space projection (SSP) and the projection operator was accounted for during source reconstruction (141). Epochs of 6150 ms duration were defined (i.e., -2050 to 4100 ms) with 0 ms defined as movement onset and the baseline being the -2050 to -1550 ms window. Initially, we rejected trials based on having a reaction time longer than 1250 ms or taking more than 3000 ms to complete the entire motor sequence, which would disrupt the baseline period. Next, epochs containing artifacts were rejected based on a fixed threshold method, supplemented with visual inspection. On average,

127 trials per participant were used for further analysis and the amount of trials accepted did not significantly differ by group ($p = .088$).

Artifact-free epochs were transformed into the time-frequency domain using complex demodulation (142), and the resulting spectral power estimations per sensor were averaged over trials to generate time-frequency plots of mean spectral density. The sensor-level data per time-frequency bin were normalized using the mean power per frequency during the -2050 to -1550 ms baseline period. The specific time-frequency windows used for imaging were determined through a two-stage, data-driven approach involving statistical analysis of the sensor-level spectrograms across all participants and trials. First, paired-sample t-tests against baseline were conducted on each data point, with the output spectrogram of t-values initially thresholded at $p < .05$ to define time-frequency bins containing potentially significant oscillatory deviations. To reduce the risk of false positive results due to multiple comparisons, the time-frequency bins that survived that initial threshold were temporally and/or spectrally clustered with neighboring bins that were also significant, and a cluster value was derived by summing all of the t-values of all data points in the cluster. Nonparametric permutation testing (10,000 permutations) was then used to derive a distribution of cluster values and the significance level of the observed clusters were tested directly using this distribution. Based on this analysis, the time-frequency periods that contained significant oscillatory events across all participants were subjected to beamforming analyses (i.e., the peri-movement beta activity). Further details of this method and our processing pipeline can be found in recent papers (62, 75, 143, 144).

MEG Source Imaging

Cortical oscillatory networks were imaged through the dynamic imaging of coherent sources (DICS) beamformer (145), which uses the cross-spectral density matrices to calculate source power for the entire brain volume. These images are typically referred to as pseudo-t

maps, with units (pseudo-t) that reflect noise-normalized power differences (i.e., active vs. passive) per voxel. Following convention, we computed noise-normalized, source power per voxel in each participant using baseline periods of equal duration and bandwidth (146). MEG preprocessing and imaging used the Brain Electrical Source Analysis (Version 7.0; BESA) software.

Normalized source power was computed over the entire brain volume per participant at $4.0 \times 4.0 \times 4.0$ mm resolution for the time-frequency periods identified through the sensor level analyses. Prior to statistical analysis, each participant's MEG data, which were coregistered to native space structural MRI prior to beamforming, were transformed into standardized space using the transform previously applied to the structural MRI volume and spatially resampled. The resulting 3D maps of brain activity were averaged across all participants to assess the neuroanatomical basis of the significant oscillatory responses identified through the sensor-level analysis. Source power was then extracted from peak voxels per time bin (i.e., planning and execution phases) and participant and underwent statistical modeling.

Isolation of Peripheral Blood Mononuclear Cells and Respiration Analysis

Whole blood was collected into EDTA tubes by venous puncture for all participants. Buffy coats were submitted to a Ficoll-Paque Plus (GE Healthcare) gradient centrifugation for isolation of the mononuclear fraction. Peripheral blood mononuclear cells (PBMC) were cryopreserved in Fetal Bovine Serum with 10% DMSO. Cells were thawed within 6 weeks of isolation and underwent assessment using the Seahorse XF96 Analyzer (Seahorse Bioscience) to quantify oxygen consumption rate (OCR) using the mitochondrial stress test assay. Specifically, PBMCs were plated at 500,000 cells/well and 3 OCR measurements were taken sequentially on 5-6 technical replicate wells prior to and upon serial injection of 3.5 μ M oligomycin (Sigma; complex V inhibitor), 1 μ M fluoro-carbonyl cyanide phenylhydrazone (FCCP; Sigma; mitochondrial oxidative phosphorylation uncoupler) and 14 μ M rotenone + 14 μ M antimycin A (Sigma; complex

I and III inhibitors, respectively) to evaluate measures of mitochondrial respiration including basal respiration, ATP-linked respiration, proton leak, maximal respiration, spare respiratory capacity (SRC) and non-mitochondrial respiration. All bioenergetic data were normalized to protein in the well for subsequent analyses. For data calculation, the Seahorse Wave software (v2.2.0) was used.

Quantification of the Redox Environment

Cellular levels of superoxide were assessed using Electron Paramagnetic Resonance (EPR) Spectroscopy of whole blood incubated with a superoxide-sensitive spin probe (1-hydroxy-3-methoxycarbonyl-1,2,2,5,5-tetramethylpyrrolidine: CMH) for 1 hour under physiologic conditions (37°C), as previously described (111). Specifically, immediately after sample collection, 200 μ M of CMH was reconstituted into EPR buffer (Krebs Hepes Buffer) supplemented with metal chelators (5 μ M sodium diethyldithiocarbamate trihydrate and 25 μ M deferoxamine) and incubated with 200 μ L of whole blood. EPR measurements were performed with a Bruker eScan EPR spectrometer (Bruker BioSpin GmbH, Rheinstetten/Karlsruhe, Germany), with the following parameters: field sweep width, 100.0 G; center field, 3482 G; microwave frequency, 9.75 kHz; microwave power, 1.10 mW; modulation amplitude, 5.94 G; conversion time, 10.24 ms; time constant, 40.96 ms. The resulting EPR spectra amplitude is expressed as arbitrary units (a.u.) that are directly proportional to the amount of total cellular superoxide in the sample.

Antioxidant activity levels were quantified in erythrocytes for key enzymatic and non-enzymatic contributors to the mitochondrial redox environment including superoxide dismutase (SOD), catalase, and glutathione. Specifically, we used the SOD Assay Kit-WST (DOJINDO, Inc.) to measure total SOD activity, the OxiSelect Catalase Activity Assay Kit (Cell Biolabs, Inc.) for catalase, and the GSSG/GSH Quantification kit (DOJINDO, Inc.) for total (tGSH), oxidized (GSSG) and reduced glutathione (GSH) according to the manufacturers' guidelines.

Statistical Analysis

To evaluate the predictive capacity of the mitochondrial redox environment on movement-related neural oscillations serving behavior, we conducted a group-based path analysis, which provides parameter estimates simultaneously for PLWH versus uninfected controls (all two-tailed p-values reported). Importantly, all statistical analyses were performed following standard data trimming procedures whereby measures that exceeded 2.5 standard deviations above or below the group's mean were excluded from subsequent analyses. Our primary hypotheses were that movement-related beta oscillatory activity during planning and execution phases of movement would predict task performance, and that these dynamics would be differentially modulated by the mitochondrial redox environment as a function of serostatus. Predictive capacities of each path were evaluated by direct comparisons of unstandardized coefficients in PLWH versus controls. In addition, we conducted a multiple mediation model whereby measures of mitochondrial function (i.e., spare respiratory capacity) predicted movement-related oscillations and subsequent behavioral performance through changes in the redox environment (i.e., superoxide, SOD, catalase, GSSG/tGSH ratio), for superoxide-sensitive and H₂O₂-sensitive paths, separately. Importantly, we examined the 95% confidence intervals of bias-corrected bootstrapped confidence intervals based on 1000 bootstrapped samples (147), which provides a robust estimate of asymmetrical mediation effects (148). All analyses were conducted with full information maximum likelihood estimation for missing data using MPlus (v.8.1).

Results:

Sequential Movement Performance

Following initial rejection of trials with anomalous performance (i.e., reaction times > 1250 ms; movement durations > 3000 ms), an average of 127 trials per participant remained for

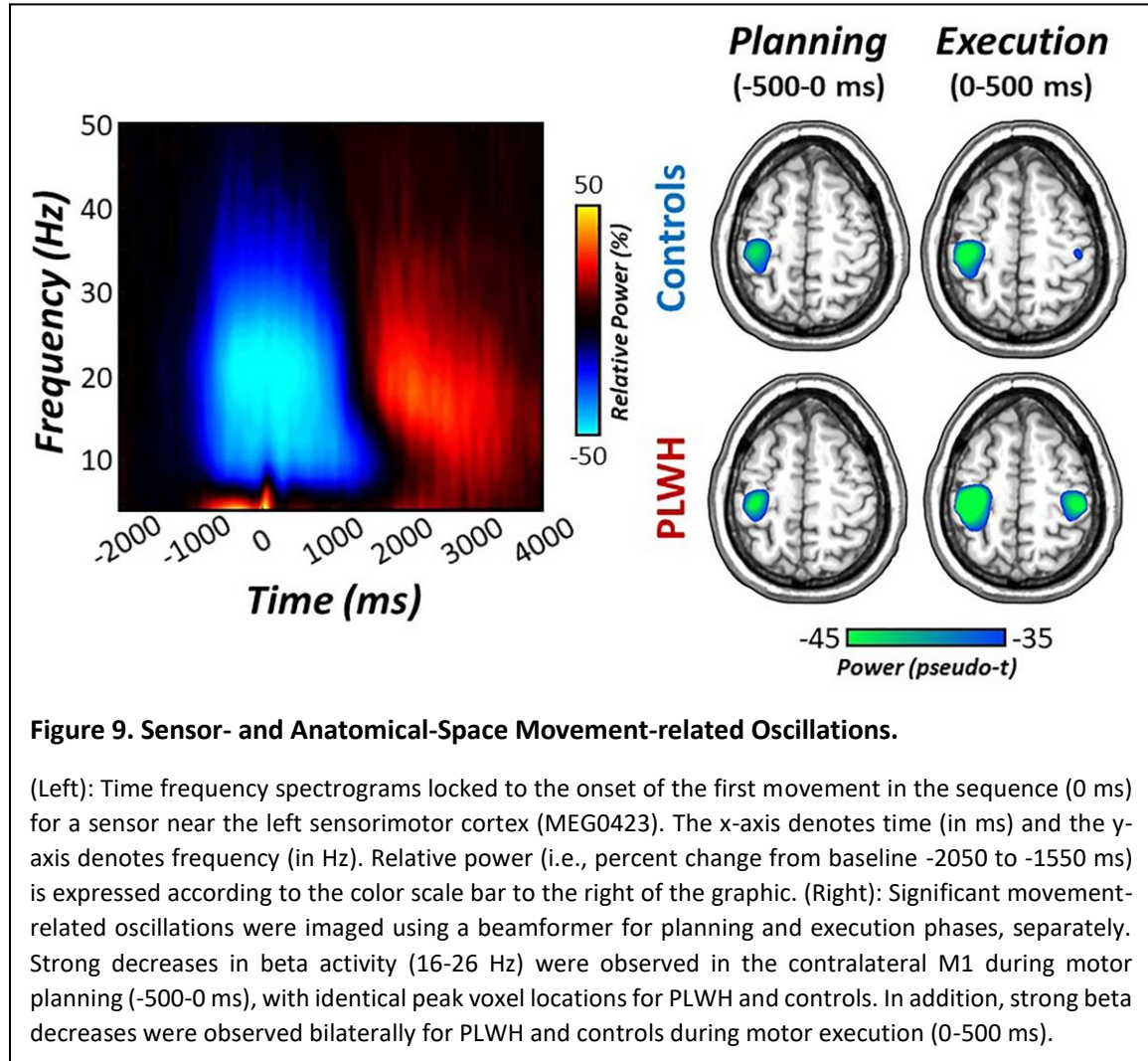
subsequent statistical modeling. Participants performed generally well on the task, with an average accuracy of 92.71% (Controls: $93.92 \pm 4.76\%$; PLWH: $91.41 \pm 10.81\%$), that did not differ as a function of group ($t(71) = -1.31, p = .195$). In contrast, reaction time (i.e., response time to the first button press) was significantly slower for PLWH (620.89 ± 224.24 ms) compared to uninfected controls (479.17 ± 139.76 ms; $t(71) = 3.27, p = .002$). Finally, movement duration (i.e., time to complete the entire motor sequence) did not significantly differ as a function of HIV infection (Controls: 831.44 ± 234.47 ms; PLWH: 907.74 ± 312.70 ms; $t(71) = 1.19, p = .240$).

MEG Sensor- and Source-level Analyses

Time-frequency analyses locked to the first movement in the sequence indicated significant peri- and post-movement oscillatory responses in gradiometers near the contralateral sensorimotor strip across all participants regardless of group ($p < .001$, Figure 9). Specifically, decreases in peri-movement beta activity (16-26 Hz) were observed prior to and following movement (i.e., -500 to 0 ms and 0 to 500 ms for planning and execution, respectively). In addition, we observed transient increases in theta oscillatory activity surrounding movement onset, while more sustained decreases during movement onset were observed in the alpha range (Figure 9). Finally, we observed post-movement increases in beta activity following motor execution. Given the known role of beta oscillations in motor planning, execution and behavioral performance, oscillatory responses in the theta and alpha range, as well as post-movement oscillations in the beta band did not undergo source reconstruction analyses, as they were outside the scope of the study.

To identify the neural origins of oscillations seen at the sensor level, planning and execution phases were imaged separately using a beamformer. The resulting maps indicated that pre-movement decreases in beta power were strongest in left M1 contralateral to movement (i.e., -500-0 ms, Figure 9), while more bilateral recruitment of beta power was demonstrated

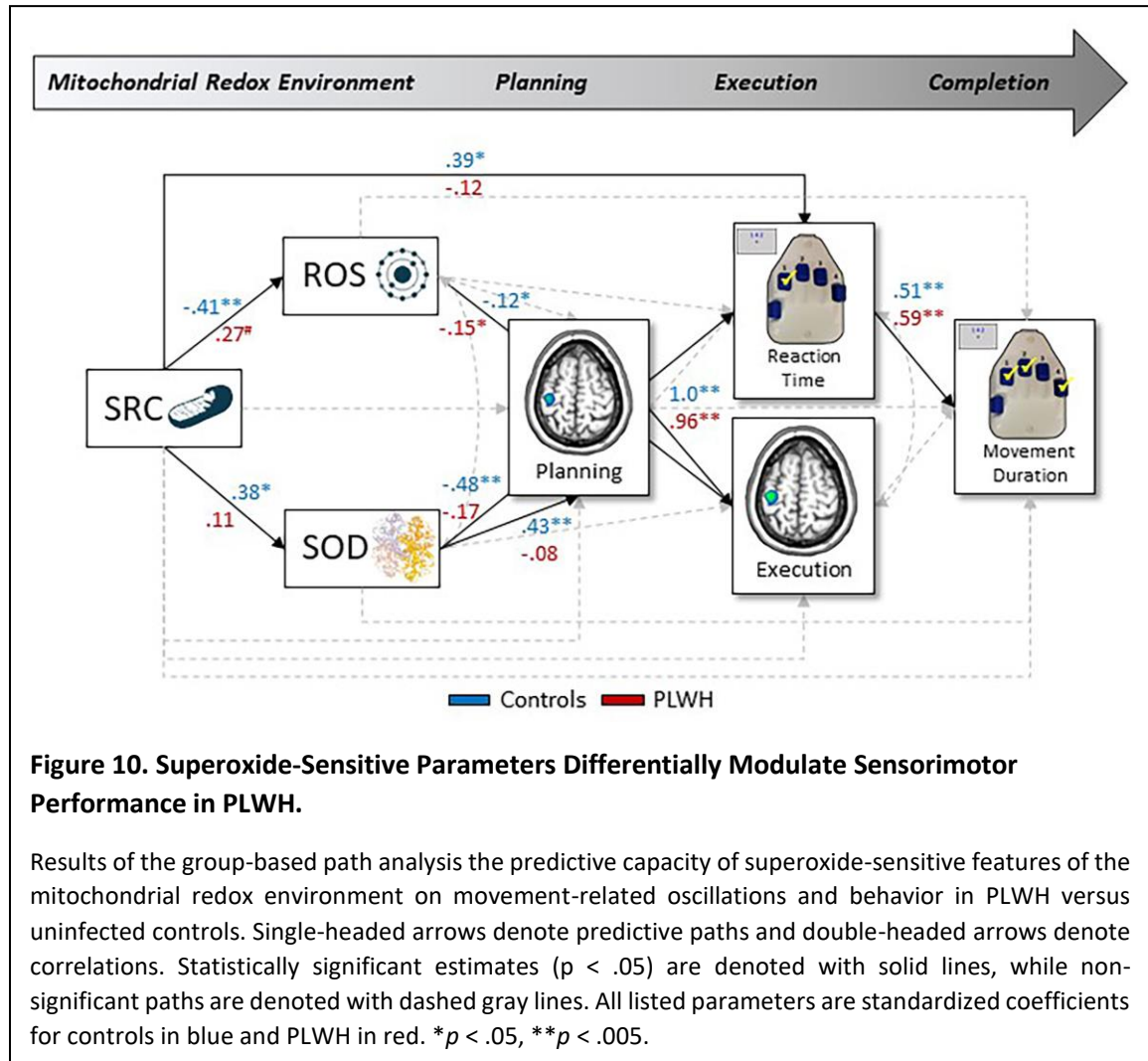
during the execution phase of movement (i.e., 0-500 ms), regardless of group. Peak voxel values (i.e., pseudo-t) were then extracted from the left M1 per time bin and underwent subsequent statistical modeling.



Superoxide-sensitive Redox Environments Mediate Brain-Behavior Dynamics in Controls, but not in PLWH

As described in the methods, we tested a multiple mediation model using a group-based path analysis to determine the direct effect of superoxide-sensitive features of the mitochondrial redox environment (i.e., SRC, superoxide, SOD) on brain-behavior relationships serving motor performance, which simultaneously calculated the effects for PLWH versus uninfected controls. In addition, direct comparisons of unstandardized coefficients were assessed per predictive path

to identify differences a function of group. Similar to our model described in Chapter 2, our brain-behavior relationships included paths whereby beta oscillatory activity during the planning period (-500 to 0 ms) predicted reaction time, as well as beta activity during motor execution (0 to 500 ms). Variables during planning and execution phases then predicted movement duration (i.e., time to complete the entire sequence). For a full model visualization, see Figure 10.



To begin, our participants exhibited a robust relationship between reaction time and movement duration on the task, such that faster responses to the first number in the sequence led to faster sequence completion times for PLWH ($\beta = .59, p < .001$) and uninfected controls ($\beta = .51, p = .001$). In addition, as expected, beta activity during the planning period strongly predicted

activity during the execution phase in the left M1 contralateral to movement in both groups (Controls: $\beta = 1.0$, $p < .001$; PLWH: $\beta = .96$, $p < .001$). Interestingly, while beta activity prior to movement did not significantly predict reaction time nor movement duration in either group ($ps > .109$), weaker beta decreases during motor execution were marginally predictive of faster sequence completion times in uninfected controls (i.e., movement duration; $\beta = -1.09$, $p = .065$), while PLWH did not exhibit this same relationship ($\beta = -.25$, $p = .628$).

In regard to superoxide-sensitive redox environments, uninfected controls exhibited a robust relationship between mitochondrial SRC, superoxide and its scavenger (SOD), such that decreases in SRC were associated with increased levels of cellular superoxide ($\beta = -.41$, $p = .005$), and reduced levels of total SOD activity ($\beta = .38$, $p = .013$). Contrary to these relationships in controls, PLWH only exhibited marginal associations among mitochondrial SRC and superoxide, such that increased mitochondrial energetic reserve was marginally associated with increased levels of superoxide ($\beta = .27$, $p = .087$). Importantly, these data suggest an immediate separable pattern of the influence of mitochondrial energetics on superoxide-sensitive redox parameters between PLWH and uninfected controls.

In regard to the influence of the mitochondrial redox environment on brain-behavior dynamics, we observed no direct effects of mitochondrial function on peri-movement oscillatory activity in the contralateral M1 ($ps > .105$), although decreases in SRC were predictive of faster reaction times in controls ($\beta = .39$, $p = .035$; Figure 8), and marginally predictive of slower movement durations in PLWH ($\beta = -.25$, $p = .078$). In contrast, we observed robust direct effects of the redox environment on brain-behavior relationships (Figure 10). Briefly, levels of cellular superoxide were robust predictors of beta activity during motor execution, while increased activity levels of superoxide's scavenger (i.e., SOD) were predictive of weaker planning-related responses in the left M1 and faster reaction times on the motor sequence task in uninfected

controls. In contrast, only cellular levels of superoxide were direct predictors of execution-related beta oscillations in PLWH, such that increased levels of superoxide were associated with stronger beta responses during motor execution ($\beta = -.15$, $p = .002$).

Next, we examined all potential mediating effects of the redox environment on mitochondrial-related changes in motor cortical dynamics and behavioral performance (Table 3). As described in the methods, statistical significance of indirect effects was determined by using bias-corrected bootstrapped confidence intervals (147, 148), thus exact p-values are not available for indirect effects. As discussed in Chapter 2, we observed five statistically significant indirect

Controls				PLWH			
Mitochondrial SRC to Movement Duration							
Path	Total	Direct	Indirect	Path	Total	Direct	Indirect
SRC→SOD→RT→MD	.13	.02	-.09*	SRC→SOD→RT→MD	-.41*	-.25	-.01
Mitochondrial SRC to Reaction Time							
SRC→SOD→RT	.16*	.39*	-.18*	SRC→SOD→RT	-.23	-.11	-.01
Mitochondrial SRC to Motor Execution							
SRC→EPR→Exec	-.13*	-.08*	.05*	SRC→EPR→Exec	.09	.01	-.04
SRC→SOD→Plan→Exec	-.13*	-.08*	.16*	SRC→SOD→Plan→Exec	.09	.01	-.09
Mitochondrial SRC to Motor Planning							
SRC→SOD→Plan	-.09	-.19*	.16*	SRC→SOD→Plan	.13	.14	-.01

Table 3. Results of the Group-based Superoxide-Sensitive Mediation Analyses using Structural Equation Modeling.

Indirect effects were assessed for statistical significance using the bias-corrected bootstrapped confidence intervals. Significant indirect effects are bolded for visualization. All reported parameters are standardized coefficients. **p* < .05.

effects ($p < .05$) for uninfected controls, which implicated levels of superoxide as strong mediators of bioenergetic-neural pathways involved in motor execution, while SOD activity mediated this change during the planning phase of movement (see Table 3). Further, we observed that superoxide-sensitive features of the redox environment and mitochondrial function together accounted for 34.9% of the variance in movement duration in healthy controls ($p < .001$).

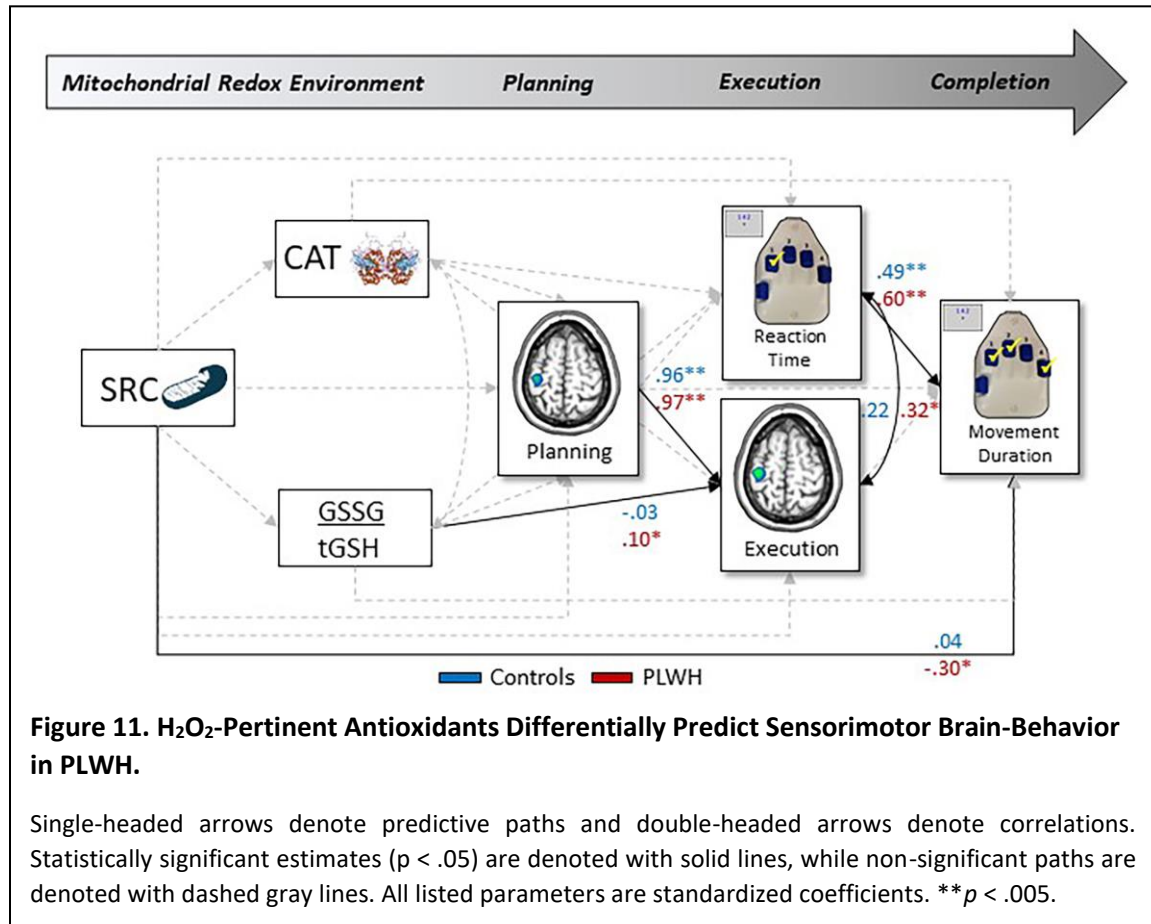
In contrast, we observed no mediating effects of the redox environment on these bioenergetic-neural pathways in PLWH, suggesting an uncoupling of the redox environment to

differentially modulate sensorimotor brain-behavior dynamics in PLWH (see Table 3). Nevertheless, we evaluated whether the predictive capacities of these relationships differed as a function of group by directly comparing the unstandardized coefficients associated with each path. Interestingly, this analysis confirmed significantly different predictive capacities of the relationships between mitochondrial SRC and superoxide ($\Delta b = 0.03$, $p = .005$), as well as SOD activity and planning-related beta responses in the left M1 ($\Delta b = -9.38$, $p = .031$) in PLWH versus uninfected controls. Importantly, these parameters sensitive to superoxide redox mechanisms in the system explained 52.8% of the variance in movement duration in virally-suppressed PLWH ($p < .001$).

H₂O₂-sensitive Pathways Predict Sensorimotor Brain-Behavior Dynamics in PLWH, but not Controls

Next, we evaluated the predictive capacity of H₂O₂-sensitive redox environments and mitochondrial function on brain-behavior relationships serving sensorimotor control using group-based path analyses. Importantly, our measures of the redox environment were now comprised of catalase activity and GSSG/tGSH ratios as continuous predictors of movement-related beta activity during motor planning and execution phases, as well as behavior on the task (see Figure 11 for model visualization). Similar to our superoxide-sensitive model, reaction time was a robust predictor of movement duration in both groups (Controls: $\beta = .49$, $p = .001$; PLWH: $\beta = .60$, $p < .001$; Figure 11). Likewise, planning-related decreases in M1 beta power predicted execution-related beta activity regardless of group (Controls: $\beta = .96$, $p < .001$; PLWH: $\beta = .97$, $p < .001$). Finally, in uninfected controls, weaker oscillatory activity during motor execution was marginally predictive of shorter movement completion times ($\beta = -.99$, $p = .068$), although this relationship was not present in PLWH ($p = .361$). As discussed in Chapter 2, we observed no direct effects of mitochondrial SRC nor H₂O₂-sensitive antioxidants on brain-behavior relationships serving motor

function in healthy controls (Figure 11). In addition, we observed no mediating effects of the redox environment between mitochondrial function, neural and behavioral indices (Figure 11).



In contrast, PLWH exhibited a direct effect of mitochondrial energetic capacity on movement duration ($\beta = -.30, p = .027$), such that decreased SRC was associated with longer time to complete the entire motor sequence. In addition, PLWH demonstrated a significant association among GSSG/tGSH ratios and execution-related beta decreases in the left M1 ($\beta = .10, p = .040$), such that an attenuated glutathione reducing capacities (i.e., higher GSSG/tGSH ratio) were associated with stronger beta decreases during motor execution in the contralateral M1 (Figure 11). Interestingly, while we observed no significant mediating effects of H₂O₂-pertinent redox parameters in PLWH, direct comparisons between the unstandardized coefficients of each path revealed significantly different predictive capacities between PLWH and uninfected controls in

the relationships among mitochondrial SRC and movement duration ($\Delta b = -55.66$, $p = .035$), as well as glutathione reducing capacity (i.e., GSSG/tGSH ratios) and movement execution ($\Delta b = 7.92$, $p = .041$), suggesting a differential coupling of these H_2O_2 -pertinent redox parameters with brain and behavior in PLWH versus their uninfected counterparts.

Discussion:

In the current study, we used advanced neurophysiology and systems biology approaches to determine the predictive capacity of the mitochondrial redox environment on sensorimotor brain-behavior dynamics in a large sample of virally-suppressed PLWH and demographically matched uninfected controls. Specifically, we observed differential effects of superoxide-sensitive redox parameters, such that in uninfected controls, increases in superoxide and SOD activity levels were robust predictors of execution-related and planning-related beta oscillations in the contralateral M1, respectively, while only intracellular levels of superoxide were strong predictors of execution-related beta power in PLWH. In addition, superoxide and SOD were strong mediators of the relationship between mitochondrial SRC and brain-behavior relationships serving motor control in seronegative participants, while we observed no mediating effects of the redox environment in PLWH, suggesting a bioenergetic-neural uncoupling as a function of serostatus. Finally, our data suggest H_2O_2 -sensitive mechanisms are direct modulators of sensorimotor neural dynamics in PLWH, but not in uninfected controls. Below, we discuss the implications of these novel findings for understanding the contribution of the mitochondrial redox environment in HIV-infection and sensorimotor function.

Our most important finding was likely the contribution of superoxide-sensitive parameters of the redox environment on brain-behavior relationships serving sensorimotor control in PLWH. As discussed previously, increases in SOD and superoxide were associated with weaker planning- and execution-related decreases in M1 beta power in uninfected controls,

respectively. In contrast, only intracellular levels of superoxide were predictors of execution-related neural oscillations in PLWH, such that elevated levels of superoxide were associated with stronger movement-related beta responses. In addition, decreases in mitochondrial SRC were marginally predictive of slower sequence completion times on the task in seropositive adults. This is an important distinction between normative and pathological systems, as in uninfected controls, these results coincided with a well-established pattern of brain-behavior dynamics that typically serve healthy motor function.

Essentially, weaker M1 beta responses during the planning period were predictive of weaker beta power during motor execution and subsequent better task performance (i.e., faster movement durations (125, 160)). However, this relationship among beta power in the contralateral M1 and behavior was absent in PLWH and further, our data suggest that disparate increases in superoxide and decreases in mitochondrial energetic capacity (i.e., SRC) led to less optimal oscillatory-behavioral profiles (i.e., stronger beta decreases, worse performance on the task, respectively). However, it is important to note that our lack of relationship between M1 beta oscillatory dynamics and behavior in PLWH could be attributable, at least in part, to the fact that we interrogated the oscillatory dynamics within M1, as opposed to other regions that comprise the extended sensorimotor network. In fact, numerous studies suggest that the parietal cortices are superior predictors of sequence-related motor performance above and beyond M1-involvement alone (60, 143, 161, 162). This is also corroborated by the notion that PLWH typically exhibit a greater degree of activation relative to uninfected controls in association cortices (i.e., prefrontal and parietal cortices) during more complex tasks, often reflecting a mechanism employed by seropositive adults to compensate for less efficient neural systems to achieve task demands (41–44). Thus, the study of beta oscillations within the parietal cortices may provide

unique insight into motor sequence performance and importantly, its differential modulation by the mitochondrial redox environment in seropositive adults.

The notion that superoxide-sensitive redox parameters are pertinent to sensorimotor function is not new, although this line of research has only been interrogated in animal models. Essentially, using SOD knockout models (i.e., cytosolic isoforms of SOD), investigators have genetically mutated SOD in the system, which leads to dramatic depletions in antioxidant activity and subsequent increases in superoxide, giving rise to a host of motor deficits observed most commonly in animal models of neurodegeneration (e.g., amyotrophic lateral sclerosis) (91–93). Importantly, while our data suggest that healthy systems (i.e., uninfected controls) exhibit mechanistic increases in superoxide and SOD to serve *better* brain-behavior profiles in humans, deficient mitochondrial respiration and alternatively, increases in superoxide were associated with less optimal brain-behavior dynamics serving sensorimotor function PLWH, perhaps reflective of redox-regulated neurodegenerative properties emerging in seropositive adults. This relationship between mitochondrial bioenergetics and sensorimotor brain and behavioral function was also robustly mediated by levels of superoxide and SOD in healthy controls, while no mediating effects were observed in PLWH. The lack of bioenergetic-neural coupling in PLWH may be attributable, at least in part, to the disparate predictive capacities of the redox environment observed between our groups. Essentially, we observed that deficiencies in the bioenergetic capacity of the mitochondria (i.e., reduced SRC) were related to decreased levels of superoxide in PLWH, which contradicts prior work in cART-treated and treatment-naïve humans (101), albeit this result was not surprising (see Chapter 1) and could be related to the cellular composition of our PBMC samples (101). Nevertheless, this pattern of findings points to dissociable, rather than dependent, mechanisms by which superoxide and mitochondrial respiration modulate brain and

behavior in PLWH, as opposed to the robust coupling of the mitochondrial redox environment to modulate brain-behavior dynamics in the seronegative population.

Finally, we observed a direct modulation of sensorimotor oscillatory dynamics by H_2O_2 -pertinent antioxidants in the system in PLWH, which was not present in seronegative controls. Briefly, in virally-suppressed PLWH, attenuated glutathione reducing capacities (i.e., higher GSSG/tGSH ratios) were associated with stronger beta decreases in the contralateral M1 during motor execution and importantly, direct comparisons of unstandardized coefficients revealed disparate predictive capacities of this relationship between PLWH and uninfected controls. This result was not surprising, as a depletion in peripheral glutathione levels has long been revered as a key marker of oxidative stress in HIV-infection (114, 116, 117), and was related to sub-optimal oscillatory recruitment (i.e., stronger beta responses) in the present study. Importantly, this study expands upon prior work, as the distinction between oxidizing, reducing and total forms of glutathione (i.e., GSSG, GSH, tGSH, respectively) had yet to be examined. This is unfortunate, as the study of distinct oxidative properties of glutathione provides unique insight into the reducing capacity of peroxides in the system above and beyond absolute levels of this cofactor alone. Nevertheless, it is important to note that future work will undoubtedly benefit from the direct quantification of H_2O_2 , along with the H_2O_2 -sensitive scavengers as measured in the current study to better understand the link between H_2O_2 redox mechanisms and sensorimotor function in PLWH.

In conclusion, our study was the first to directly quantify features of mitochondrial function and the redox environment to the oscillatory neural dynamics serving motor control in virally-suppressed PLWH and uninfected controls. Importantly, our results provided evidence for a differential modulation of both superoxide- and H_2O_2 -sensitive redox pathways on M1 beta oscillatory activity and motor sequence performance in PLWH, while only superoxide-sensitive

features modulated brain-behavior dynamics in uninfected controls. However, future studies directly quantifying levels of H_2O_2 in the system will be of utmost importance, as the current study now sheds light on the involvement of H_2O_2 -pertinent redox parameters in pathological sensorimotor function. In addition, we observed disparate trajectories by which mitochondrial respiration predicted changes in the redox environment in PLWH versus uninfected controls. Importantly, our data suggest separable mechanisms of action among the mitochondria and superoxide-sensitive redox parameters in PLWH, as opposed to the dependency of the redox environment on bioenergetic-neural relationships in the seronegative population. Future work will benefit from the direct quantification of these redox parameters within the mitochondria (e.g., mitochondrial origin of SOD: MnSOD and superoxide levels from isolated mitochondria), to support the notion of mitochondrial-induced bioenergetic uncoupling present in HIV-infected adults. Alternatively, evaluating other cellular sources of ROS (e.g., NOX enzymes (120)) and their relation to the superoxide redox environment as measured in the current study will be critical to fully unravel the origin of redox-regulated neural oscillatory profiles in PLWH. Nevertheless, our data suggest that blood-based markers of mitochondrial function and the redox environment serve as important modulators of beta oscillatory dynamics serving motor control in both healthy and pathological systems and further, may serve as targets for remedying more severe forms of motor and cognitive dysfunction in PLWH in the future.

CHAPTER 4. CLINICAL MARKERS OF HIV PREDICT REDOX-REGULATED NEURAL AND BEHAVIORAL FUNCTION IN THE SENSORIMOTOR SYSTEM

Introduction:

HIV-infection is now a chronic but manageable condition, with people living with HIV (PLWH) living longer than ever before thanks to effective and stable regimens of combination antiretroviral therapy (cART). However, prolonged longevity often coincides with a host of age-related comorbidities including cognitive and behavioral dysfunction that remain a major concern in seropositive populations, even in the modern cART era. In fact, approximately 35-70% of all PLWH develop some form of cognitive impairment (i.e., HIV-associated neurocognitive disorder: HAND) (3–7), with the most common abnormalities first manifesting as deficits in motor control (e.g., gait, coordination, strength, motor dexterity) (19–22). This is an important consideration, as motor deficits likely contribute to higher-order cognitive symptoms and will profoundly impact the functional dependence PLWH experience as they grow older. In addition to age, important risk factors for developing neurocognitive impairment and overall poorer prognoses also include clinical measures pertinent to HIV such as CD4 nadir (i.e., lowest lifetime CD4+ T-cell count), time since diagnosis and delay of cART initiation. For example, CD4+ T-cells are important indicators of immune system stability, as their levels substantially decrease immediately upon infection (32, 33) and further, lower CD4 nadir values have been directly linked to accelerated aging phenotypes (e.g., DNA methylation) and the risk for developing neurocognitive impairment in PLWH (35–37, 163). Thus, the evaluation of relevant clinical and demographic factors (e.g., HIV-related clinical metrics, age) that may contribute to the motor dysfunction seen in PLWH is incredibly important.

Beyond pertinent age- and disease-related markers of HIV-infection that may contribute to functional decline are the underlying neural and molecular mechanisms that give rise to behavioral changes in PLWH. For example, prior work has demonstrated a role for mitochondrial function (e.g., oxygen consumption, ATP production) and associated redox interactions (e.g.,

generation of reactive oxygen species (ROS) and engagement of antioxidant defenses) in regulating neuronal function (78, 82, 87, 88, 92, 128–130) and in turn, behavioral performance (88, 91, 93, 94), albeit its role in *human* neurophysiology and behavior is less well understood. In regard to HIV-infection, previous studies by our lab and others have characterized features sensitive to both superoxide (e.g., intracellular superoxide, superoxide dismutase (SOD)) and hydrogen peroxide (H_2O_2 ; e.g., catalase, glutathione) redox systems and generally, these studies suggest that mitochondrial respiration decreases in seropositive adults, indicative of a reduced energetic capacity of the mitochondria that is concomitant with elevations in superoxide ((101), see Chapter 1). In contrast, antioxidants pertinent to the mitochondrial redox environment (i.e., SOD, catalase, glutathione) have demonstrated discrepant trajectories as a function of serostatus, although this could largely be attributable to differences in sample characteristics across studies (e.g., sample size, cART treatment regimens) ((114–117), see Chapter 1).

In regard to the brain, recent work by our lab has provided evidence for a redox-regulated neural oscillatory profile that differentially predicts motor function in health and disease (i.e., HIV-infection). Briefly, volitional movement requires a rich, multispectral recruitment of population-level neural oscillatory activity during planning, execution and termination phases of movement in a distributed sensorimotor network, particularly in the beta band (e.g., 15-30 Hz). The study of beta oscillations in motor control are particularly important, as peri-movement beta decreases have been shown to be pertinent to movement planning and selection factors (55, 57, 60–63), scale in magnitude with participant characteristics (e.g., chronological age, neurodegeneration (76, 125–127, 164–166)), and are intimately tied to behavioral performance (60, 125, 143, 167–170). Concerning HIV-infection, our previous work suggests that beta power during planning and execution phases of movement are differentially modulated by the mitochondrial redox environment (Chapter 3). In uninfected controls, our data suggest that increases in superoxide

and its scavenger (i.e., SOD) are robust predictors of more optimal neural oscillatory response profiles serving motor control (i.e., weaker beta responses during movement, faster reaction times, shorter movement durations), and further, fully mediate the relationship between mitochondrial function, neural and behavioral metrics (Chapter 2). In contrast, superoxide levels and mitochondrial energetic capacities demonstrated separable (rather than dependent) associations with beta activity in the contralateral M1 and motor performance, indicative of an uncoupling of bioenergetic-neural pathways in PLWH (Chapter 3). Importantly, while Chapters 2 and 3 provided novel insight regarding the role of the mitochondrial redox environment in sensorimotor brain-behavior dynamics in humans, the precise factors contributing to the disruption in HIV-related bioenergetic-neural sensorimotor pathways is not clear.

To this end, we enrolled 69 virally-suppressed PLWH and used advanced systems biology and neurophysiology approaches to evaluate the contribution of key demographic and HIV clinical markers on the bioenergetic-neural-behavioral pathways shown to be disrupted in PLWH (Chapter 3). Specifically, we used Seahorse Analyzer of mitochondrial stress tests to assess mitochondrial respiration in real time, Electron Paramagnetic Resonance (EPR) Spectroscopy of whole blood to quantify intracellular superoxide levels, antioxidant activity assays and magnetoencephalography (MEG) to directly quantify beta oscillatory activity during a sequential movement task. In addition, we used structural equation modeling to evaluate the effect of HIV clinical markers (i.e., CD4 nadir, exposure time: time since diagnosis—time on cART) and chronological age on the pathway by which the mitochondrial redox environment differentially predicts planning- and execution-related M1 beta oscillations and behavioral performance, sequentially.

Methods:

Participant Demographics

Sixty-nine HIV-infected adults ($M_{\text{age}} = 45.3$ years old, range: 21-65 years) were enrolled in the current study. All PLWH were receiving effective cART and had viral suppression defined as <50 copies/mL. Exclusion criteria included any medical illness affecting CNS function (except HIV), any psychiatric or neurological disorder, history of head trauma, current pregnancy, and current substance use. For a comprehensive list of HIV-relevant clinical metrics, see Table 4. The University of Nebraska Medical Center Institutional Review Board approved the study and all participants provided written informed consent.

<i>Demographics (Mean \pm SD)</i>	
N	69
Age (yrs)	45.3 \pm 13.0
Sex (% males)	81.2
Handedness (% right handed)	89.9
Education (yrs)	13.8 \pm 2.5
BMI	29.6 \pm 6.1
CD4 Nadir (cells/ μ L)	264 \pm 220
Current CD4 (cells/ μ L)	755 \pm 354
Time since diagnosis (yrs)	13.4 \pm 9.2
Time on ART (yrs)	11.0 \pm 7.7
Exposure Time (yrs)	2.9 \pm 5.6

Table 4. HIV-infected Participant Demographics and Clinical Metrics.

Experimental Paradigm

Participants were seated in a nonmagnetic chair with their head positioned within the MEG helmet-shaped sensor array. Participants were initially asked to fixate on a crosshair for 3750 ms (\pm 350 ms), followed by a presentation of three numbers for 500 ms, each corresponding to a finger on the hand (Figure 5). Upon the presentation of a visual cue (i.e., numbers turning blue), participants were asked to tap the fingers corresponding to the numbers sequentially and given 2250 ms to complete the movement. A total of 160 trials were completed, making the overall recording time approximately 17 minutes.

For each participant, reaction time (RT: the time to respond to the first number in the sequence) and movement duration (MD: the time to complete the entire motor sequence) data were extracted for each trial and incorrect trials were excluded from all analyses. In addition, individual trial data was initially rejected based on behavioral performance metrics that exceeded a standard threshold that would ultimately impact MEG data analyses (i.e., RT > 1250 ms and MD > 3000 ms). The remaining RT and MD data was then averaged per participant and subjected to subsequent statistical analyses using structural equation modeling.

MEG Data Acquisition and Coregistration with Structural MRI

All recordings were performed in a one-layer magnetically-shielded room with active shielding engaged for environmental noise compensation. With an acquisition bandwidth of 0.1-330 Hz, neuromagnetic responses were sampled continuously at 1 kHz using an MEGIN/Elektta MEG system (MEGIN, Helsinki, Finland) with 306 magnetic sensors, including 204 planar gradiometers and 102 magnetometers. Throughout data acquisition, participants were monitored using a real-time audio-video feed from inside the magnetically-shielded room. MEG data from each participant were individually corrected for head motion and subjected to noise reduction using the signal space separation method with a temporal extension (140). Each participant's MEG data were coregistered with their structural T1-weighted MRI data prior to imaging analyses using BESA MRI (Version 2.0). Structural MRI data were aligned parallel to the anterior and posterior commissures and transformed into standardized space. After beamformer analysis (see below), each subject's functional images were transformed into standardized space using the transform that was previously applied to the structural MRI volume and spatially resampled.

MEG Preprocessing and Sensor-Level Statistics

Cardiac and ocular artifacts were removed from the data using signal-space projection (SSP) and the projection operator was accounted for during source reconstruction (141). Epochs

of 6150 ms duration were defined (i.e., -2050 to 4100 ms) with 0 ms defined as movement onset and the baseline being the -2050 to -1550 ms window. Initially, we rejected trials based on having a reaction time longer than 1250 ms or taking more than 3000 ms to complete the entire motor sequence, which would disrupt the baseline period. Next, epochs containing artifacts were rejected based on a fixed threshold method, supplemented with visual inspection. On average, 130 trials per participant were used for further analysis.

Artifact-free epochs were transformed into the time-frequency domain using complex demodulation (142), and the resulting spectral power estimations per sensor were averaged over trials to generate time-frequency plots of mean spectral density. The sensor-level data per time-frequency bin were normalized using the mean power per frequency during the -2050 to -1550 ms baseline period. The specific time-frequency windows used for imaging were determined through a two-stage, data-driven approach involving statistical analysis of the sensor-level spectrograms across all participants and trials. First, paired-sample t-tests against baseline were conducted on each data point, with the output spectrogram of t-values initially thresholded at $p < .05$ to define time-frequency bins containing potentially significant oscillatory deviations. To reduce the risk of false positive results due to multiple comparisons, the time-frequency bins that survived that initial threshold were temporally and/or spectrally clustered with neighboring bins that were also significant, and a cluster value was derived by summing all of the t-values of all data points in the cluster. Nonparametric permutation testing (10,000 permutations) was then used to derive a distribution of cluster values and the significance level of the observed clusters were tested directly using this distribution. Based on this analysis, the time-frequency periods that contained significant oscillatory events across all participants were subjected to beamforming analyses (i.e., the peri-movement beta activity). Further details of this method and our processing pipeline can be found in recent papers (62, 75, 143, 144).

MEG Source Imaging

Cortical oscillatory networks were imaged through the dynamic imaging of coherent sources (DICS) beamformer (145), which uses the cross-spectral density matrices to calculate source power for the entire brain volume. These images are typically referred to as pseudo-t maps, with units (pseudo-t) that reflect noise-normalized power differences (i.e., active vs. passive) per voxel. Following convention, we computed noise-normalized, source power per voxel in each participant using baseline periods of equal duration and bandwidth (146). MEG preprocessing and imaging used the Brain Electrical Source Analysis (Version 7.0; BESA) software.

Normalized source power was computed over the entire brain volume per participant at $4.0 \times 4.0 \times 4.0$ mm resolution for the time-frequency periods identified through the sensor level analyses. Prior to statistical analysis, each participant's MEG data, which were coregistered to native space structural MRI prior to beamforming, were transformed into standardized space using the transform previously applied to the structural MRI volume and spatially resampled. The resulting 3D maps of brain activity were averaged across all participants to assess the neuroanatomical basis of the significant oscillatory responses identified through the sensor-level analysis. Source power was then extracted from peak voxels per time bin (i.e., planning and execution phases) and participant and underwent statistical modeling.

Isolation of Peripheral Blood Mononuclear Cells and Respiration Analysis

Whole blood was collected into EDTA tubes by venous puncture for all participants. Buffy coats were submitted to a Ficoll-Paque Plus (GE Healthcare) gradient centrifugation for isolation of the mononuclear fraction. Peripheral blood mononuclear cells (PBMC) were cryopreserved in Fetal Bovine Serum with 10% DMSO. Cells were thawed within 6 weeks of isolation and underwent assessment using the Seahorse XF96 Analyzer (Seahorse Bioscience) to quantify oxygen consumption rate (OCR) using the mitochondrial stress test assay. Specifically, PBMCs

were plated at 500,000 cells/well and 3 OCR measurements were taken sequentially on 5-6 technical replicate wells prior to and upon serial injection of 3.5 μ M oligomycin (Sigma; complex V inhibitor), 1 μ M fluoro-carbonyl cyanide phenylhydrazone (FCCP; Sigma; mitochondrial oxidative phosphorylation uncoupler) and 14 μ M rotenone + 14 μ M antimycin A (Sigma; complex I and III inhibitors, respectively) to evaluate measures of mitochondrial respiration including basal respiration, ATP-linked respiration, proton leak, maximal respiration, spare respiratory capacity (SRC) and non-mitochondrial respiration. All bioenergetic data were normalized to protein in the well for subsequent analyses. For data calculation, the Seahorse Wave software (v2.2.0) was used.

Quantification of the Redox Environment

Cellular levels of superoxide were assessed using Electron Paramagnetic Resonance (EPR) Spectroscopy of whole blood incubated with a superoxide-sensitive spin probe (1-hydroxy-3-methoxycarbonyl-1-2,2,5,5-tetramethylpyrrolidine: CMH) for 1 hour under physiologic conditions (37°C), as previously described (111). Specifically, immediately after sample collection, 200 μ M of CMH was reconstituted into EPR buffer (Krebs Hepes Buffer) supplemented with metal chelators (5 μ M sodium diethyldithiocarbamate trihydrate and 25 μ M deferoxamine) and incubated with 200 μ L of whole blood. EPR measurements were performed with a Bruker eScan EPR spectrometer (Bruker BioSpin GmbH, Rheinstetten/Karlsruhe, Germany), with the following parameters: field sweep width, 100.0 G; center field, 3482 G; microwave frequency, 9.75 kHz; microwave power, 1.10 mW; modulation amplitude, 5.94 G; conversion time, 10.24 ms; time constant, 40.96 ms. The resulting EPR spectra amplitude is expressed as arbitrary units (a.u.) that are directly proportional to the amount of total cellular superoxide in the sample.

Antioxidant activity levels were quantified in erythrocytes for key enzymatic and non-enzymatic contributors to the mitochondrial redox environment including superoxide dismutase (SOD), catalase, and glutathione. Specifically, we used the SOD Assay Kit-WST (DOJINDO, Inc.) to

measure total SOD activity, the OxiSelect Catalase Activity Assay Kit (Cell Biolabs, Inc.) for catalase, and the GSSG/GSH Quantification kit (DOJINDO, Inc.) for total (tGSH), oxidized (GSSG) and reduced glutathione (GSH) according to the manufacturers' guidelines.

Statistical Analysis

To evaluate the contribution of clinically-relevant HIV markers and age on the bioenergetic-neural-behavioral pathway outlined as aberrant in Chapter 3, we used structural equation modeling in a larger sample (~2x) of virally-suppressed PLWH. Specifically, we evaluated the predictive capacity of CD4 nadir (i.e., the lowest lifetime CD4+ T-cell count) and HIV exposure time (i.e., time since diagnosis – time on cART; time PLWH were not virally suppressed) as independent measures of HIV disease history while controlling for participant age. Our primary hypotheses were that CD4 nadir and exposure time would differentially modulate the path by which the mitochondrial redox environment predicts neural dynamics and motor function, sequentially. Further, we anticipated that clinical HIV metrics would be unique predictors of bioenergetic-neural pathways above and beyond the effects of age alone. For comparison with previous studies discussed in this document, parameters pertinent to superoxide and H₂O₂ were examined separately. We evaluated all potential mediating effects by examining the 95% confidence intervals of bias-corrected bootstrapped confidence intervals based on 1000 bootstrapped samples (147) to provide a robust estimate of asymmetrical mediation effects. All analyses were conducted with full information maximum likelihood estimation for missing data using MPlus (v.8.1).

Results:

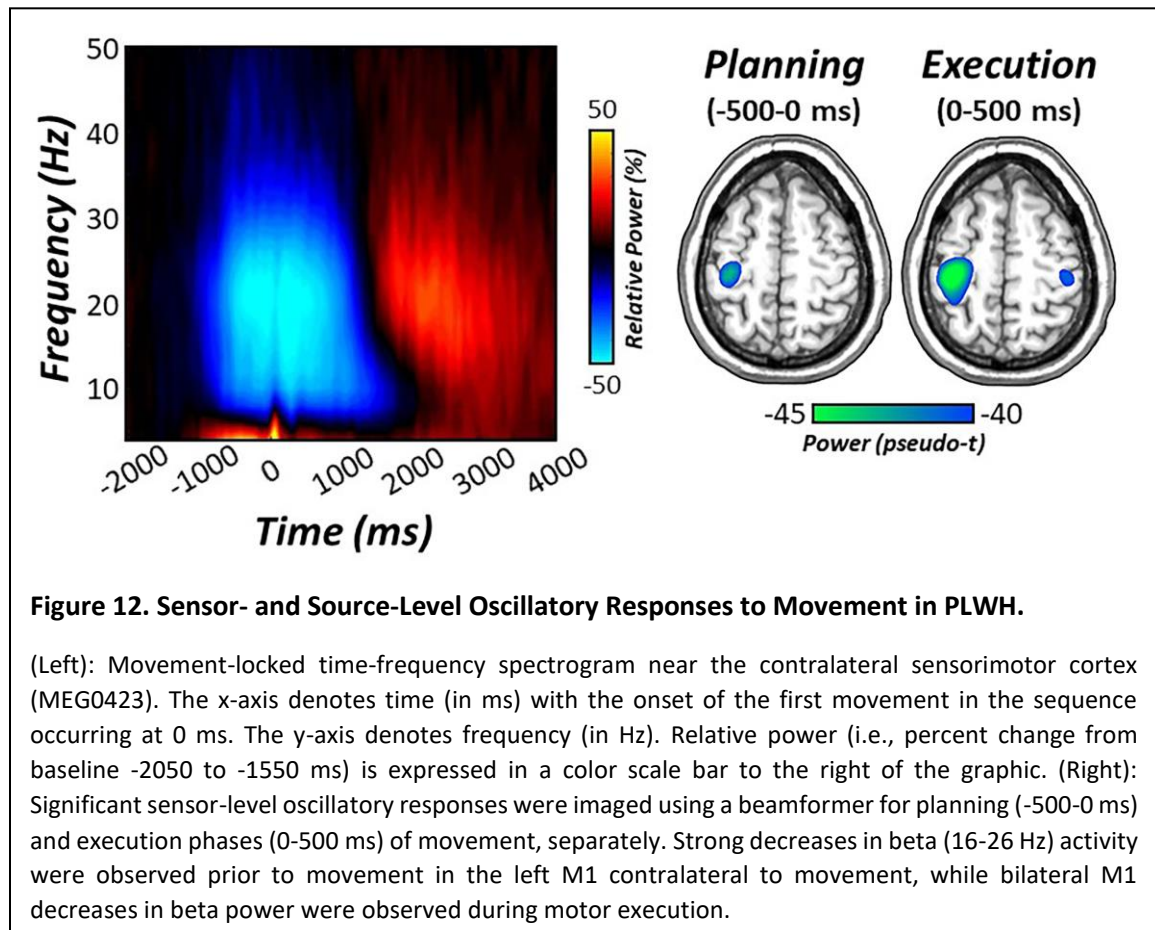
Sequential Movement Performance

First, individual trials were rejected based on anomalous performance (i.e., reaction times > 1250 ms; movement durations > 3000 ms). In this sample, an average of 130 trials per

participant remained for subsequent statistical modeling. Participants performed generally well on the task, with an average accuracy of $90.81 \pm 10.98\%$. Likewise, average reaction time was 566.90 ± 202.72 ms, while the time to complete the entire motor sequence was 888.44 ms on average (± 280.08 ms), which corresponds well with our previous reports in normative and clinical populations ((60), Chapters 2,3).

MEG Sensor- and Source-level Analyses

Statistical analysis of time-frequency spectrograms near the sensorimotor cortex revealed significant peri-movement beta oscillatory activity (16-26 Hz) during planning (i.e., -500-0 ms) and execution phases (i.e., 0-500 ms; $p < .001$, Figure 12). In addition, we observed peri-movement increases and decreases in oscillatory activity surrounding movement onset (for theta and alpha, respectively), while more sustained post-movement increases in beta activity followed



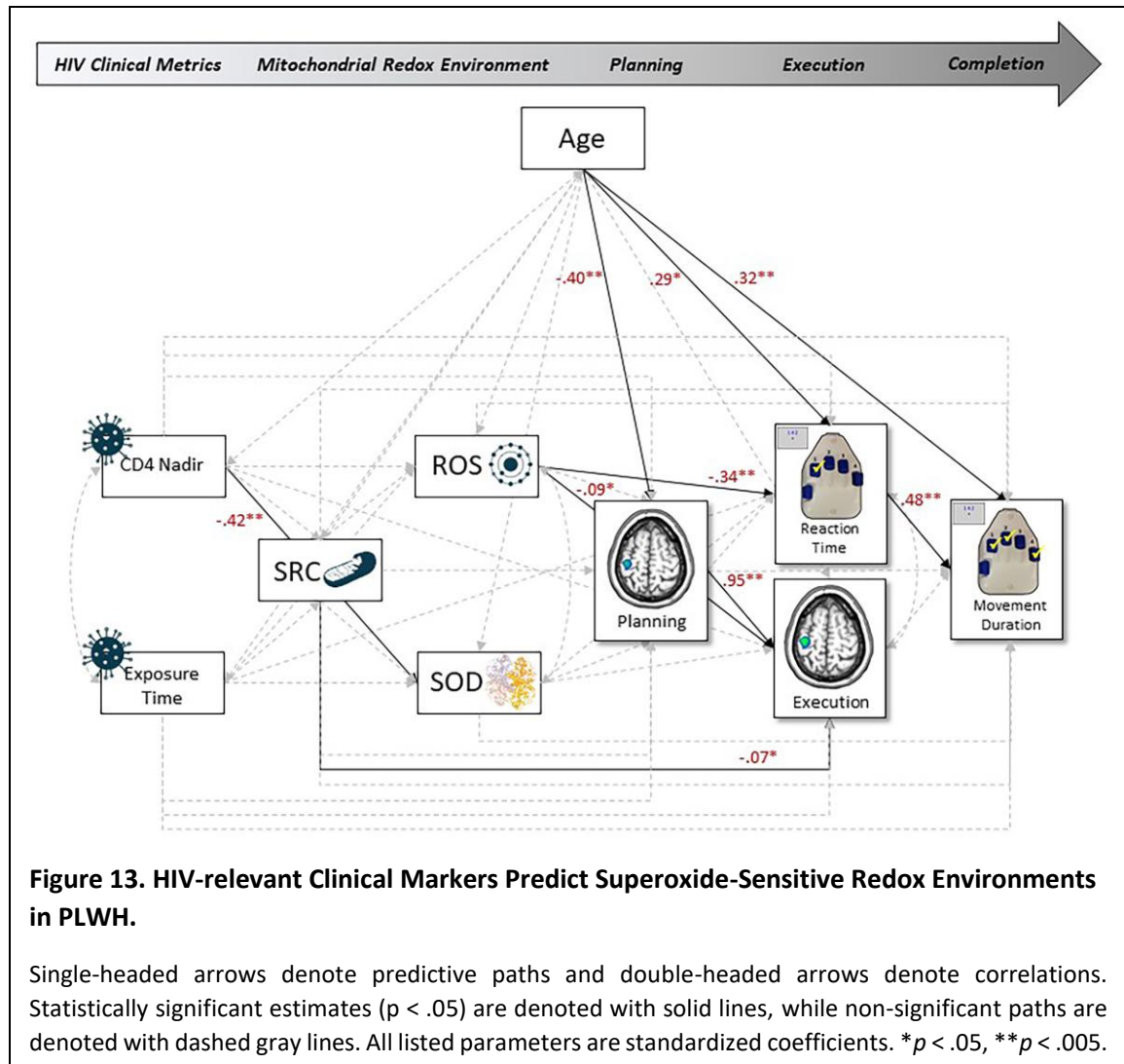
motor execution. However, we focused our analyses on peri-movement oscillations in the beta range given the known contribution of this activity to motor planning and execution, as well as behavioral performance.

To identify the neural origins of significant sensor-level time-frequency clusters, planning and execution windows in the beta range were imaged separately using a beamformer. The resulting maps indicated that robust decreases in beta power prior to movement were the strongest in left M1 contralateral to movement (i.e., -500-0 ms, Figure 12), while more bilateral recruitment of beta power was present during the execution phase of movement (i.e., 0-500 ms; Figure 12). Peak voxel values (i.e., pseudo-t) were then extracted from the left M1 per time bin and underwent subsequent statistical modeling.

Clinical Measures of HIV Disease Status Predict Superoxide-Sensitive Bioenergetic-Neural Changes in Behavior

As described in the methods, we tested a multiple mediation structural equation model to determine the direct effect of clinical HIV metrics (i.e., CD4 nadir and exposure time) and age on superoxide-sensitive features of the mitochondrial redox environment (i.e., SRC, superoxide, SOD) and brain-behavior relationships serving motor performance, sequentially. Importantly, this approach simultaneously controlled for the effects of age in our large sample. For a full model visualization, see Figure 13.

As expected, we observed robust relationships between reaction time and movement duration ($\beta = .48, p < .001$), that was preceded by a strong coupling of planning- and execution-related beta power in the contralateral M1 ($\beta = .95, p < .001$), although peri-movement beta activity did not significantly predict reaction time nor movement duration on the task ($ps > .145$). However, increasing age significantly predicted stronger planning-related decreases in M1 beta power ($\beta = -.40, p = .001$), as well as worse performance on the task (reaction time: $\beta = .29, p = .029$; movement duration: $\beta = .32, p = .004$).



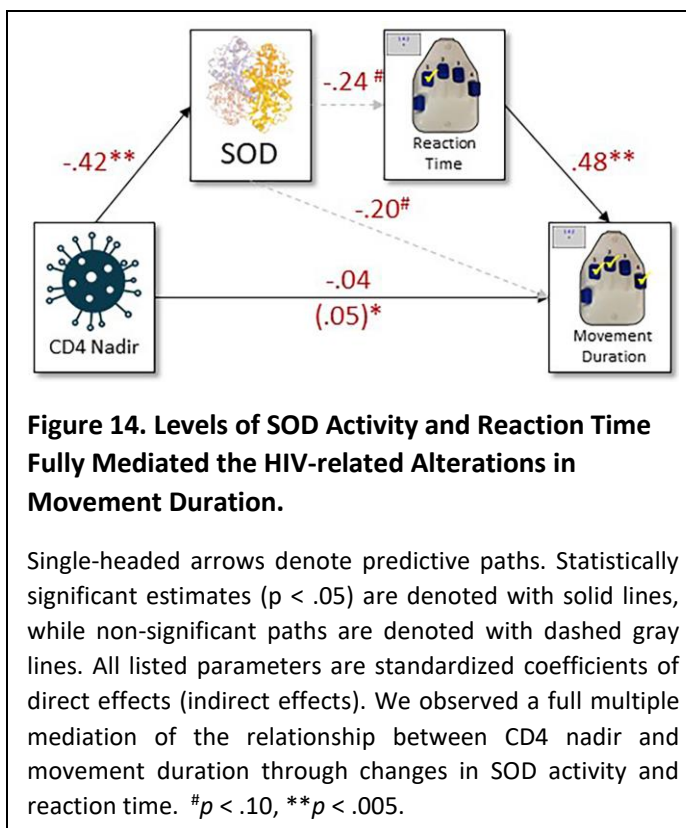
In regard to superoxide-sensitive mitochondrial redox environments, PLWH exhibited no direct effects of mitochondrial energetic capacity on levels of superoxide nor SOD activity ($ps > .103$), although an imbalance of the redox environment was trending in HIV-infected adults, as increased levels of superoxide were marginally associated with attenuated SOD activity ($\beta = -.28$, $p = .055$). In regard to their influence on brain-behavior dynamics, we observed a direct effect of mitochondrial SRC on motor execution oscillatory responses in the contralateral M1 ($\beta = 0.07$, $p = .050$), such that decreases in SRC were associated with stronger movement-related beta activity during motor execution. In addition, we observed direct effects of the redox environment on brain-behavior relationships (Figure 13). Specifically, increased levels of superoxide were

associated with stronger execution-related beta activity in the left M1 ($\beta = -.09, p = .014$), as well as faster reaction times on the task ($\beta = -.34, p = .007$), while elevated levels of SOD activity were marginally predictive of both faster response times ($\beta = -.24, p = .082$) and total sequence completion times on the task ($\beta = -.20, p = .067$).

Next, we evaluated whether clinical HIV metrics were modulators of the bioenergetic-neural pathway above and beyond the effects of age alone. Interestingly, HIV exposure time was marginally predictive of movement duration, such that greater time exposed to HIV without effective cART was associated with worse performance on the task ($\beta = .17, p = .065$). In contrast, CD4 nadir (i.e., the lowest CD4 count ever reported) was robustly predictive of SOD activity levels, such that lower CD4 nadir (indicative of poorer clinical outcomes) was associated with currently elevated levels of total SOD activity ($\beta = -.42, p < .001$). Importantly, CD4 nadir and HIV exposure time were not associated with one another ($\beta = .03, p = .823$), nor participant age (CD4 nadir and age: $\beta = -.09, p = .485$; exposure time and age: $\beta = .18, p = .151$), suggesting that these metrics are indeed independent proxies of HIV disease status and have unique effects on this pathway above and beyond the effects of age alone.

Finally, we examined all potential mediating effects of the mitochondrial redox environment on disease-related changes in motor cortical dynamics and behavioral performance by determining the statistical significance of indirect effects by using bias-corrected bootstrapped confidence intervals (147, 148). Interestingly, we observed a full multiple mediation of the relationship between CD4 nadir and movement duration through levels of SOD activity and RT ($\beta_{\text{indirect}} = .05, b_{\text{indirect}} = 8.77, 95\% \text{ CI } [1.49, 31.06]$). Essentially, historically lower CD4 nadir counts were associated with currently elevated activity levels of SOD in the system, which led to faster reaction times ($\beta = -.24, p = .082$) and subsequently faster movement durations ($\beta = .48, p < .001$).

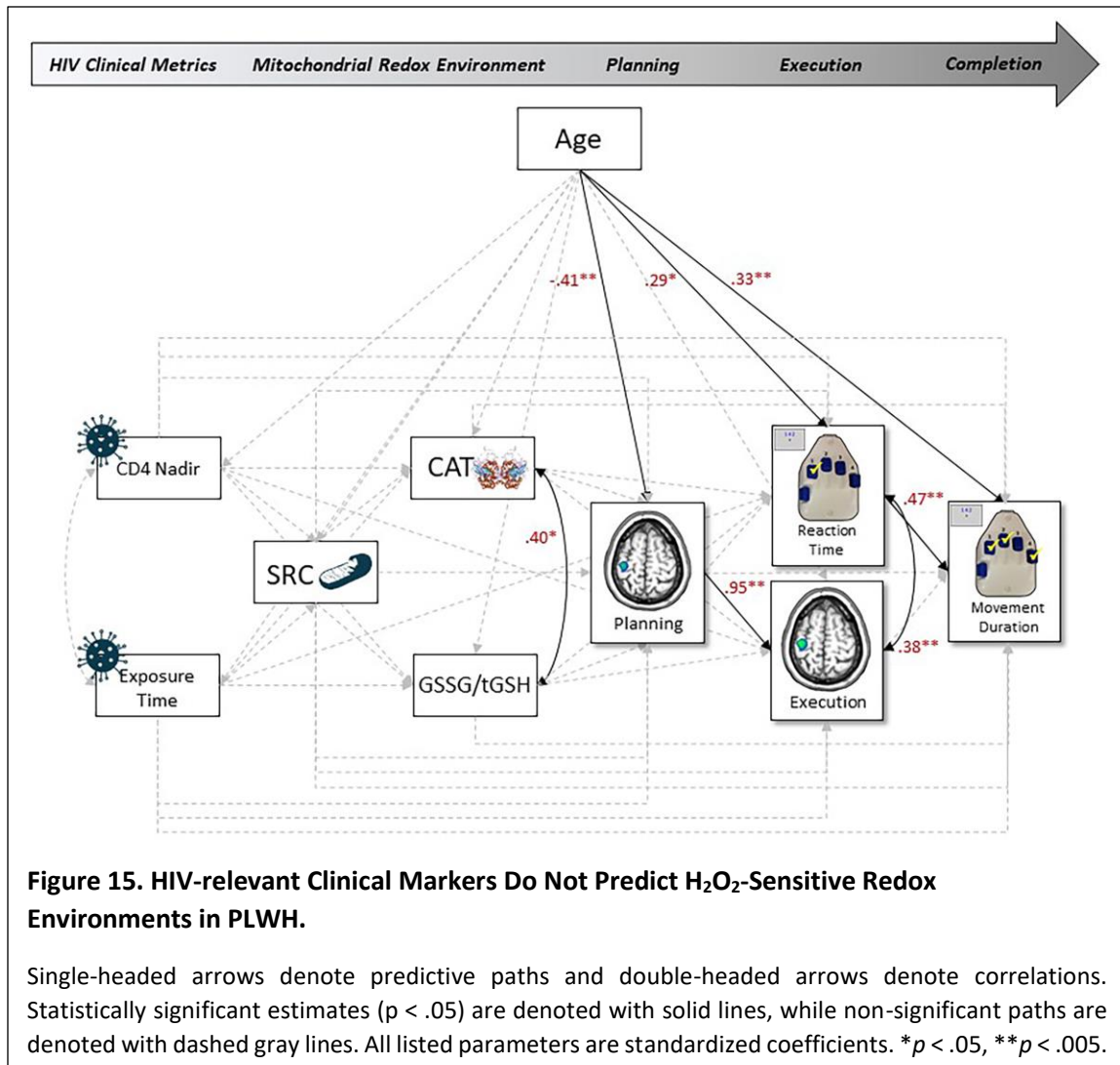
as assessed in their current state of effective viral suppression (Figure 14). In contrast, we observed no mediating effects of superoxide-sensitive redox parameters (i.e., SRC, superoxide, SOD) on the relationship between HIV exposure time, neural and behavioral metrics. Similarly, there were no mediating effects on the age-related change in motor function observed in the current study (i.e., stronger



planning-related beta decreases: $\beta = -.40$, $p = .001$, slower reaction times: $\beta = .29$, $p = .029$, longer movement durations: $\beta = .32$, $p = .004$). Taken together, clinical HIV metrics and the mitochondrial redox environment accounted for 55.7% of the variance in movement duration in virally-suppressed PLWH.

H₂O₂-Pertinent Redox Parameters are Not Modulated by HIV Clinical Characteristics

Finally, to evaluate the predictive capacity of age and HIV clinical markers on bioenergetic-neural-behavioral pathways serving motor function, we conducted a path analysis using the same regression equation described above. However, in this model, our measures of the redox environment now comprised antioxidants important for scavenging H₂O₂ (i.e., catalase activity and glutathione reducing capacity (GSSG/tGSH ratios)). For a full model visualization, see Figure 15. As with the first model, reaction time was a significant predictor of movement duration ($\beta = .47$, $p < .001$; Figure 15), such that faster reaction times were associated with shorter time to



complete the entire motor sequence. This was preceded by a robust coupling between planning- and execution-related beta oscillations in the contralateral M1 ($\beta = .95$, $p < .001$). However, movement-related beta oscillations in M1 were not predictive of behavior ($ps > .157$).

Unlike our model evaluating features of superoxide redox systems, clinical HIV metrics were not significant predictors of H₂O₂-pertinent redox parameters, nor brain-behavior relationships in PLWH while controlling for age (Figure 15). In contrast, as expected, age was significantly associated with planning-related decreases in beta power and behavior, such that increasing age was associated with stronger beta responses ($\beta = -.41$, $p = .001$), as well as slower reaction times ($\beta = .29$, $p = .041$) and longer total movement completion times ($\beta = .33$, $p = .004$).

Finally, we observed no direct nor mediating effects of mitochondrial function and H₂O₂-pertinent redox parameters on the relationship between HIV clinical metrics or age on neural and behavioral metrics.

Discussion:

In the present study, we evaluated the contribution of important demographics and clinical HIV risk factors on the bioenergetic-neural-behavioral pathways underlying motor control in a large sample of virally-suppressed PLWH. Specifically, we observed differential effects of superoxide-, but not H₂O₂-sensitive redox systems on the neural dynamics serving motor function in PLWH. In addition, historical measures of immune stability (i.e., CD4 nadir) and duration of compromise (i.e., exposure time) demonstrated dissociable effects on this pathway, above and beyond the aging process alone. Finally, peripheral antioxidant scavengers (i.e., SOD) fully mediated the relationship between lowest lifetime CD4+ T-cell counts and current behavioral performance, perhaps indicative of persistent oxidative environments serving behavior in the presence of virologic suppression in HIV. The implications of these novel findings are discussed below.

Our most important finding was likely the effect of clinically-relevant HIV risk factors on redox-regulated neural dynamics and behavioral performance in PLWH. Specifically, HIV exposure time had marginal effects on behavior, such that longer times exposed to HIV without being virally suppressed were associated with longer movement durations on the task. This relationship, although marginal in the current study, was not surprising, as HIV disease duration and delayed initiation of cART have demonstrated relationships with the risk for developing neurocognitive impairment despite current virologic suppression. For example, studies have shown that longer durations exposed to HIV prior to cART leads to shorter life expectancies, progression and/or fluctuation in HAND stage, and the development of non-AIDS related comorbidities (e.g., vascular

diseases) (38, 171–173). This may be attributable, at least in part, to the stage of immune compromise that individuals experience upon infection, as low levels of CD4+ T-cell counts that are sustained in the absence of virologic suppression remain one of the best predictors of clinical degradation and poorer prognoses in PLWH (7, 35, 36, 173). Of note, clinical metrics reliant on parameters such as HIV duration (i.e., exposure time) can be somewhat unreliable, as the exact timepoint of transmission is often unknown by patients (174), thus future studies are needed to replicate and confirm these findings.

In addition to HIV exposure time, lower CD4 nadir (i.e., worse immune response) was related to currently elevated SOD activity in the periphery. Further, levels of SOD activity were full mediators of the relationship between CD4 nadir and behavior on the task, such that historically lower levels of CD4 nadir were associated with increased levels of SOD activity, which were related to subsequently faster reaction times and movement durations on the task. This finding may seem counterintuitive at first glance but considering the dynamic interactions between immune responses and redox environments may help clarify this mechanism. Essentially, upon response to infections and pathogens, immune cell mitochondria shift their role as primary producers of energy to the purposeful generators of ROS (e.g., superoxide) in the system. In turn, the excessive production of ROS, and engagement of the redox environment (i.e., increased antioxidant defenses) contribute to downstream processes to fight invading pathogens and promote inflammation (84–86, 99). Thus, we propose that this mitochondrial-induced “oxidative burst” that occurs during acute infection in HIV may lead to substantial increases in antioxidants important for scavenging superoxide in the system (e.g., SOD), which compensates for chronically elevated levels in response to infection with HIV, and these elevations are sustained even through viral suppression (175). In turn, the currently elevated levels of SOD that have persisted are related to better functioning in cART-treated individuals included in the current study.

Importantly, this hypothesis is speculative, and future studies would greatly benefit from evaluation of redox parameters in PLWH at early stages of infection, as well as at numerous longitudinal follow-ups to support this conclusion of persistently elevated oxidative environments serving behavioral performance in the modern cART era. Alternatively, this relationship could also be linked to excessive H_2O_2 in the periphery of PLWH. As the direct result of the superoxide-SOD scavenging reaction is H_2O_2 , elevations in total SOD activity and superoxide of PLWH would inherently produce more H_2O_2 in the environment ((118), see Chapter 1), which could also be an important mediator of the relationship between historically-pertinent HIV immune stability and behavior, rather than superoxide-dependent mechanisms alone.

Another important finding of the current study confirms the role of superoxide-sensitive redox parameters in modulating the neural dynamics serving motor function in PLWH, as opposed to H_2O_2 -pertinent antioxidants in the system. Briefly, we observed direct effects of levels of superoxide on motor cortical beta oscillations during motor execution and behavioral performance, such that increased levels of superoxide were associated with stronger beta responses in the contralateral M1, and also faster reaction times on the task. In addition, decreases in mitochondrial SRC were also associated with stronger execution-related beta responses in the contralateral M1. Finally, current elevations in total SOD activity were marginally related to faster reaction times and shorter movement completion times on the task. These results align well with prior studies by our lab, which demonstrated direct, but separable effects of mitochondrial function and superoxide-sensitive parameters on sensorimotor brain-behavior dynamics in PLWH and uninfected controls (see Chapters 2 and 3), albeit the current study expands upon prior work and suggests that elevations in superoxide redox parameters are also associated with better motor performance on the motor sequence task, which had yet to be established. This discrepancy could be attributable to sample size differences, as the current study

is nearly 2x larger than previous reports (Chapter 3). In contrast to superoxide-pertinent mechanisms in PLWH, we observed no direct nor mediating effects of H_2O_2 -sensitive redox parameters on sensorimotor brain-behavior dynamics. Similarly, neither clinical HIV risk factors nor age significantly predicted subsequent pathways. However, the direct quantification of H_2O_2 will be essential to clarify the importance of H_2O_2 redox systems in this pathway.

Finally, we observed no effects of age on mitochondrial function nor superoxide- and H_2O_2 -sensitive redox systems in PLWH, which was surprising, as there is extensive literature implicating a mitochondrial-induced redox imbalance in aging systems (79–81, 88, 93–95). Although recent evidence suggests that PLWH exhibit premature or accelerated aging phenotypes (34, 104, 176), our data suggest that peripheral mitochondrial and redox parameters as measured in the current study were not dependent on the aging process. In fact, HIV-relevant clinical markers that were related to bioenergetic-neural-behavioral pathways were not related to age, suggesting that alterations in this path are specific to HIV disease status. In contrast, we observed robust effects of age on beta oscillations during motor planning and behavior on the task, such that increasing age was associated with stronger planning-related beta responses, slower reaction times and longer movement durations, which aligns well with prior work in the healthy aging motor system (125, 127). Taken together, these data suggest that clinical HIV risk factors and age exhibit separable mechanisms of action to modulate sensorimotor brain and behavioral function, with redox biology being especially pertinent to HIV-related modulation of motor function, rather than age-dependent mechanisms in the system.

In conclusion, the current study was the first to identify the role of important demographic and clinical HIV risk factors in the bioenergetic-neural-behavioral pathway serving sensorimotor function in virally-suppressed PLWH. Importantly, our results provided evidence for a preferential modulation of superoxide-regulated neural and behavioral profiles by clinical HIV

risk factors, above and beyond the effects of age alone. Similarly, the relationship between historically lower levels of CD4+ T-cells and behavior were fully dependent on levels of SOD activity in the periphery, which is not surprising given the wealth of literature implicating SOD deficiencies to numerous clinical pathologies and behavioral dysregulation (90–93), albeit our findings suggest that currently *elevated* levels of total SOD activity were predictive of *better* motor function. This discrepancy could be attributable to persistently elevated oxidative environments induced by acute infection with HIV, but are not necessarily detrimental when individuals are effectively virally-suppressed. Nevertheless, future studies directly quantifying levels of H_2O_2 , as well as conducting longitudinal studies of redox status in acute and chronic HIV-infection will be profoundly important to clarify the role of SOD in clinically-modulated behavioral performance. Finally, our results suggest that aging produces dissociable effects on brain and behavioral function in PLWH, which may not rely on the redox profile. To close, our findings suggest that clinical parameters pertinent to HIV disease status are direct modulators of the bioenergetic-neural-behavioral pathway underlying motor function, while controlling for participant age. This is an important consideration regarding the ever-growing population of aging adults with HIV and suggests that disease-related risk factors are better predictors of current redox, neural and behavioral profiles, which may provide effective proxies for other instances of chronic inflammation (e.g., neurodegenerative diseases) and related functional decline in the future.

CONCLUSIONS

These studies are the first to support the notion that mitochondrial function and associated redox environments modulate *human* neurophysiological function and behavior, and that these parameters have dissociable mechanisms of action for modulating planning- and execution-related neural dynamics serving motor function in health and disease. Importantly, this work not only expands our knowledge regarding sensorimotor processing and behavior in HIV-infection, a disease that presents first and most commonly with motor deficits despite effective cART, but illuminates potential targets for therapeutic intervention in other instances of chronic inflammation and neurocognitive dysfunction in the future (e.g., healthy aging, Alzheimer's disease, Parkinson's disease).

In regard to the healthy motor system, we found that peripheral markers sensitive to superoxide, rather than H_2O_2 , were predictive of more optimal planning- and execution-related neural responses in the contralateral M1 and better behavioral performance, sequentially. These patterns of findings coincided with a well-established relationship between M1 beta oscillations and behavior in humans, such that weaker beta responses during motor execution are related to faster sequence completion times on the task (125). In addition, we observed a dynamic coupling of the bioenergetic-neural-behavioral pathway through discrete elevations in superoxide and SOD (Chapter 2). Together, these results suggest that more *optimal* brain-behavioral profiles of motor function (i.e., weaker beta responses, faster reaction times, shorter movement durations) were related to *increases* in peripheral oxidative environments (i.e., superoxide and SOD), which aligns well with prior work suggesting that *depletions* in these metrics lead to behavioral *decrements* in animal models of disease (91–93, 177). Furthermore, these data provide support for the notion that ROS and associated antioxidant defenses are not merely byproducts of mitochondrial metabolism, but have direct influences on neurophysiology and behavior, which has now been

extended to humans. Importantly, the differential effects of SOD and superoxide on planning- and execution-related activity in the brain provide support for the study of neural oscillatory dynamics at the sub-second level using MEG, as opposed to other functional neuroimaging techniques with coarser temporal resolutions that may otherwise obscure these effects (e.g., fMRI).

In contrast, PLWH exhibited dissociable effects of mitochondrial function and redox interactions on the neural dynamics serving motor performance. First, unlike healthy controls, PLWH did not exhibit relationships between M1 neural activity and behavior on the task. This was unexpected, but could be attributable to the notion that an extended sensorimotor network is recruited in instances of complex or sequential motor performance (60, 143, 161, 162), thus examining regions directly outside of M1 (e.g., parietal cortices) may better index complex motor control in HIV-infection. In regard to the redox environment, we found that increases in superoxide, as well as attenuated glutathione reducing capacities were predictive of stronger execution-related beta responses in the contralateral M1, while mitochondrial respiratory capacities were related to worse behavioral outcomes (i.e., longer movement durations; Chapter 3). In addition, neither superoxide nor H_2O_2 redox systems mediated the relationship between mitochondrial, brain or behavioral metrics, suggesting a bioenergetic-neural-behavioral uncoupling present in instances of chronic HIV-infection. Of note, future studies would greatly benefit from the evaluation of other measures of mitochondrial function known to be disrupted in PLWH (e.g., basal respiration, ATP-linked respiration; see Chapter 1). As the mitochondria are known to work through numerous mechanisms to modulate neuronal function and in turn, behavior in animals (e.g., changes in mitochondrial motility, morphology, ATP production (78, 82, 87, 88)), the evaluation of other parameters pertinent to mitochondrial physiology beyond the influence of spare respiratory capacities alone, may illuminate alternative bioenergetic-redox coupling mechanisms that better index sensorimotor brain-behavior dynamics in PLWH. Finally,

we found that clinical measures of HIV disease status preferentially predicted motor function through discrete elevations in the redox environment (i.e., SOD), while demographic characteristics (i.e., age) did not demonstrate this relationship (Chapter 4). These findings provide novel insight regarding the effect of virally-suppressed HIV-infection on motor cortical and behavioral dynamics, and suggest that the reliance on redox parameters to modulate behavior as evidenced in previous studies (Chapter 3) is specific to HIV-infection itself, above and beyond age-related functional alterations alone.

Mechanistically, the influence of mitochondrial function and redox status on population-level neural oscillations in M1 could be attributable, at least in part to changes in GABAergic inhibitory interneuronal pools. Briefly, the majority of the signal recorded by MEG is comprised of summated magnetic fields surrounding active populations of pyramidal cells (178). Recent neurophysiological studies suggest that the modulation of pyramidal cells and further, population-level oscillations are driven by GABAergic input. This interneuronal drive has been shown to give rise to numerous spectral profiles including higher frequency beta and gamma oscillations (132, 134, 149–151), especially within motor and visual networks (72, 137, 138, 152, 153). In regard to mitochondrial redox biology, the generation of higher frequency oscillators requires enormous amounts energy in the brain (78, 129, 130), and pharmacologically manipulating superoxide and H_2O_2 -sensitive features of this environment has direct consequences on the integrity of inhibitory interneuronal pools (e.g., interneuronal pool degradation, decreased parvalbumin expression) in animal models (128). Thus, we propose that the mitochondrial redox-regulated mechanisms observed in the current studies could be acting through modulation of GABAergic inhibitory interneuronal pools to modify the strength of population-level neural oscillations in the beta range. Notably, the indices of redox status as measured in the current study were extracted from peripheral sources. However, prior work has

found that there is good correspondence between bioenergetic indices derived from the periphery (e.g., PMBC) and those measured in the brain (e.g., isolated neuronal mitochondria) (139), as well as other highly metabolically active tissues (e.g., skeletal muscle) (179), which suggests that peripheral, blood-based markers of mitochondrial function and redox biology may provide effective proxies for *systemic* changes in the redox environment. Future work in this area will be invaluable to fully unravel the nature of bioenergetic-oscillatory coupling in the sensorimotor cortices.

Finally, the current studies undoubtedly illuminate the precursors important for modulating sensorimotor neural and behavioral profiles in health and disease, which may serve as effective targets to help ameliorate aging- and disease-related declines in the future. *En masse*, our studies suggest that parameters sensitive to superoxide in the system (i.e., intracellular superoxide levels and total SOD activity) were the best, and most consistent predictors of motor function (Chapters 2, 3 and 4), such that increases in these features were predictive of more optimal brain-behavior profiles in healthy controls, while they had divergent effects in PLWH. The notion that redox parameters may serve as effective therapeutic targets for disease is not new, as clinical trials using cocktails of naturally occurring antioxidants or mimetics have been readily employed in various populations (e.g., cancer, hypertension, neurodegeneration) (180–182). However, most of these trials have yielded disappointing results, as the administration of antioxidant therapies is quite nuanced, and investigators must consider numerous experimental factors such as the antioxidant profile, pharmacological dosage, cellular target, and the mechanism of action. For example, in our study, we observed that increases in superoxide and SOD were evident in PLWH (Chapter 1), which led to downstream alterations in neural-behavioral profiles (e.g., stronger beta responses during motor execution, see Chapter 3 and 4). While it may seem intuitive to employ antioxidant therapies to remedy increases in ROS, our studies confirmed

the involvement of *total* SOD activity, which comprises each mammalian isoform of SOD, as opposed to the mitochondrial origin alone. Future work will benefit from the direct quantification of mitochondrial-SOD to corroborate the current findings, but also to confirm the cellular target (i.e., extracellular or mitochondrial) that would be necessary for therapeutic intervention. In addition, many of the clinical trials to date have utilized physiologically-irrelevant doses of antioxidants, as well as inaccurate antioxidant profiles due to availability limitations, which greatly increases the probability of trial failure in patient populations.

In conclusion, our studies suggest that elevations in redox parameters are not necessarily detrimental to the system (e.g., in healthy systems and HIV, see Chapters 2 and 4), as previously proposed in theories such as the mitochondrial free radical theory of aging (79–81). This was in direct opposition with our hypotheses based on aging- and disease-related mitochondrial-induced redox imbalances in the system. In fact, despite aberrations in redox profiles and mitochondrial energetics present in PLWH, parameters of the redox environment disparately predicted better behavioral outcomes in the presence of virologic suppression (Chapter 4). While speculative, this could be attributable to elevated oxidative environments that have persisted since their inception upon HIV transmission, which have since normalized to serve “healthier” motor function when patients are effectively virally-suppressed. This is an important distinction that could be the result of our sample’s characteristics, as individuals with comorbidities known to affect neural, behavioral or redox parameters (e.g., substance abuse) were excluded from the current studies. However, future work quantifying these parameters in the context of these comorbid presentations may clarify these mechanisms, and better generalize to the diverse HIV-infected population as a whole, especially regarding those with more severe forms of neurocognitive impairment whom were not included in these series of studies. Nevertheless, the current studies demonstrate the promise of integrating data across systems biology and neurophysiological

methods for understanding the mechanisms and pathways underlying neural and behavioral function in humans. Finally, the study of relatively healthy, virally-suppressed PLWH not only expands our knowledge of these mechanisms on motor function in the context of chronic infection that has since been immunologically-normalized (i.e., cART-treated individuals), but also provides the foundation for groundbreaking new studies in adults with neurological disorders or those with chronic inflammation that present with motor, cognitive and behavioral aberrations (e.g., Parkinson's disease, Alzheimer's disease, healthy aging).

BIBLIOGRAPHY

1. A. Antinori, *et al.*, Updated research nosology for HIV-associated neurocognitive disorders. *Neurology* **69**, 1789–99 (2007).
2. L. A. Cysique, B. J. Brew, Neuropsychological functioning and antiretroviral treatment in HIV/AIDS: a review. *Neuropsychol Rev* **19**, 169–85 (2009).
3. R. K. Heaton, *et al.*, HIV-associated neurocognitive disorders persist in the era of potent antiretroviral therapy: CHARTER Study. *Neurology* **75**, 2087–96 (2010).
4. R. K. Heaton, *et al.*, HIV-associated neurocognitive disorders before and during the era of combination antiretroviral therapy: differences in rates, nature, and predictors. *J Neurovirol* **17**, 3–16 (2011).
5. K. R. Robertson, *et al.*, The prevalence and incidence of neurocognitive impairment in the HAART era. *AIDS* **21**, 1915–21 (2007).
6. S. Simioni, *et al.*, Cognitive dysfunction in HIV patients despite long-standing suppression of viremia. *AIDS* **24**, 1243–50 (2010).
7. D. Saylor, *et al.*, HIV-associated neurocognitive disorder — pathogenesis and prospects for treatment. *Nature Reviews Neurology* **12**, 15 (2016).
8. A. Kamkwala, P. Newhouse, Mechanisms of Cognitive Aging in the HIV-Positive Adult. *Curr Behav Neurosci Rep* **4**, 188–197 (2017).
9. L. Varatharajan, S. A. Thomas, The transport of anti-HIV drugs across blood-CNS interfaces: summary of current knowledge and recommendations for further research. *Antiviral Res* **82**, A99-109 (2009).
10. W. G. van Gorp, J. P. Baerwald, S. J. Ferrando, M. C. McElhiney, J. G. Rabkin, The relationship between employment and neuropsychological impairment in HIV infection. *J Int Neuropsychol Soc* **5**, 534–9 (1999).
11. R. K. Heaton, *et al.*, The impact of HIV-associated neuropsychological impairment on everyday functioning. *J Int Neuropsychol Soc* **10**, 317–31 (2004).
12. R. M. Kaplan, *et al.*, Validity of the Quality of Well-Being Scale for persons with human immunodeficiency virus infection. HNRC Group. HIV Neurobehavioral Research Center. *Psychosom Med* **57**, 138–47 (1995).
13. S. M. Albert, *et al.*, Neuropsychologic impairment in early HIV infection. A risk factor for work disability. *Arch Neurol* **52**, 525–30 (1995).
14. R. K. Heaton, *et al.*, Neuropsychological impairment in human immunodeficiency virus-infection: implications for employment. HNRC Group. HIV Neurobehavioral Research Center. *Psychosomatic Medicine* **56**, 8–17 (1994).

15. T. D. Marcotte, *et al.*, A multimodal assessment of driving performance in HIV infection. *Neurology* **63**, 1417–1422 (2004).
16. S. DeVaughn, E. M. Müller-Oehring, B. Markey, H. M. Brontë-Stewart, T. Schulte, Aging with HIV-1 Infection: Motor Functions, Cognition, and Attention – A Comparison with Parkinson’s Disease. *Neuropsychol Rev* **25**, 424–438 (2015).
17. M. Reger, R. Welsh, J. Razani, D. J. Martin, K. B. Boone, A meta-analysis of the neuropsychological sequelae of HIV infection. *J Int Neuropsychol Soc* **8**, 410–424 (2002).
18. B. M. Ances, D. B. Clifford, HIV-Associated Neurocognitive Disorders and the Impact of Combination Antiretroviral Therapies. *Curr Neurol Neurosci Rep* **8**, 455–461 (2008).
19. V. Valcour, *et al.*, Aging exacerbates extrapyramidal motor signs in the era of highly active antiretroviral therapy. *Journal of NeuroVirology* **14**, 362–367 (2008).
20. I. M. Elicer, D. Byrd, U. S. Clark, S. Morgello, J. Robinson-Papp, Motor function declines over time in human immunodeficiency virus and is associated with cerebrovascular disease, while HIV-associated neurocognitive disorder remains stable. *J. Neurovirol.* **24**, 514–522 (2018).
21. J. Robinson-Papp, *et al.*, Characteristics of Motor Dysfunction in Longstanding Human Immunodeficiency Virus. *Clinical Infectious Diseases* **71**, 1532–1538 (2020).
22. J. W. Wilkins, P. D, K. R. Robertson, P. D, C. R. Snyder, *Implications of Self-Reported Cognitive and Motor Dysfunction in HIV-Positive Patients.*
23. J. L. Montoya, *et al.*, Inflammation Relates to Poorer Complex Motor Performance Among Adults Living With HIV on Suppressive Antiretroviral Therapy. *JAIDS Journal of Acquired Immune Deficiency Syndromes* **80**, 15–23 (2019).
24. J. T. Becker, *et al.*, Subcortical brain atrophy persists even in HAART-regulated HIV disease. *Brain Imaging and Behavior* **5**, 77–85 (2011).
25. R. A. Cohen, *et al.*, Effects of nadir CD4 count and duration of human immunodeficiency virus infection on brain volumes in the highly active antiretroviral therapy era. *Journal of NeuroVirology* **16**, 25–32 (2010).
26. K. M. Clifford, *et al.*, Progressive Brain Atrophy Despite Persistent Viral Suppression in HIV Patients Older Than 60 Years. *JAIDS Journal of Acquired Immune Deficiency Syndromes* **76**, 289–297 (2017).
27. K. Hestad, *et al.*, Regional brain atrophy in HIV-1 infection: association with specific neuropsychological test performance. *Acta Neurologica Scandinavica* **88**, 112–118 (1993).
28. P. M. Thompson, *et al.*, Thinning of the cerebral cortex visualized in HIV/AIDS reflects CD4+ T lymphocyte decline. *PNAS* **102**, 15647–15652 (2005).

29. J. C. Stout, Progressive Cerebral Volume Loss in Human Immunodeficiency Virus Infection: A Longitudinal Volumetric Magnetic Resonance Imaging Study. *Arch Neurol* **55**, 161 (1998).
30. M. Küper, *et al.*, Structural gray and white matter changes in patients with HIV. *J Neurol* **258**, 1066–1075 (2011).
31. R. Sanford, *et al.*, Longitudinal Trajectories of Brain Volume and Cortical Thickness in Treated and Untreated Primary Human Immunodeficiency Virus Infection. *Clinical Infectious Diseases* **67**, 1697–1704 (2018).
32. S. Serrano-Villar, *et al.*, HIV-infected individuals with low CD4/CD8 ratio despite effective antiretroviral therapy exhibit altered T cell subsets, heightened CD8+ T cell activation, and increased risk of non-AIDS morbidity and mortality. *PLoS Pathog* **10**, e1004078 (2014).
33. V. Leung, *et al.*, Predictors of CD4:CD8 ratio normalization and its effect on health outcomes in the era of combination antiretroviral therapy. *PLoS One* **8**, e77665 (2013).
34. A. M. Gross, *et al.*, Methylome-wide Analysis of Chronic HIV Infection Reveals Five-Year Increase in Biological Age and Epigenetic Targeting of HLA. *Mol Cell* **62**, 157–168 (4).
35. V. Tozzi, *et al.*, Prevalence and risk factors for human immunodeficiency virus-associated neurocognitive impairment, 1996 to 2002: results from an urban observational cohort. *J Neurovirol* **11**, 265–73 (2005).
36. J. A. Muñoz-Moreno, *et al.*, Nadir CD4 cell count predicts neurocognitive impairment in HIV-infected patients. *AIDS Res Hum Retroviruses* **24**, 1301–7 (2008).
37. R. J. Ellis, *et al.*, CD4 nadir is a predictor of HIV neurocognitive impairment in the era of combination antiretroviral therapy. *AIDS* **25**, 1747–51 (2011).
38. M. May, *et al.*, Impact of late diagnosis and treatment on life expectancy in people with HIV-1: UK Collaborative HIV Cohort (UK CHIC) Study. *BMJ* **343**, d6016 (2011).
39. D. F. Passos, *et al.*, CD4/CD8 ratio, comorbidities, and aging in treated HIV infected individuals on viral suppression. *Journal of Medical Virology* **92**, 3254–3264 (2020).
40. K. J. Towgood, *et al.*, Mapping the brain in younger and older asymptomatic HIV-1 men: Frontal volume changes in the absence of other cortical or diffusion tensor abnormalities. *Cortex* **48**, 230–241 (2012).
41. T. Ernst, L. Chang, J. Jovicich, N. Ames, S. Arnold, Abnormal brain activation on functional MRI in cognitively asymptomatic HIV patients. *Neurology* **59**, 1343–9 (2002).
42. L. Chang, *et al.*, Adaptation of the attention network in human immunodeficiency virus brain injury. *Ann Neurol* **56**, 259–72 (2004).

43. L. Chang, R. Yakupov, H. Nakama, B. Stokes, T. Ernst, Antiretroviral treatment is associated with increased attentional load-dependent brain activation in HIV patients. *J Neuroimmune Pharmacol* **3**, 95–104 (2008).
44. T. Ernst, *et al.*, Declined neural efficiency in cognitively stable human immunodeficiency virus patients. *Ann Neurol* **65**, 316–25 (2009).
45. C. S. Hakkers, *et al.*, Review of functional MRI in HIV: effects of aging and medication. *J Neurovirol* **23**, 20–32 (2017).
46. M. C. Masters, B. M. Ances, Role of Neuroimaging in HIV-Associated Neurocognitive Disorders. *Semin Neurol* **34**, 89–102 (2014).
47. B. M. Ances, A. C. Roc, M. Korczykowski, R. L. Wolf, D. L. Kolson, Combination antiretroviral therapy modulates the blood oxygen level—dependent amplitude in human immunodeficiency virus—seropositive patients. *Journal of NeuroVirology* **14**, 418–424 (2008).
48. S. B. Juengst, H. J. Aizenstein, J. Figurski, O. L. Lopez, J. T. Becker, Alterations in the hemodynamic response function in cognitively impaired HIV/AIDS subjects. *Journal of Neuroscience Methods* **163**, 208–212 (2007).
49. J. Rothwell, *Motor Control*, Second (Elsevier, 2004).
50. D. M. Wolpert, R. C. Miall, Forward Models for Physiological Motor Control. *Neural Netw* **9**, 1265–1279 (1996).
51. D. M. Wolpert, Z. Ghahramani, M. I. Jordan, An internal model for sensorimotor integration. *Science* **269**, 1880–2 (1995).
52. E. Bizzi, F. A. Mussa-Ivaldi, Neural basis of motor control and its cognitive implications. *Trends Cogn Sci* **2**, 97–102 (1998).
53. T. W. Wilson, E. Heinrichs-Graham, A. L. Proskovec, T. J. McDermott, Neuroimaging with magnetoencephalography: A dynamic view of brain pathophysiology. *Transl Res* **175**, 17–36 (2016).
54. T. Grent-'t-Jong, R. Oostenveld, O. Jensen, W. P. Medendorp, P. Praamstra, Competitive interactions in sensorimotor cortex: oscillations express separation between alternative movement targets. *J Neurophysiol* **112**, 224–32 (2014).
55. C. Tzagarakis, N. F. Ince, A. C. Leuthold, G. Pellizzer, Beta-band activity during motor planning reflects response uncertainty. *J Neurosci* **30**, 11270–7 (2010).
56. T. W. Wilson, *et al.*, An extended motor network generates beta and gamma oscillatory perturbations during development. *Brain Cogn* **73**, 75–84 (2010).

57. E. Heinrichs-Graham, D. J. Arpin, T. W. Wilson, Cue-related Temporal Factors Modulate Movement-related Beta Oscillatory Activity in the Human Motor Circuit. *J Cogn Neurosci* **28**, 1039–51 (2016).
58. P. Praamstra, D. Kourtis, K. Nazarpour, Simultaneous preparation of multiple potential movements: opposing effects of spatial proximity mediated by premotor and parietal cortex. *J Neurophysiol* **102**, 2084–95 (2009).
59. J. Kaiser, N. Birbaumer, W. Lutzenberger, Event-related beta desynchronization indicates timing of response selection in a delayed-response paradigm in humans. *Neurosci Lett* **312**, 149–52 (2001).
60. E. Heinrichs-Graham, T. W. Wilson, Coding complexity in the human motor circuit. *Hum Brain Mapp* **36**, 5155–67 (2015).
61. T. Grent-'t-Jong, R. Oostenveld, O. Jensen, W. P. Medendorp, P. Praamstra, Oscillatory dynamics of response competition in human sensorimotor cortex. *Neuroimage* **83**, 27–34 (2013).
62. A. I. Wiesman, S. M. Koshy, E. Heinrichs-Graham, T. W. Wilson, Beta and gamma oscillations index cognitive interference effects across a distributed motor network. *Neuroimage*, 116747 (2020).
63. E. Heinrichs-Graham, J. M. Hoburg, T. W. Wilson, The peak frequency of motor-related gamma oscillations is modulated by response competition. *NeuroImage* **165**, 27–34 (2018).
64. W. Gaetz, M. Macdonald, D. Cheyne, O. C. Snead, Neuromagnetic imaging of movement-related cortical oscillations in children and adults: age predicts post-movement beta rebound. *Neuroimage* **51**, 792–807 (2010).
65. E. Heinrichs-Graham, M. J. Kurz, J. E. Gehringer, T. W. Wilson, The functional role of post-movement beta oscillations in motor termination. *Brain Struct Funct* **222**, 3075–3086 (2017).
66. M. T. Jurkiewicz, W. C. Gaetz, A. C. Bostan, D. Cheyne, Post-movement beta rebound is generated in motor cortex: evidence from neuromagnetic recordings. *Neuroimage* **32**, 1281–9 (2006).
67. G. Pfurtscheller, F. H. Lopes da Silva, Event-related EEG/MEG synchronization and desynchronization: basic principles. *Clin Neurophysiol* **110**, 1842–57 (1999).
68. A. K. Engel, P. Fries, Beta-band oscillations--signalling the status quo? *Curr Opin Neurobiol* **20**, 156–65 (2010).
69. J. Igarashi, Y. Isomura, K. Arai, R. Harukuni, T. Fukai, A θ - γ oscillation code for neuronal coordination during motor behavior. *J Neurosci* **33**, 18515–30 (2013).

70. A. Tomassini, L. Ambrogioni, W. P. Medendorp, E. Maris, Theta oscillations locked to intended actions rhythmically modulate perception. *Elife* **6** (7).
71. S. D. Muthukumaraswamy, Functional properties of human primary motor cortex gamma oscillations. *J Neurophysiol* **104**, 2873–85 (2010).
72. W. Gaetz, J. C. Edgar, D. J. Wang, T. P. Roberts, Relating MEG measured motor cortical oscillations to resting γ -aminobutyric acid (GABA) concentration. *Neuroimage* **55**, 616–21 (2011).
73. T. W. Wilson, *et al.*, Abnormal gamma and beta MEG activity during finger movements in early-onset psychosis. *Dev Neuropsychol* **36**, 596–613 (2011).
74. W. Gaetz, C. Liu, H. Zhu, L. Bloy, T. P. Roberts, Evidence for a motor gamma-band network governing response interference. *Neuroimage* **74**, 245–53 (2013).
75. R. K. Spooner, A. I. Wiesman, A. L. Proskovec, E. Heinrichs-Graham, T. W. Wilson, Prefrontal theta modulates sensorimotor gamma networks during the reorienting of attention. *Hum Brain Mapp* **41**, 520–529 (2020).
76. T. W. Wilson, *et al.*, Functional brain abnormalities during finger-tapping in HIV-infected older adults: a magnetoencephalography study. *J Neuroimmune Pharmacol* **8**, 965–74 (2013).
77. K. M. Becker, *et al.*, Decreased MEG beta oscillations in HIV-infected older adults during the resting state. *J. Neurovirol.* **19**, 586–594 (2013).
78. O. Kann, R. Kovács, Mitochondria and neuronal activity. *American Journal of Physiology-Cell Physiology* **292**, C641–C657 (2007).
79. E. Cadenas, K. J. A. Davies, Mitochondrial free radical generation, oxidative stress, and aging¹¹This article is dedicated to the memory of our dear friend, colleague, and mentor Lars Ernster (1920–1998), in gratitude for all he gave to us. *Free Radical Biology and Medicine* **29**, 222–230 (2000).
80. D. Harman, Aging: a theory based on free radical and radiation chemistry. *J Gerontol* **11**, 298–300 (1956).
81. D. Harman, Free radical theory of aging: an update: increasing the functional life span. *Ann N Y Acad Sci* **1067**, 10–21 (2006).
82. M. Vos, E. Lauwers, P. Verstreken, Synaptic Mitochondria in Synaptic Transmission and Organization of Vesicle Pools in Health and Disease. *Front. Synaptic Neurosci.* **2** (2010).
83. C. López-Otín, M. A. Blasco, L. Partridge, M. Serrano, G. Kroemer, The hallmarks of aging. *Cell* **153**, 1194–217 (2013).
84. D. G. Franchina, C. Dostert, D. Brenner, Reactive Oxygen Species: Involvement in T Cell Signaling and Metabolism. *Trends Immunol* **39**, 489–502 (6).

85. G. J. van der Windt, *et al.*, Mitochondrial respiratory capacity is a critical regulator of CD8⁺ T cell memory development. *Immunity* **36**, 68–78 (2012).
86. L. A. Sena, *et al.*, Mitochondria are required for antigen-specific T cell activation through reactive oxygen species signaling. *Immunity* **38**, 225–36 (2013).
87. T. Sun, H. Qiao, P. Y. Pan, Y. Chen, Z. H. Sheng, Motile axonal mitochondria contribute to the variability of presynaptic strength. *Cell Rep* **4**, 413–419 (2013).
88. Y. Hara, *et al.*, Presynaptic mitochondrial morphology in monkey prefrontal cortex correlates with working memory and is improved with estrogen treatment. *Proc Natl Acad Sci U S A* **111**, 486–91 (2014).
89. T. Ahmad, *et al.*, Computational classification of mitochondrial shapes reflects stress and redox state. *Cell Death Dis* **4**, e461 (2013).
90. M. Khacho, *et al.*, Mitochondrial dysfunction underlies cognitive defects as a result of neural stem cell depletion and impaired neurogenesis. *Human Molecular Genetics* **26**, 3327–3341 (2017).
91. F. Johnson, C. Giulivi, Superoxide dismutases and their impact upon human health. *Molecular Aspects of Medicine* **26**, 340–352 (2005).
92. Andrew. G. Reaume, *et al.*, Motor neurons in Cu/Zn superoxide dismutase-deficient mice develop normally but exhibit enhanced cell death after axonal injury. *Nat Genet* **13**, 43–47 (1996).
93. C. Sims-Robinson, *et al.*, The role of oxidative stress in nervous system aging. *PLoS One* **8**, e68011 (2013).
94. S. S. Ali, *et al.*, Initial evidence linking synaptic superoxide production with poor short-term memory in aged mice. *Brain Res* **1368**, 65–70 (2011).
95. S. S. Ali, *et al.*, Gender differences in free radical homeostasis during aging: shorter-lived female C57BL6 mice have increased oxidative stress. *Aging cell* **5**, 565–574 (2006).
96. S. Przedborski, K. Tieu, C. Perier, M. Vila, MPTP as a Mitochondrial Neurotoxic Model of Parkinson's Disease. *J Bioenerg Biomembr* **36**, 375–379 (2004).
97. S. Przedborski, H. Ischiropoulos, Reactive oxygen and nitrogen species: weapons of neuronal destruction in models of Parkinson's disease. *Antioxid Redox Signal* **7**, 685–93 (2005).
98. C. E. Lambert, S. C. Bondy, Effects of MPTP, MPP⁺ and paraquat on mitochondrial potential and oxidative stress. *Life Sciences* **44**, 1277–1284 (1989).
99. B. Akkaya, *et al.*, Increased Mitochondrial Biogenesis and Reactive Oxygen Species Production Accompany Prolonged CD4. *J Immunol* **201**, 3294–3306 (12).

100. S. Hong, W. A. Banks, Role of the immune system in HIV-associated neuroinflammation and neurocognitive implications. *Brain Behav Immun* **45**, 1–12 (2015).
101. M. Korencak, *et al.*, Effect of HIV infection and antiretroviral therapy on immune cellular functions. *JCI Insight* **4** (2019).
102. X. Wang, *et al.*, Oxidative stress and mitochondrial dysfunction in Alzheimer's disease. *Biochimica et Biophysica Acta (BBA) - Molecular Basis of Disease* **1842**, 1240–1247 (2014).
103. I. González-Casacuberta, D. L. Juárez-Flores, C. Morén, G. Garrabou, Bioenergetics and Autophagic Imbalance in Patients-Derived Cell Models of Parkinson Disease Supports Systemic Dysfunction in Neurodegeneration. *Front. Neurosci.* **13** (2019).
104. T. M. Rickabaugh, *et al.*, Acceleration of age-associated methylation patterns in HIV-1-infected adults. *PLoS One* **10**, e0119201 (2015).
105. D. L. Zanet, *et al.*, Association between short leukocyte telomere length and HIV infection in a cohort study: No evidence of a relationship with antiretroviral therapy. *Clin Infect Dis* **58**, 1322–32 (2014).
106. C. Gemma, J. Vila, A. Bachstetter, P. C. Bickford, *Oxidative Stress and the Aging Brain: From Theory to Prevention* (Taylor & Francis Group, LLC, 2007).
107. J. K. Anderson, Oxidative stress in neurodegeneration: cause or consequence? *Nature Medicine*, **8** (2004).
108. M. Picard, B. S. McEwen, Mitochondria impact brain function and cognition. *Proc Natl Acad Sci U S A* **111**, 7–8 (2014).
109. C. Akay, *et al.*, Antiretroviral drugs induce oxidative stress and neuronal damage in the central nervous system. *J Neurovirol* **20**, 39–53 (2014).
110. K. L. Stauch, K. Emanuel, B. G. Lamberty, B. Morsey, H. S. Fox, Central nervous system-penetrating antiretrovirals impair energetic reserve in striatal nerve terminals. *J Neurovirol* **23**, 795–807 (2017).
111. I. M. Ahmad, J. B. Temme, M. Y. Abdalla, M. C. Zimmerman, Redox status in workers occupationally exposed to long-term low levels of ionizing radiation: A pilot study. *Redox Rep* **21**, 139–45 (2016).
112. V. Avdoshina, *et al.*, The HIV Protein gp120 Alters Mitochondrial Dynamics in Neurons. *Neurotox Res* **29**, 583–593 (2016).
113. A. Shah, A. Kumar, HIV-1 gp120-Mediated Mitochondrial Dysfunction and HIV-Associated Neurological Disorders. *Neurotox Res* **30**, 135–7 (8).
114. M. Repetto, *et al.*, Oxidative stress in blood of HIV infected patients. *Clin Chim Acta* **255**, 107–17 (1996).

115. L. Gil, D. Pérez, R. Tápanes, J. Pérez, T. Grune, Does mitochondrial dysfunction during antiretroviral therapy in human immunodeficiency virus infection suggest antioxidant supplementation as a beneficial option? *Redox Rep* **10**, 113–9 (2005).
116. G. W. Pace, C. D. Leaf, The role of oxidative stress in HIV disease. *Free Radic Biol Med* **19**, 523–8 (1995).
117. L. Gil, *et al.*, Contribution to characterization of oxidative stress in HIV/AIDS patients. *Pharmacol Res* **47**, 217–24 (2003).
118. S. Liochev, I. Fridovich, The effects of superoxide dismutase on H₂O₂ formation. *Free Radical Biology and Medicine* **42**, 5 (2007).
119. F. G. Tahrir, *et al.*, Dysregulation of mitochondrial bioenergetics and quality control by HIV-1 Tat in cardiomyocytes. *Journal of Cellular Physiology* **233**, 748–758 (2018).
120. J. D. Lambeth, NOX enzymes and the biology of reactive oxygen. *Nature Reviews Immunology* **4**, 181–189 (2004).
121. H. A. Funes, *et al.*, Neuronal bioenergetics and acute mitochondrial dysfunction: a clue to understanding the central nervous system side effects of efavirenz. *J Infect Dis* **210**, 1385–95 (2014).
122. R. Polo, S. Martinez, P. Madrigal, M. Gonzalez-Muñoz, Factors associated with mitochondrial dysfunction in circulating peripheral blood lymphocytes from HIV-infected people. *J Acquir Immune Defic Syndr* **34**, 32–6 (2003).
123. T. W. Wilson, E. Heinrichs-Graham, K. M. Becker, Circadian modulation of motor-related beta oscillatory responses. *Neuroimage* **102 Pt 2**, 531–9 (2014).
124. A. Fry, *et al.*, Modulation of post-movement beta rebound by contraction force and rate of force development. *Hum Brain Mapp* **37**, 2493–511 (7).
125. E. Heinrichs-Graham, T. W. Wilson, Is an absolute level of cortical beta suppression required for proper movement? Magnetoencephalographic evidence from healthy aging. *Neuroimage* **134**, 514–21 (2016).
126. E. Heinrichs-Graham, *et al.*, Hypersynchrony despite pathologically reduced beta oscillations in patients with Parkinson's disease: a pharmaco-magnetoencephalography study. *J Neurophysiol* **112**, 1739–47 (2014).
127. H. E. Rossiter, E. M. Davis, E. V. Clark, M. H. Boudrias, N. S. Ward, Beta oscillations reflect changes in motor cortex inhibition in healthy ageing. *Neuroimage* **91**, 360–5 (2014).
128. L. A. Hasam-Henderson, *et al.*, NMDA-receptor inhibition and oxidative stress during hippocampal maturation differentially alter parvalbumin expression and gamma-band activity. *Scientific Reports* **8**, 9545 (2018).

129. O. Kann, The interneuron energy hypothesis: Implications for brain disease. *Neurobiology of Disease* **90**, 75–85 (2016).
130. O. Kann, I. E. Papageorgiou, A. Draguhn, Highly Energized Inhibitory Interneurons are a Central Element for Information Processing in Cortical Networks. *J Cereb Blood Flow Metab* **34**, 1270–1282 (2014).
131. O. Kann, J.-O. Hollnagel, S. Elzoheiry, J. Schneider, Energy and Potassium Ion Homeostasis during Gamma Oscillations. *Front. Mol. Neurosci.* **9** (2016).
132. M. Bartos, I. Vida, P. Jonas, Synaptic mechanisms of synchronized gamma oscillations in inhibitory interneuron networks. *Nat Rev Neurosci* **8**, 45–56 (2007).
133. G. Buzsáki, A. Draguhn, Neuronal oscillations in cortical networks. *Science* **304**, 1926–9 (2004).
134. G. Buzsáki, X. J. Wang, Mechanisms of gamma oscillations. *Annu Rev Neurosci* **35**, 203–25 (2012).
135. W. Singer, Neuronal synchrony: a versatile code for the definition of relations? *Neuron* **24**, 49–65, 111–25 (1999).
136. M. Vinck, T. Womelsdorf, E. A. Buffalo, R. Desimone, P. Fries, Attentional modulation of cell-class-specific gamma-band synchronization in awake monkey area v4. *Neuron* **80**, 1077–89 (2013).
137. S. D. Hall, *et al.*, The role of GABAergic modulation in motor function related neuronal network activity. *Neuroimage* **56**, 1506–10 (2011).
138. S. D. Muthukumaraswamy, *et al.*, The effects of elevated endogenous GABA levels on movement-related network oscillations. *Neuroimage* **66**, 36–41 (2013).
139. D. J. Tyrrell, *et al.*, Blood-Based Bioenergetic Profiling Reflects Differences in Brain Bioenergetics and Metabolism. *Oxid Med Cell Longev* **2017**, 7317251 (2017).
140. S. Taulu, J. Simola, Spatiotemporal signal space separation method for rejecting nearby interference in MEG measurements. *Phys Med Biol* **51**, 1759–68 (2006).
141. M. A. Uusitalo, R. J. Ilmoniemi, Signal-space projection method for separating MEG or EEG into components. *Med Biol Eng Comput* **35**, 135–40 (1997).
142. C. K. Kovach, P. E. Gander, The demodulated band transform. *J Neurosci Methods* **261**, 135–54 (2016).
143. E. Heinrichs-Graham, *et al.*, Parietal Oscillatory Dynamics Mediate Developmental Improvement in Motor Performance. *Cerebral Cortex* **30**, 6405–6414 (2020).
144. R. K. Spooner, *et al.*, Prefrontal gating of sensory input differentiates cognitively impaired and unimpaired aging adults with HIV. *Brain Commun* **2**, fcaa080 (2020).

145. J. Gross, *et al.*, Dynamic imaging of coherent sources: Studying neural interactions in the human brain. *Proc Natl Acad Sci U S A* **98**, 694–9 (2001).
146. A. Hillebrand, K. D. Singh, I. E. Holliday, P. L. Furlong, G. R. Barnes, A new approach to neuroimaging with magnetoencephalography. *Hum Brain Mapp* **25**, 199–211 (2005).
147. B. Efron, R. Tibshirani, Bootstrap Methods for Standard Errors, Confidence Intervals, and Other Measures of Statistical Accuracy. *Statist. Sci.* **1**, 54–75 (1986).
148. M. S. Fritz, D. P. MacKinnon, Required Sample Size to Detect the Mediated Effect. *Psychol Sci* **18**, 233–239 (2007).
149. P. Fries, D. Nikolić, W. Singer, The gamma cycle. *Trends Neurosci* **30**, 309–16 (2007).
150. P. J. Uhlhaas, *et al.*, Neural synchrony in cortical networks: history, concept and current status. *Front Integr Neurosci* **3**, 17 (2009).
151. P. J. Uhlhaas, W. Singer, Neuronal dynamics and neuropsychiatric disorders: toward a translational paradigm for dysfunctional large-scale networks. *Neuron* **75**, 963–80 (2012).
152. R. A. Edden, S. D. Muthukumaraswamy, T. C. Freeman, K. D. Singh, Orientation discrimination performance is predicted by GABA concentration and gamma oscillation frequency in human primary visual cortex. *J Neurosci* **29**, 15721–6 (2009).
153. S. D. Muthukumaraswamy, R. A. Edden, D. K. Jones, J. B. Swettenham, K. D. Singh, Resting GABA concentration predicts peak gamma frequency and fMRI amplitude in response to visual stimulation in humans. *Proc Natl Acad Sci U S A* **106**, 8356–61 (2009).
154. , Nomenclature and research case definitions for neurologic manifestations of human immunodeficiency virus-type 1 (HIV-1) infection. Report of a Working Group of the American Academy of Neurology AIDS Task Force. *Neurology* **41**, 778–785 (1991).
155. Y. Zhou, *et al.*, Motor-related brain abnormalities in HIV-infected patients: a multimodal MRI study. *Neuroradiology* **59**, 1133–1142 (2017).
156. X. Wang, *et al.*, Abnormalities in Resting-State Functional Connectivity in Early Human Immunodeficiency Virus Infection. *Brain Connectivity* **1**, 207–217 (2011).
157. B. M. Ances, *et al.*, HIV infection and aging independently affect brain function as measured by functional magnetic resonance imaging. *J Infect Dis* **201**, 336–40 (2010).
158. B. M. Ances, *et al.*, Resting cerebral blood flow: a potential biomarker of the effects of HIV in the brain. *Neurology* **73**, 702–8 (2009).
159. B. Ances, F. Vaida, R. Ellis, R. Buxton, Test-retest stability of calibrated BOLD-fMRI in HIV- and HIV+ subjects. *Neuroimage* **54**, 2156–62 (2011).
160. E. Heinrichs-Graham, *et al.*, The lifespan trajectory of neural oscillatory activity in the motor system. *Dev Cogn Neurosci* **30**, 159–168 (4).

161. A. Yokoi, J. Diedrichsen, Neural Organization of Hierarchical Motor Sequence Representations in the Human Neocortex. *Neuron* **103**, 1178-1190.e7 (2019).
162. M. Samuel, *et al.*, Evidence for lateral premotor and parietal overactivity in Parkinson's disease during sequential and bimanual movements. A PET study. *Brain* **120**, 963–976 (1997).
163. A. M. Gross, *et al.*, Methylome-wide Analysis of Chronic HIV Infection Reveals Five-Year Increase in Biological Age and Epigenetic Targeting of HLA. *Molecular Cell* **62**, 157–168 (2016).
164. E. Heinrichs-Graham, *et al.*, Neuromagnetic evidence of abnormal movement-related beta desynchronization in Parkinson's disease. *Cereb Cortex* **24**, 2669–78 (2014).
165. B. Pollok, *et al.*, Motor-cortical oscillations in early stages of Parkinson's disease. *The Journal of Physiology* **590**, 3203–3212 (2012).
166. P. Brown, "Bad oscillations in Parkinson's disease" in *Parkinson's Disease and Related Disorders*, P. Riederer, H. Reichmann, M. B. H. Youdim, M. Gerlach, Eds. (Springer Vienna, 2006), pp. 27–30.
167. M. Bologna, *et al.*, Transcranial Alternating Current Stimulation Has Frequency-Dependent Effects on Motor Learning in Healthy Humans. *Neuroscience* **411**, 130–139 (7).
168. R. A. Joundi, N. Jenkinson, J. S. Brittain, T. Z. Aziz, P. Brown, Driving oscillatory activity in the human cortex enhances motor performance. *Curr Biol* **22**, 403–7 (2012).
169. E. Santarnecchi, *et al.*, High-gamma oscillations in the motor cortex during visuo-motor coordination: A tACS interferential study. *Brain Res Bull* **131**, 47–54 (2017).
170. A. Guerra, *et al.*, Effects of Transcranial Alternating Current Stimulation on Repetitive Finger Movements in Healthy Humans. *Neural Plast* **2018**, 4593095 (2018).
171. J. T. Becker, *et al.*, Vascular risk factors, HIV serostatus, and cognitive dysfunction in gay and bisexual men. *Neurology* **73**, 1292–1299 (2009).
172. N. Sacktor, K. Robertson, Evolving clinical phenotypes in HIV-associated neurocognitive disorders. *Curr Opin HIV AIDS* **9**, 517–520 (2014).
173. C. A. Sabin, Do people with HIV infection have a normal life expectancy in the era of combination antiretroviral therapy? *BMC Medicine* **11**, 251 (2013).
174. A. J. McMichael, P. Borrow, G. D. Tomaras, N. Goonetilleke, B. F. Haynes, The immune response during acute HIV-1 infection: clues for vaccine development. *Nat Rev Immunol* **10**, 11–23 (2010).
175. A. Angajala, *et al.*, Diverse Roles of Mitochondria in Immune Responses: Novel Insights Into Immuno-Metabolism. *Front Immunol* **9** (2018).

176. V. Appay, S. L. Rowland-Jones, Premature ageing of the immune system: the cause of AIDS? *Trends Immunol* **23**, 580–5 (2002).
177. J. Magrané, M. A. Sahawneh, S. Przedborski, Á. Estévez, G. Manfredi, Mitochondrial dynamics and bioenergetic dysfunction is associated with synaptic alterations in mutant SOD1 motor neurons. *J Neurosci* **32**, 229–42 (2012).
178. M. Hämäläinen, R. Hari, R. J. Ilmoniemi, J. Knuutila, O. V. Lounasmaa, Magnetoencephalography---theory, instrumentation, and applications to noninvasive studies of the working human brain. *Rev. Mod. Phys.* **65**, 413–497 (1993).
179. D. J. Tyrrell, *et al.*, Respirometric Profiling of Muscle Mitochondria and Blood Cells Are Associated With Differences in Gait Speed Among Community-Dwelling Older Adults. *J Gerontol A Biol Sci Med Sci* **70**, 1394–9 (2015).
180. R. Marchioli, C. Schweiger, G. Levantesi, L. Tavazzi, F. Valagussa, Antioxidant vitamins and prevention of cardiovascular disease: Epidemiological and clinical trial data. *Lipids* **36**, S53–S63 (2001).
181. P. Mecocci, M. C. Polidori, Antioxidant clinical trials in mild cognitive impairment and Alzheimer's disease. *Biochimica et Biophysica Acta (BBA) - Molecular Basis of Disease* **1822**, 631–638 (2012).
182. M. Goodman, R. M. Bostick, O. Kucuk, D. P. Jones, Clinical trials of antioxidants as cancer prevention agents: Past, present, and future. *Free Radical Biology and Medicine* **51**, 1068–1084 (2011).